Thermal processing

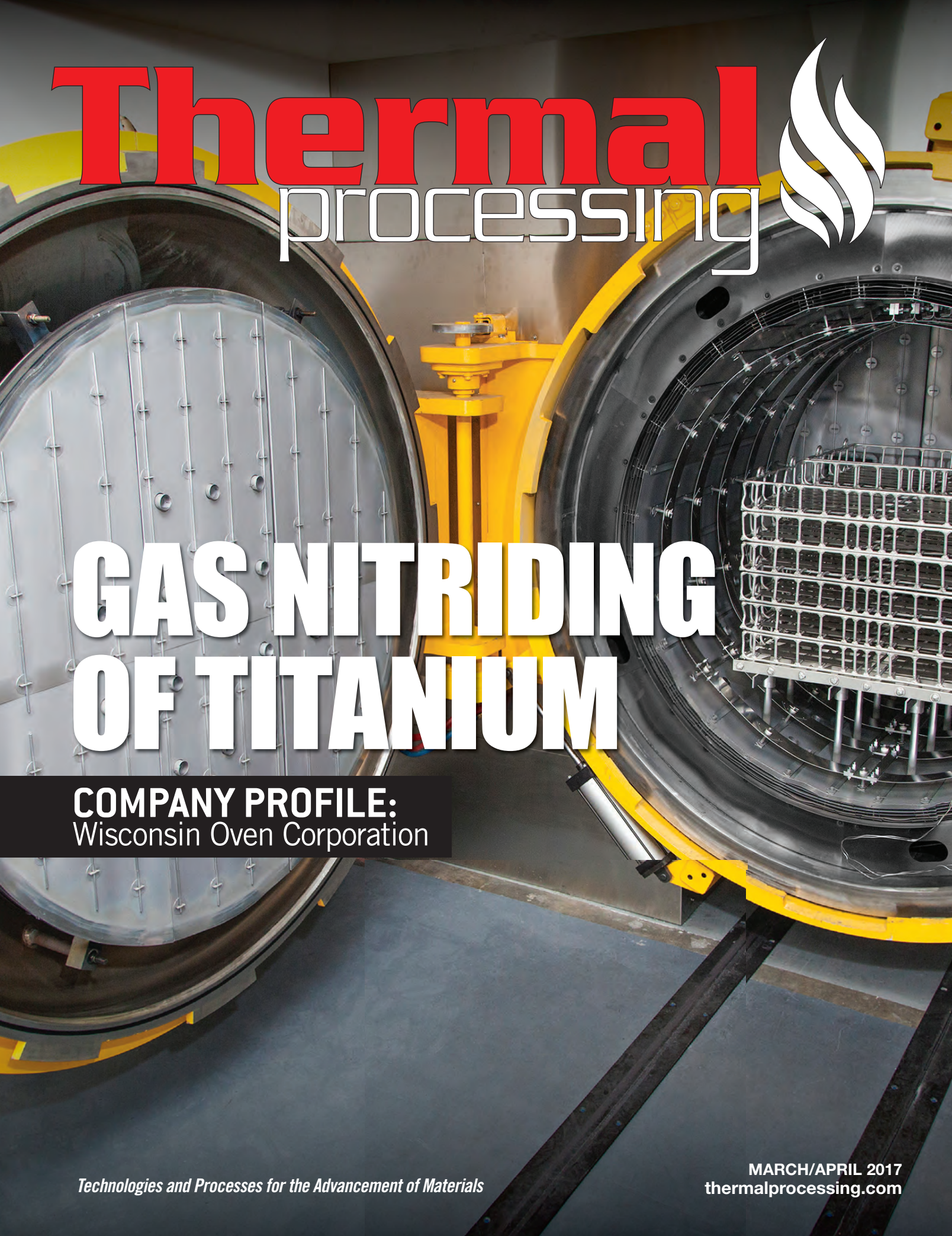

GAS NITRIDING OF TITANIUM

COMPANY PROFILE:
Wisconsin Oven Corporation

Technologies and Processes for the Advancement of Materials

MARCH/APRIL 2017
thermalprocessing.com

First-Time Heat Treater Streamlines Production, Reducing Lead Times by Nearly 85%

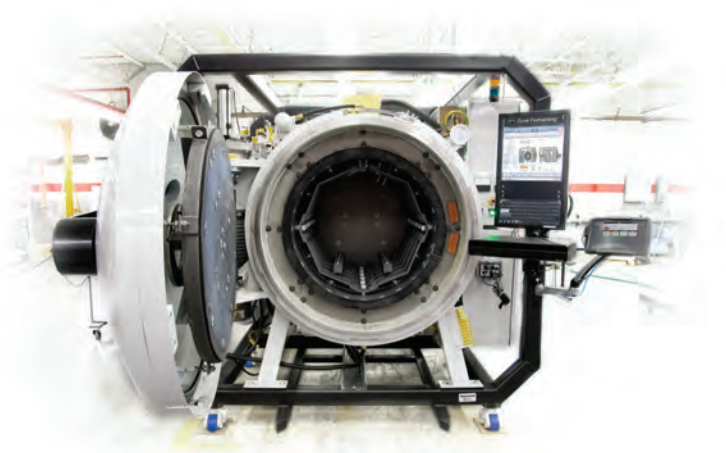

Customer Story

A manufacturer of Aerospace-grade fasteners wanted to streamline their production process and shorten lead times while still keeping costs low. They realized that to meet their objectives they needed to bring heat treatment in-house.

While the decision to bring heat treatment in-house made sense, this would be their first vacuum furnace. Ipsen's TITAN® product line appealed to them as it was built on the principle that everyone can be heat treater, whether you are new to the industry or an expert. As such, all TITAN furnaces are carefully designed and crafted with the end user in mind.

"We used to send our products to a local heat treater before bringing them back in-house to finish the production process ... In the end, this strategy just wasn't working for us. It created long lead times and a convoluted in-house workflow that simply wasn't sustainable."

However, they not only needed a heat-treating system that could run their required processes, but also a company that had the resources to support them throughout the process. This included assistance with on-site installation, expert training and timely field support. In the end …

Discover this customer's winning outcome:

www.IpsenUSA.com/Customer-Stories

Download *Quick Scan* or *QR Droid* app to scan code

LEGENDARY PERFORMANCE

WHEN JACK BEAVERS DESIGNED THE BEAVERMATIC INTERNAL QUENCH FURNACE (IQF) ALMOST 60 YEARS AGO, HE CREATED THE SIGNATURE TECHNOLOGY IN AN INDUSTRY WORKHORSE THAT STILL SETS THE STANDARDS TODAY.

The BeaverMatic IQF's rugged design combined with a unique load transfer mechanism for high-production output is the reason for so many successful installations around the world.

- World's largest Internal Quench Furnace with 15,000 pound workload
- Users experience substantial improvement in work flow
- Simplified designs for ease of operation and maintenance
- Reliable, performance proven equipment
- Excellent and efficient processing results

Today Premier Furnace Specialists builds the BeaverMatic IQF incorporating modern process controls and materials, keeping the legend alive and reliable as ever. The legend doesn't end there, Premier Furnace Specialists offers a complete range of furnaces to suit any industrial heating process.

248-596-9000
premierfurnace.com • beavermatic.com
sales@premierfurnace.com




Premier Furnace Specialists, Inc.

FEATURES

MARCH/APRIL 2017

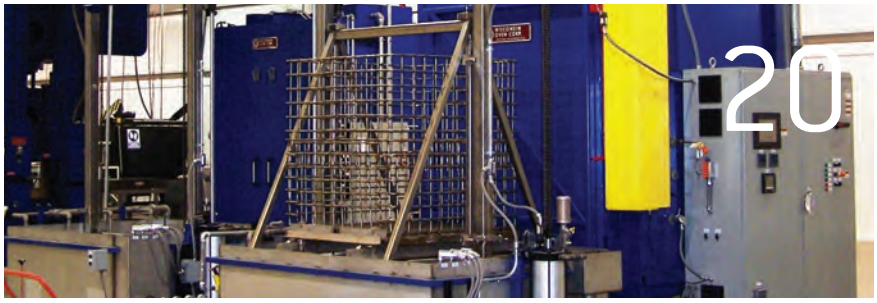

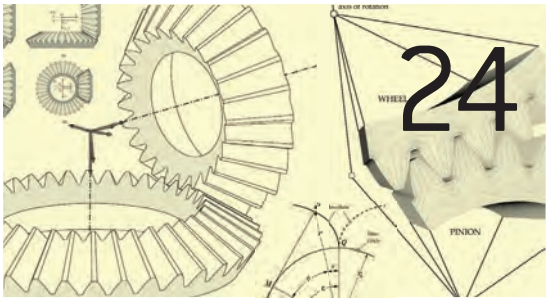

LOW COST, HIGH PRECISION NITRIDING

Tested ZeroFlow® Process – Exceptional Quality & Low Operating Costs.

If you are looking for a market-proven, innovative approach to nitriding and ferritic nitrocarburizing, SECO/WARWICK's ZeroFlow® technology will be of interest to you. With dozens of operating units installed globally, you'll be glad to know that you can trust this money-saving technology to help improve your business.

SECO/WARWICK
INVENTION MEETS RELIABILITY

Mark Hemsath, Nitriding Product Manager | Mob. +1 419 356 3500
E-mail: mark.hemsath@secowarwick.com | www.secowarwick.com

DEPARTMENTS

MARCH/APRIL 2017
Volume 6 / Number 2

UPDATE
NEW PRODUCTS, TRENDS, SERVICES, AND DEVELOPMENTS

08

QUALITY COUNTS
By Jim Oakes

THE RIGHT PREPARED ATMOSPHERE

12

METAL URGENCY
By Lee M. Rothleutner

COUPLING ALLOY AND PROCESS SELECTION

14

HOT SEAT
By Jack Titus

HEAT TREATING, FURNACES, AND UNINTENDED CONSEQUENCES

16

MAINTENANCE MATTERS
By Jim Grann

VACUUM FURNACE LEAKS

18

Q&A
Joe Stambaugh

Forging Products Group Leader, Ajax Tocco Magnethermic

56

RESOURCES

Cover photo: Solar Atmospheres

Thermal Processing is published semi-annually by Media Solutions, Inc., 266D Yeager Parkway Pelham, AL 35124. Phone (205) 380-1573 Fax (205) 380-1580 International subscription rates: $105.00 per year. Postage Paid at Pelham AL and at additional mailing offices. Printed in the USA. POSTMASTER: Send address changes to *Thermal Processing* magazine, P.O. Box 1210 Pelham AL 35124. Return undeliverable Canadian addresses to P.O. Box 503 RPO West Beaver Creek Richmond Hill, ON L4B4R6.

Vacuum Heat Treating Services

…because quality is critical

Our leading edge vacuum technology and expertise provides precise control and repeatability for consistently superior parts. Solve your toughest thermal processing challenges by utilizing our brain-trust of metallurgists, chemists and engineers.

- Over 60 vacuum furnaces – lab-sized to 48' long
- Argon, nitrogen and helium quenching up to 20 bar
- Operating range of -320°F to +3,600°F
- On-site metallurgical testing lab
- 24/7 Operations

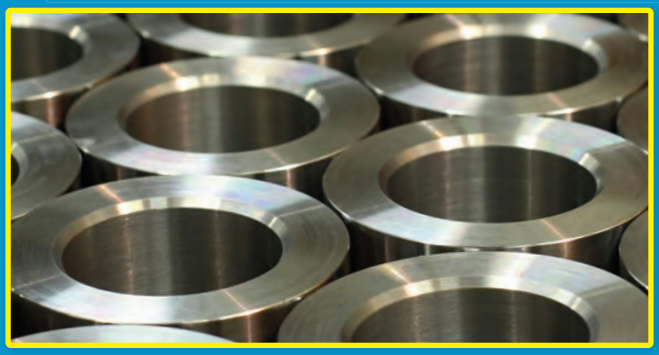

Vacuum Heat Treating

Annealing	Hardening
Age Hardening	Hydriding
Brazing	Dehydriding
Carburizing	Gas Nitriding
Degassing	Stress Relieving
Diffusion Bonding	Tempering

For more information or a quote, call 1-855-WE-HEAT-IT or visit solaratm.com

SOLAR ATMOSPHERES

MedAccred Accredited Heat Treating

Accredited Nadcap™ Heat Treating Nondestructive Testing

AS ISO 9001:2008 9100C registered

MedAccred accredited for Heat Treating at our Souderton, PA facility only | Nadcap Accredited for Nondestructive Testing at our Hermitage, PA facility only

Philadelphia Pittsburgh Southern California South Carolina

VACUUM PROCESSING **Heat Treating • Brazing • Carburizing • Nitriding**

LETTER FROM THE EDITOR

Welcome to the March/April issue of *Thermal Processing* magazine!

With a few months of 2017 already behind us, it's clear that this year is moving at an overwhelming pace. Constant changes from our new administration, industry advancements, and regulations, to name a few, can be challenging.

A great way to keep up with what's going on in the industry is to attend industry association events, and there are a plethora scheduled for this year.

On April 4-6, Forge Fair will take place in Cleveland, Ohio. Sponsored by the Forging Industry Association, this technical trade show offers a way for forging professionals to connect with each other and gain knowledge from exhibitor presentations. In this issue's Q&A, we had a chance to speak with one of the exhibitors, Joe Stambaugh with Ajax Tocco Magnethermic, to hear a little about what they will be highlighting at their booth. If you're attending or exhibiting, I hope you have a successful show and an enjoyable trip.

We also present a technical paper by Alfonso Fuentes, a professor at the Rochester Institute of Technology. The authors developed a computerized generation of straight bevel gears with spherical involute profiles, which can be applied for bevel gears manufactured by forging.

You'll also read about using infrared temperature measurement to understand the technology and consider all the relevant application parameters.

For our focus on materials used in heat treating, we bring you a preliminary study from authors at Solar Atmospheres who show how partial pressure of nitrogen when gas nitriding Ti-6Al-4V in a vacuum furnace can have a significant effect on the nitrided case characteristics.

Lastly, a technical paper from authors at Scania compares Ca-treated carburizing steel grade to a standard steel grade. Machining tests were performed at the transmission machining site at Scania in order to evaluate the PCBN cutting tool life as defined by the generated surface roughness during actual production.

Thermal Processing columnists Jack Titus, Jim Oakes, and Jim Grann return this issue to share their experience and valuable tips. We also would like to welcome a new contributing writer for the Metal Urgency column. Lee Rothleutner is a principal development engineer with The Timken Company, and his research experience includes microstructural evolution during induction hardening, torsional fatigue, and vanadium microalloying. We are so excited to have him on board.

For the company profile this month, *Thermal Processing* associate editor Kenneth Carter talked with Wisconsin Oven. Located in East Troy, Wisconsin, the company offers a variety of standard pre-engineered ovens as well as custom-designed ovens for specific applications.

We hope you enjoy this issue, and as always, thanks for reading!

Molly J. Rogers

Molly J. Rogers
Editor
Thermal Processing magazine
editor@thermalprocessing.com
(800) 366-2185 x205

Thermal processing for Gear Solutions

David C. Cooper
PUBLISHER
Chad Morrison
ASSOCIATE PUBLISHER

EDITORIAL
Molly J. Rogers
EDITOR
Kenneth Carter
ASSOCIATE EDITOR

SALES
Chad Morrison
ASSOCIATE PUBLISHER
Dave Gomez
REGIONAL SALES MANAGER

CIRCULATION
Teresa Cooper
MANAGER
Jamie Willett
ASSISTANT
Cole Morrison
ASSISTANT

ART
Shane Bell
CREATIVE DIRECTOR
Michele Hall
GRAPHIC DESIGNER

CONTRIBUTING WRITERS
NICLAS ÅNMARK
THOMAS BJÖRK
ALFONSO FUENTES-AZNAR
IGNACIO GONZALEZ-PEREZ
JIM GRANN
DONALD JORDAN
JOHN MERCHANT
JIM OAKES
VIRGINIA OSTERMAN
HARISH K. PASAPULA
LEE M. ROTHLEUTNER
JACK TITUS

Media solutions

PUBLISHED BY MEDIA SOLUTIONS, INC.
P. O. BOX 1987 • PELHAM, AL 35124
(800) 366-2185 • (205) 380-1580 FAX

David C. Cooper
PRESIDENT
Chad Morrison
VICE PRESIDENT

Teresa Cooper
OPERATIONS

The Solution

ALD Thermal Treatment, Inc.

High Tech is our Business

ALD is a leader in vacuum process technology and Heat treatment services.

LEADERS IN THE CONTROL OF DISTORTION

+ Low Pressure Carburizing
+ High pressure gas quenching
+ Gas Nitriding
+ Ferritic Nitro-Carburizing
+ Plasma Carburizing
+ Normalizing
+ Hardening
+ Annealing
+ Brazing
+ Cryogenic Treatments
+ Engineering services and process development
+ Prototype and trials

Global Service Centers

- Limbach-Oberfrohna Germany
- Port Huron, Michigan USA
- Ramos Arizpe, Coahuila Mexico

www.aldtt.net

Enrique Lopez – Sales and Marketing
Email: sales@aldtt.net
Phone +1 (810) 357-0685

ALD Thermal Treatment, Inc.
2656 24th Street
Port Huron, MI 48060, USA

ALD is a subsidiary of AMG Advanced Metallurgical Group N.V.

Heavy Carbon Awarded Patent for Method of Carburizing

On January 10, 2017, the United States Patent and Trademark Office awarded patent number 9,540,721 to George Barbour, president of Heavy Carbon Company, for a method of carburizing, which allows a carburizing process in a furnace at high temperatures in a protective atmosphere. The primary function of this method of carburizing is soot control with an atmosphere flow providing a constant low CH4 to produce a strong reaction for a high-quality atmosphere regardless of carbon potential set point.

This new method carburizes at a carbon potential well into the soot range while maintaining a controllable carbon potential with a stable CH4. This stability maintains a constant reaction, cracking an air/gas mix in a self-heated retort to a temperature of 1,825°F before entry into the furnace. The high carbon potential penetrates the steel surface at a rate up to 30-percent faster, saving time and money while producing higher quality parts.

In addition to the speed at a higher carbon potential at high temperatures, the atmosphere will also penetrate lower grade steels at lower temperatures without using ammonia to raise the HRC. The air/gas mix is cracked in a retort outside the furnace to form the atmosphere and is heated at the same high temperature of 1,825°F before entry into the furnace. In this manner, the low furnace temperature does not hinder the reaction that must take place in the furnace.

Soot control takes place simultaneously while the carburizing cycle is in operation; therefore, no time is lost to clean soot from the furnace. Instead of using furnace time to remove soot and clean the furnace, loads can be run instead. Time is money, and soot burnout takes time. Because less time is required per load, less gas and power is used, resulting in more cost savings.

The Heavy Carbon Company manufactures the patented system, the Endocarb System. The Endocarb System can be added to existing furnaces or built into a furnace at the time of manufacture.

FOR MORE INFORMATION: heavycarbon.com

Vacuum Pump Services Corp. Appoints New President

Vacuum Pump Services Corp. (VPS), a new company established July 2016, has appointed Robert Sandora Sr. as president, effective February 2017. VPS is in Hatfield, Pennsylvania, and services general industry vacuum pumps of the Rotary vane, Piston, and Roots blower types for use with high vacuum chambers and vacuum heat-treating furnaces. The VPS market area is mid-Atlantic and nearby states.

"Bob will direct all operations of the new company: sales, repair services, testing, and field service," said William R. Jones, owner of VPS. "Bob has 40 years' experience in vacuum technology and has an excellent background to head our new company."

FOR MORE INFORMATION: vacpumpservices.com

Premier Furnace/BeaverMatic Manufactures a Double-Pallet Forge Furnace for a Major Aerospace Supplier

An existing Premier Furnace/BeaverMatic customer purchased its first double-pallet forge furnace. The furnace will be used for preheating and heat-treating rolled rings. It is capable of processing two 5.5 feet (1.68 meters) wide by 5.5 feet (1.68 meters) deep by 2.75 feet (0.838 meters) high workloads with a gross weight of 9,000 pounds (4,086 kilograms) each.

The load is heated by five Kromschröder Ecomax pulse-fired self-recuperative burners. A forced convection system results in ±20°F with temperature capabilities of up to 2,150°F. A Honeywell

˜ ° ¸″″ controls and monitors the temperature process of the fur˙nace^ ˇ he ˇ L° will also allow the operator to program multiple temperature ramp rates and set points via input from one type N thermocouple assembly mounted to the rear wall^ ˇ he furnace is insulated with energy˙efficient materials to maintain a reasonable cold˙face temperature and minimize heat loss while operating at normal process parameters^ A custom˙designed door and guide system allow for an efficient and repeatable seal^

ˇ remier Furnace/BeaverMatic manufactures standard and cus˙tom, batch and continuous equipment used worldwide in the commercial heat˙treating, aerospace, automotive, fastener, gear, tool, mining, military, and power˙generation industries^ It has recently manufactured a wide range of gas˙fired and electrically heated furnaces of various sizes and types^ ˇ remier Furnace/BeaverMatic offers world˙class furnace capabilities with simplified yet sophisticated designs^

FOR MORE INFORMATION: premierfurnace.com

Baker Furnace Moves to New Facility in California

Baker Furnace has announced the relocation of its facility to Brea, ° alifornia^ ˇ he new 4″,″″ ˙square˙foot building will allow the com˙pany to continue its commitment to excellence, quality, and crafts˙manship in the engineering, design, and manufacturing of custom˙built industrial ovens, furnaces, and pollution˙control equipment^

It has also invested in new equipment, which will allow for the most accurate, high˙quality, and timely production of its custom industrial ovens^

Along with physical growth, it has also doubled the size of its dedicated team of employees^ As a leader in the industry and equip˙ment customization, the company says it is committed to meeting client needs no matter the scale of complexity of the project^

Baker Furnace is owned by ˇ hermal ˇ roduct olutions (ˇ ˇ), a leading American manufacturer of custom industrial ovens used for heat treating, finishing, drying, curing, manufacturing automation, and process control^

FOR MORE INFORMATION: thermalproductsolutions.com

PWR Performance Products Installs Controlled Atmosphere Brazing at Its U.S. Racing Facility

xpanding its plant capacity, ˇ WR ˇ erformance ˇ roducts adds a eco/Warwick ° ontrolled Atmosphere Brazing (° AB) ystem to manufacturer high˙performance aluminum heat exchangers^

“ˇ he addition of this equipment is an important step in ˇ WR ˇ erformance ˇ roducts’s global strategy to expand our reach into the North American market with the new ° &R Racing technology,” said Kees Weel, ° O and managing director at ˇ WR ˇ erformance ˇ roducts^ “We purchased our first eco/Warwick Brazing line 15 years ago for our facility in Australia as part of our overall manufacturing strategy to keep all operations in house for optimum quality control over all of our products^ ˇ he eco/Warwick brazing technology has operated with the reliable performance that we demand to produce high˙quality product^”

eco/Warwick will provide a complete ° AB manufacturing cell that will include an inline dry˙off oven and a radiation braze ° AB furnace system equipped with patented Accubraze† process control technology^ Installation is scheduled for the third quarter of “ ″1‘^

A Seco/Warwick Radiation CAB System is an ideal method for brazing similar-size products in a continuous flow environment. The furnace is designed to use a stainless steel muffle to contain the nitrogen atmosphere and provide uniform heating of the products. The heat input into the furnace chamber is proportionally controlled to heat the muffle, which, in turn, heats the products. Product results are consistently high, and fully automated material handling provides maximum efficiency with minimal operator intervention.

FOR MORE INFORMATION: secowarwick.com

Lindberg/MPH Ships Atmosphere Box Furnace for Research and Development

The maximum temperature rating for this furnace is 1,100°C and has a work chamber of 36" W x 48" D x 36" H making it ideal for heat treating a variety of part sizes. The atmosphere box furnace has a wide temperature range of 760°C to 1,100°C. The heat-treating furnace is constructed with mild steel construction and structural steel frame. A vacuum-formed ceramic fiber insulation is used for quick heat-up and low heat storage. A horizontal swing insulated plug door keeps the inner hot surface away from the operator when opening to charge or unload work. The programmable temperature controller is capable of running 50 programs with 500 segments. This capability allows the operator to set specific programs for the different parts that will be processed.

"By designing the furnace with a wide temperature range, it provided the customer with the flexibility to process a variety of part sizes," said Jason Dobberstein, Lindberg/MPH sales manager.

Features of this Lindberg/MPH heat-treat furnace include:

- Vacuum-formed ceramic fiber modules with low heat storage for fast heat-up rates
- Prewired, side-mounted, forced air-cooled control console
- Programmable controller
- Vacuum-formed ceramic fiber insulation
- Horizontal swing insulated door plug
- Door limit switch
- Nitrogen atmosphere

This box furnace is CSA inspected and certified. All Lindberg/MPH equipment comes with an exclusive three-year warranty, which covers all materials for all components (less wear items).

FOR MORE INFORMATION: lindbergmph.com

Ipsen Shipped 25 Furnaces in Q4, Concluding a Record Year

Ipsen wrapped up a record year by shipping 25 furnaces during the last three months of 2016. With destinations in six countries and 13 states, this equipment will support the aerospace, automotive, commercial heat treating, medical, and MIM industries. Heat-treating systems ranged from a custom-built debinding and sintering furnace to a horizontal MetalMaster® vacuum furnace with a 20,000-pound (9,072 kilograms) load capacity.

Included among the shipments were an atmosphere washer and loader, as well as several H2- and H6-sized Titan® vacuum furnaces equipped with the PdMetrics® predictive maintenance software platform. This exclusive platform helps optimize equipment performance and minimize downtime. Other vacuum furnaces shipped included horizontal and vertical MetalMaster furnaces, Titan DS (debinding and sintering) furnaces, a VerticalTurbo, a Titan LT (low-temperature), a horizontal TurboTreater®, and an HEQ (horizontal external quench) from the VFS® product line.

To best support these industries, Ipsen's global ICS (Ipsen Customer Service) team facilitates system installations, as well as provides expert training, startup assistance, and 360-degree support throughout the entire life span of the equipment for any brand.

FOR MORE INFORMATION: ipsenusa.com

POWDERMET2017

2017 International Conference on Powder Metallurgy & Particulate Materials

June 13–16, 2017
The Bellagio • Las Vegas

TECHNICAL PROGRAM
Over 200 worldwide industry experts will present the latest in powder metallurgy and particulate materials.

TRADE EXHIBITION
Over 100 companies showcasing leading suppliers of powder metallurgy and particulate materials processing equipment, powders, and products.

SPECIAL CONFERENCE EVENTS
Including special guest speakers, awards luncheons, and evening networking events.

Held in conjunction with:

AM | PM
Additive Manufacturing | With Powder Metallurgy
June 13–15, 2017 | LAS VEGAS

POWDERMET2017.ORG

METAL POWDER INDUSTRIES FEDERATION
APMI INTERNATIONAL

Getting the Right Endothermic Gas Is Essential for Producing Quality Heat-Treated Parts.

By Jim Oakes

FURNACE ATMOSPHERES ARE CRITICAL TO meeting metallurgical specifications defined by control processes. The makeup of a furnace's atmosphere in the heat-treating process varies based upon the application. In the case of neutral and carbon-rich atmospheres, carrier gas is commonly supplied by an endothermic generator. The endothermic gas provides a non-oxidizing, reducing atmosphere capable of delivering this neutral or carbon-rich atmosphere.

A typical endothermic gas generator supplies an atmosphere using air and a hydrocarbon gas, which are mixed and passed over nickel-bearing catalyst at about 1,900°F. The composition of the endothermic gas will vary based on the component gases and ratios in the mixture. Once the endothermic gas is formed, the gas is cooled to maintain the integrity of the gas composition and delivered to heat-treating furnaces through a header system. Correct cooling of the gas is critical to preventing carbon monoxide from reversing into carbon (soot) and CO_2. The cooled gas then forms the basis of the atmosphere used in the heat-treating process. This atmosphere can be measured in a number of ways, most of which are controlled via dew point or an infrared gas analysis to determine the percentage of CO_2 in the gas.

The most common method of verifying this endothermic atmosphere is to use a dew point measuring device or an oxygen sensor. (Dew point is the temperature and pressure at which gas begins to condense into a liquid.) The dew point measurement is accomplished by taking a sample of the atmosphere after the cooling process previously described.

One such method uses an oxygen sensor to measure and control the dew point via a calculation in the dew point control instrument itself. This calculation uses the oxygen millivolts generated by the sensor, the hydrogen factor of the controlling instrument (using the assumption of the $\%H_2$ in the endothermic gas), and the temperature of the oxygen sensor. The temperature is required for the calculation, but the dew point of the gas is not temperature-dependent. Other direct-measure dew point analyzers typically consist of a capacitive measurement technology providing a voltage output to a controller for a reference to the dew point.

An NDIR three-gas analyzer also can be used to measure the atmosphere in a furnace or generator. The consistency of the endothermic gas produced at the generator significantly affects all downstream processes, and since an endo generator commonly produces gas for multiple furnaces, it is critical to get this process under control. In order for the furnace atmosphere to be controlled consistently and accurately with an in-situ oxygen sensor, it assumes a consis-

tent makeup of endothermic gas. For the endothermic generator gas, values should be 18.8-20.5 for CO, and CO_2 should be 0.25-0.50 with a preferred value of 0.40. When a generator is running properly, the dew point in Fahrenheit can be calculated by multiplying the CO_2 by 100.

If methane (CH_4) has a value of 0.50 or less, the generator is performing correctly. If the CH_4 is over 0.50, there may be a problem, and it is advisable to burn out the generator as quickly as the facility can take the generator offline. If after burnout the CH_4 climbs back above 0.5 within a week or two, then replacement of the catalyst should be considered. If the catalyst is depleted, uncracked CH_4 will be present. As a result, a low dew point (uncracked CH_4 is very dry) and an increase in the air ratio will occur. The end result will be a wet gas with soot and water coming out of the generator. Downstream, the furnace will try to compensate by adding more gas, likely creating an uncontrollable atmosphere, preventing the furnace from producing the proper metallurgical results for the parts being heat-treated.

Control parameters on an endothermic generator vary based on age of the equipment and, in some cases, the specifications a heat treater must comply with. Older generators may have only manual controls for the air-gas ratio without the ability to control dew point or CO_2. This can be a real challenge based on variations of the composition of air (humidity) and gas (spiking of CH_4 from the gas company). Generators can be retrofitted to support automatic control to create a consistent carrier gas.

The latest technology in endothermic generator controls goes beyond just evaluating the composition of the carrier gas. New and retrofitted endothermic generators use sophisticated flow loop algorithms to provide demand-based control of gas generators. Instead of burning off excess unused endothermic gas, these controls evaluate the demand required by the furnaces and automate the precise delivery of gas and air to the generator to provide furnaces with the proper amount of gas at the correct dew point. It provides a low-maintenance, reliable, and environmentally friendly endothermic gas, creating a foundation for producing quality heat-treated parts.

ABOUT THE AUTHOR: Jim Oakes is vice president of business development for Super Systems Inc., where he oversees marketing and growth in multiple business channels and helps develop product innovation strategies in conjunction with customer feedback. He has extensive experience working in the heat treating and software/IT industries. This article was co-authored by Matt Specter, also with Super Systems. For more information, email joakes@supersystems.com or go to www.supersystems.com.

There Can Be Risks Associated with Heat-Treating Vanadium Microalloyed Steels.

By Lee M. Rothleutner

COMBINING BOTH ALLOYING AND PROCESSING into a single strategy to achieve a desired level of performance sounds like a simple concept, but can be challenging to accomplish. The endless pursuit of cheaper, lighter materials with reduced processing that meet or exceed previous component performance can be costly. Continual improvement practices often exploit incremental cost or performance enhancements to stay competitive in the marketplace, but not without risk.

One conceivable scenario could be slightly modifying the material of an existing part to achieve slightly higher mechanical properties and, as a result, higher perceived performance. An example increasingly seen in literature is the use of vanadium microalloyed steels in conventional heat-treated or secondary processed (e.g., induction hardened) components. This column briefly examines some of the benefits, as well as the drawbacks, of vanadium microalloyed steels in such a scenario.

VANADIUM MICROALLOYED STEEL FORGINGS

One application that successfully improves cost savings through a coupled alloying and processing strategy is direct-cooled vanadium microalloyed steel forgings. Their improved strength and hardness over plain carbon ferrite-pearlite steels is a result of nanometer-sized vanadium carbides and nitrides that precipitate from austenite during the transformation to ferrite and pearlite upon cooling. These steels have been shown to perform comparably to quench and tempered martensitic steels in specific applications [1]. Although not necessarily suitable as a comprehensive replacement for quench and tempered steels, the immense cost savings that the direct-cooling concept gains through processing reduction by far offset the cost of the 0.1 wt. % vanadium alloying addition required to achieve design requirements.

Since their introduction, these steels have seen use in a variety of applications that deviate from their original direct-cooled process design, and sometimes with mixed success. Such applications include automotive power transmission shafts, quench and tempered springs, and heavy section forgings for the oil and gas industry [2]. Improvements in specific performance characteristics such as torsional load, torsional fatigue life, and tempering resistance have been observed, but so have detrimental effects such as reduced toughness and strength [2].

VANADIUM CARBIDE AND NITRIDE SOLUBILITY

Successful implementation of vanadium microalloying into any process relies on understanding the solubility of the vanadium carbides and nitrides, since their existence within the microstructure is the reason for its improved performance. Therefore, understanding how thermal processing can influence both precipitate size and distribution is critical in implementing vanadium microalloying as an alloying strategy. The solubility of microalloy carbides and nitrides is a complex subject on which entire book chapters have been written (see Gladman [3]), so it is introduced here only for awareness.

The derivation of a solubility product is thermodynamic; however, because these products are determined experimentally, it is challenging to completely negate kinetic effects. As a result, solubility products from literature are best used only as a first approximation. For the purpose of discussion, the solubility product for vanadium nitride (VN) in austenite is:

$$log_{10}[V][N] = 2.27 - \frac{7070}{T} \qquad \text{Equation 1}$$

where vanadium (V) and nitrogen (N) are in wt.%, and solubility temperature (T) is in Kelvin [3]. This equation can be used to determine a great deal of information, but the simplest and most useful value calculated from this equation is the approximate temperature, or solubility temperature, at which a compound may either precipitate from austenite upon cooling or dissolve in austenite upon heating. In the case of a steel that contains 0.10 wt. % V and 70 ppm N, the associated solubility temperature is 1,030°C (1,886°F); therefore, if the steel is to be thermally processed, doing so above the solubility temperature allows precipitation upon cooling to be maximized.

PERFORMANCE OF VANADIUM MICROALLOYED FERRITE-PEARLITE MICROSTRUCTURES

Vanadium microalloyed steels were specifically designed for applications requiring forged and direct-cooled ferrite-pearlite microstructures, so they also work well in the hot-rolled condition. The data in Figure 1 indicate that there are multiple alloy strategies for medium-carbon hot-rolled steels that achieve similar properties, including vanadium microalloying [4]. This emphasizes the point that each process is different and needs to be fully evaluated before implementing a change of this magnitude.

One case in which vanadium may significantly reduce the performance of ferrite-pearlite medium-carbon steels is after a normalizing heat treatment. Normalizing is a common heat treatment used to refine grain size and promote a more homogenous microstructure. Applications requiring consistent performance, as well as reduced distortion and enhanced microstructural response during subsequent processing, can all benefit from normalizing [5].

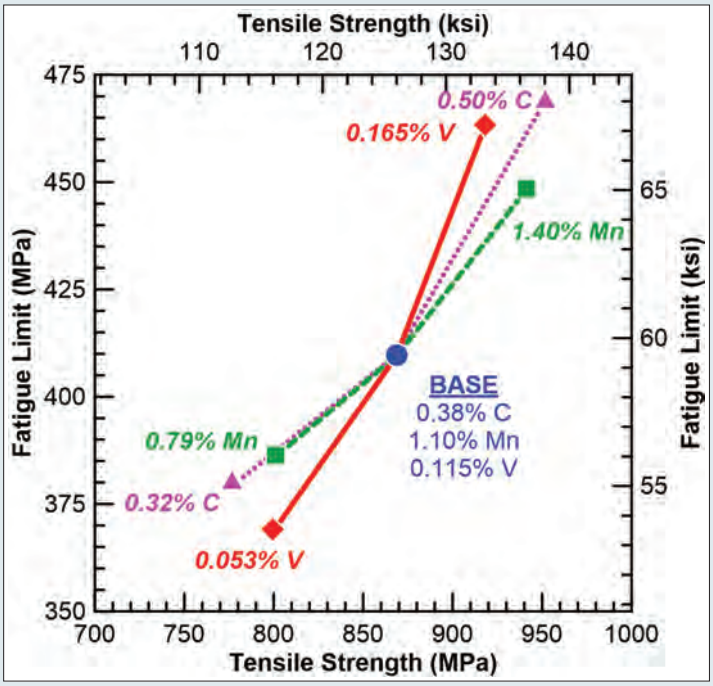

Figure 1: Influence of carbon (C), manganese (Mn), and vanadium (V) content on the strength of medium-carbon hot-rolled steels [4]

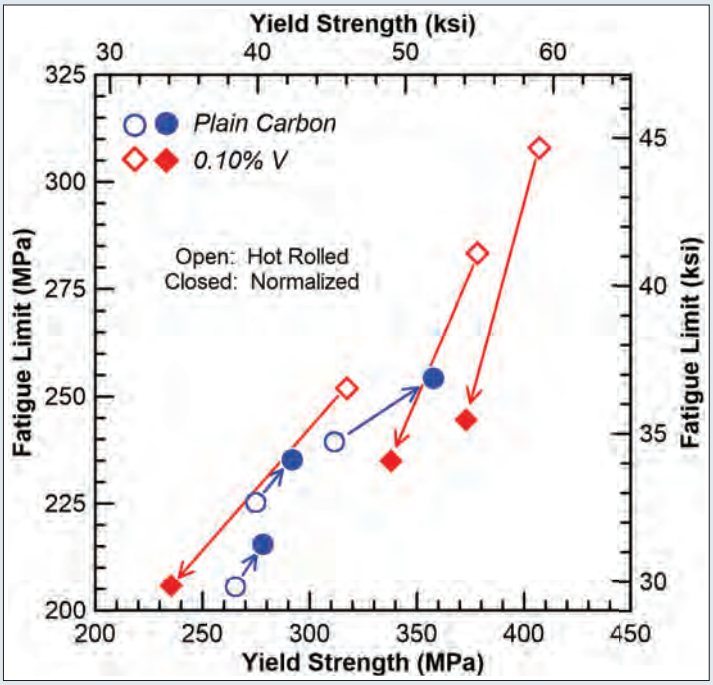

Figure 2: Influence of normalizing heat treatment on the fatigue limit and yield strength of hot-rolled plain carbon and vanadium microalloyed steels [6]

Figure 2 shows the effect a normalizing heat treatment can have on the yield strength and fatigue limit of hot-rolled plain carbon and vanadium microalloyed steels. In the hot-rolled condition, the vanadium microalloyed steels show superior yield strength and fatigue performance compared to plain carbon steels. After normalizing, the plain carbon steels' performance improves slightly, while the vanadium microalloyed steels' performance decreases sharply — the reduction in their yield strength being the most notable. One hypothesis for this decrease in the vanadium steel properties is that because the normalizing temperature is below the solubility temperature, the carbides/nitrides coarsen appreciably, making them ineffective in precipitation strengthening the steel.

CONCLUSION

Ultimately, understanding the complete processing of the material from steel supplier through final machining is the foundation for optimizing properties and minimizing costs. Direct-cooled vanadium microalloyed steels for forging applications are an excellent example of a coupled alloy processing strategy that reduces costs without sacrificing specific performance requirements. This article is a glimpse into the complexities involved in selecting the best material for an application.

REFERENCES

1. G. Krauss, Steels – Processing, Structure, and Performance, ed. 2, ASM International, Materials Park, OH, 2015.
2. L.M. Rothleutner, C.J. Van Tyne, R.J. Glodowski, J.G. Speer, and D.K. Matlock, "Contributions of Vanadium to Properties of Heat Treated Medium Carbon Forging Steels." In HSLA Steels 2015, Microalloying 2015 & Offshore Engineering Steels 2015: Conference Proceedings, John Wiley & Sons, Inc., pp. 419-425, 2015.
3. T. Gladman, Physical Metallurgy of Microalloyed Steels, Institute of Materials, 1997.
4. I. Nomura, "Influences of Microstructures of Fatigue Strength of Medium Carbon Microalloyed Steels," Tetsu-to-Hagane (J. Iron Steel Inst. Jpn.), vol. 83, no. 3, pp. 227-232, 1997.
5. D. Herring, "Metal Urgency – Compelling Reasons Normalizing Produces High Quality Gears," Thermal Processing for Gear Solutions, pp. 16-17, Nov. 2012.
6. T. Abe, T. Sampi, H. Osuzu, and I. Kozasu, "Quantitative Correlation of Static Strengthening Mechanisms to Fatigue Property in Low and Medium Carbon Steels," Tetsu-to-Hagane (J. Iron Steel Inst. Jpn.), vol. 70, no. 10, pp. 1459-1466, 1984.

ABOUT THE AUTHOR: Lee Rothleutner is a principal development engineer with The Timken Company. He received his Ph.D. in Metallurgical and Materials Engineering from the Colorado School of Mines. His research experience includes microstructural evolution during induction hardening, torsional fatigue, and vanadium microalloying. Rothleutner serves on the Heat Treating Society Membership Committee and is a veteran of the U.S. Coast Guard. He can be reached at lee.rothleutner@timken.com.

Ingenuity Can Often Negate Murphy's Law.

By Jack Titus

A FEW DECADES AGO, MY INVOLVEMENT WITH depleted uranium (DU) began in the metallurgical R&D department, developing program logic to heat treat DU in a two-chamber vacuum furnace with a water quench. (DU is a byproduct of the production of enriched uranium for fuel in nuclear reactors and in the manufacture of nuclear weapons. It's the primary penetrator material for armor piercing anti-tank projectiles.)

The furnace system that existed employed an oil quench. In 1974, the 1968 vintage 24" x 36" x 24" (600 mm x 900 mm x 600 mm) furnace hot zone was insulated with ceramic fiber and moly (molybdenum) sheet hot face, and it had graphite tube friction fit heating elements. The as-built hearth (load transfer system) was made from U-shaped moly structural members. At that time, moly was a relatively new vacuum furnace material, except for hot face sheathing and heating elements, so the hearth was purchased from Austria where moly usage was much more advanced. Likewise, graphite, except for heating elements, was not yet used in any significant quantity as a structural component. Maximum furnace load was about 800 pounds (363 kilograms), and the quench tank held approximately 800 gallons (3,028 liters) of oil (water).

This DU heat-treat process consisted of evacuation, heat and soak, backfill with nitrogen, transfer, and water quench. In addition, the load of DU bars had to descend slowly into the water quench, easily achieved with the hydraulically driven elevator, as was the inner door separating the hot zone from the vestibule.

Several months after the furnace was commissioned in R&D, there were a few relay logic and limit switch issues that continued to give us intermittent problems. While running a test load of, I believe, high speed steel, probably M2, the inner door began closing as the moly hearth was returning to the 2,200°F (1,204°C) hot zone from the quench chamber. Holding our breath, our worst fears were realized as we opened the furnace maintenance door after cooling the hot zone: the moly hearth was bent directly in the center across the three longitudinal support beams. Purchasing another moly hearth from Austria was out of the question. We made a two-prong decision: attempt to straighten the hearth and begin development of a graphite hearth. Straightening the complex eight-part moly hearth looked like an impossible task.

Moly — at that time in its development — became brittle (not doped to improve ductility) at room temperature after being heated above about 1,500°F (815°C). We knew in order to straighten the moly, we'd have to heat the entire assembly to at least 1,200°F (648°C) and probably as high as 1,500°F (815°C). The problem became how to do it.

Fortunately, another R&D department was working on automobile tire pyrolyzing and had a high-temperature low-profile horizontal hot chamber we could use. After that, the next issue became: How do we remove the hot assembly from the furnace and apply force to straighten the beams without the moly, which has high thermal conductivity, losing too much heat and cracking? Excess oxidation of the moly was also a concern, but we felt the moly would not be exposed to air in the furnace long enough to affect its strength. We wrapped the entire eight-member hearth in 2 inches of ceramic fiber to retain as much heat as possible. My cohort JGC and I donned fires suits so we could get as close as possible and manhandle the assembly hanging from a jib crane. Using a portable gantry-mounted hydraulic cylinder attached to a horizontal beam, we successfully straightened the hearth. It wasn't pretty, but it was reinstalled in the vacuum furnace and ran successfully for several months until the graphite hearth was developed.

Several months after installing the new graphite hearth, the DU arrived at our lab in the afternoon several hours later than expected. By then, we had removed the quench oil, cleaned the quench tank, added water, and were ready for the DU tests. Before unloading the DU from the truck, we were given radiation badges and gloves to handle the DU bars. DU is very dense. A cubic foot of steel weighs 490 pounds; DU weighs 1,192 pounds per cubic foot. Each 1.5-inch-diameter x 20-inch-long DU bar weighed about 24 pounds.

The DU bars were loaded vertically in fixtures and placed on the elevator in the two-chamber vestibule. We opened the inner door via pushbutton and enabled the hearth to drive from the cold hot zone into the vestibule where the elevator forks lowered the DU onto the hearth, then enabled the hearth to drive back into the hot zone. When moving back to the hot zone, we noticed that the hearth sounded different. We moved the hearth back to the vestibule for inspection and discovered a cracked graphite cross beam. We unloaded the DU and proceeded to replace the cross beam. After an hour or two, the hearth was again ready. After the DU technicians left that late evening, the hearth was moved several times back-and-forth from vestibule to hot zone to confirm that all worked as expected for tests the following day.

Then it happened — for reasons I cannot explain to this day, I manually enabled the elevator to lower into the quench (without limit switch stops via the elevator hydraulic valve over-ride), not realizing that the hearth was in the vestibule. The elevator forks lowered right through four of the five graphite cross beams. After all these years, I can still hear that sound of graphite beams being crushed. Luckily, the one intact beam kept the broken beams from falling into the water quench. Needless to say, that was a long night cutting new hearth beams with a DoAll vertical band saw from a slab of graphite. But the next morning, we did successfully conduct the tests. And upon leaving, the DU technicians asked for our radiation badges, explaining that they were for our own peace of mind as gamma ray badges would not detect the weaker alpha radiation from the primary emitter from DU.

Next is an incident that won't be soon forgotten by the engineers associated with it, even though it happened a few decades ago involving the solution portion of a solution-and-age pusher system for 7000 series aluminum ogive portions of an artillery round.

The 6-inch-diameter by 2-inch-thick parts were loaded on edge in rod frame alloy baskets located on 30-square-inch alloy trays in a single-row pusher furnace about 30 feet long. There were maybe 56 parts in a

basket. During startup, temperature uniformity tests revealed non-uniformity in portions of the furnace. After cooling the furnace, an engineer proceeded to work his way through the furnace, adjusting directional baffles to redirect air to the cold areas of the zones. Startup and dry-out again continued without any problems. Production commenced after proving that the temperature uniformity had improved.

As time passed, no one at first realized that the rod frame baskets exiting the solution furnace were empty. Then, as more attention was payed to the push schedule, it was discovered that parts should have been coming out of the furnace long ago, but no parts were coming out. The baskets were empty. Again, after cooling the furnace, inspection revealed that all of the production parts entering the furnace were lying in puddles on the furnace floor. So what happened? As the engineer was adjusting baffles inside the solution furnace, he would hit his head on thermocouples protruding from the refractory walls, pushing them all in so he wouldn't break the protection tubes, but he forgot to reposition them when he finished with the adjustments. Since the thermocouples were now positioned in the refractory wall, they could not sense the true zone temperature and caused the controllers to overheat and melt the aluminum as they passed through the furnace.

Lastly, this episode involves an atmosphere box carburizing furnace. Commissioning had been proceeding successfully until it was time for refractory dry-out. The startup engineer began the normal step-up heating procedure. Periodically, he would open the furnace door to visually check for any abnormalities. During an inspection after lunch, he noticed that the horizontally mounted radiant tubes had mysteriously grown, pushing the burners away from the furnace case so much so that he could see red heat where the tubes entered the sidewalls. This was not normal. Opening the furnace door, he was blasted with white heat way above the 1,750°F (954°C) he expected. There were no electrical or high-limit failures since the high limit was set to 50°F (10°C) above the set point at 1,800°F (982°C) and the controller did indicate 1,750°F.

After an exhaustive investigation, it was discovered that the control and high-limit thermocouples were type K as required, but the temperature controller and high-limit instruments were configured for type J. When the type K furnace thermocouple reached 1,750°F equaling 39.5 millivolts, the type J controller set for 1,750°F only indicated 1,303°F. The type J controller continued calling for heat to reach the 55.2 millivolts corresponding to 1,750°F. When the type J controller finally reached 1,750°F, the furnace was over 2,500°F (1,371°C), well above the melting point of the radiant tubes, roof fan, and alloy work support.

ABOUT THE AUTHOR: Jack Titus can be reached at (248) 668-4040 or jtitus@afc-holcroft.com. Go to www.afc-holcroft.com.

Understanding Linear Leak Rates and Common Causes of Leaks in Vacuum Furnaces Can Save Valuable Production Time.

By Jim Grann

THE PROCESS OF FINDING LEAKS IN YOUR vacuum heat-treating system can sometimes be a lengthy process. However, a deeper understanding of best practices for finding and correcting leaks can go a long way in simplifying the process.

While one of the more common ways to perform a leak check is with a helium mass spectrometer, there is also the rate of rise test, commonly known as the CDE (clean, dry, empty) linear leak rate. This comes later, when you want to know the rate of rise, or the true linear leak rate, of your vacuum furnace. To determine the true linear leak rate, you should:

1. Pump the furnace down.
2. Let it sit for a predetermined amount of time (depending on the temperature of the furnace and the processes you are running).
3. Stop the process cycle, which separates the vacuum pumping system from the furnace.
4. Watch the rate of rise over a one-hour time period.

However, this is an area where some people often fail their mandated leak rate. This is because you do not necessarily obtain a true linear leak rate in a one-hour time sample since no one can truly ascertain linearity from one sample. Rather, you need to take multiple samples.

For example, you require a leak rate of 5 microns per hour or less. If you pump the vacuum furnace down to 1 micron, shut it off, and come back in an hour to find it has gone up to 8 microns, then the leak rate is 7 microns/hour. If you look at just this sample, you would fail your mandated leak rate.

Looking at the same situation again, you come back in one hour to find the leak rate is 7 microns/hour. Instead of stopping at that point, though, you let it sit for another hour because, if it is truly linear, it will double (go up by 7 microns) in another hour. Then you could say it is linear and it fails. However, if in that second hour, it instead goes from 8 to 10 microns, then you would divide 10 by two hours, and you would get a leak rate of 5 microns/hour, thus meeting your required leak rate.

So many people give up prematurely during this process, and they have to either leak-check the furnace again, run a cleanup cycle, or call maintenance. As a result, they end up losing a solid 24 hours of production time because they didn't let the furnace sit for one more hour. By letting it sit another hour, you can confirm either: (a) it was linear and truly leaking, or (b) it was not linear yet, but now it passes, and you are back in production after two hours rather than investing in 24 additional hours.

VACUUM VALVE TROUBLESHOOTING

If your leak rate is linear and fails, this is an indication that you might need to perform a leak check. One of the first things you should do is conduct a conventional leak check with a helium mass spectrometer. Sometimes, this is all you will need as you will quickly find the leak and be back to production.

However, it is also important to consider your vacuum valves as an extension of leaks because they can also cause issues with the furnace. There is truly nothing worse than opening up your vacuum furnace after you have run a load and your parts are blue or something other than bright and shiny. Valves (e.g., backfill valves, partial pressure valves, vacuum valves, and process gas valves) can leak between adjacent systems, which can then affect your leak rate, part colors, and quality in your vacuum furnace.

To validate the sealing condition of vacuum valves with no test equipment, you would do the following:

Main Valve

To check the O-ring seal integrity of the main valve, perform the following steps:

1. Pump down the vacuum chamber to 1,000 microns or less.
2. Press the Process Cycle Stop button to stop the pumping of the furnace.
3. Select the vacuum sensor tube that is reading the vacuum level of the diffusion pump. Normally, this will read somewhere in the range of 20 to 200 microns.
4. While you are watching the vacuum level in the diffusion pump, press the Chamber Release button.
5. As the inert gas enters the vacuum chamber, there should be no upward movement (loss in vacuum) in the diffusion pump's vacuum reading.
6. If the diffusion pump seems to be backfilling at the same rate as the chamber, there is a leak at the main valve dish seal.

Roughing Valve

To check the seal integrity of the roughing valve, perform the following steps:

1. Pump down the vacuum chamber to 1,000 microns or less.
2. Press the Process Cycle Stop button to stop the pumping of the furnace.
3. While the vacuum level in the main chamber begins to slowly climb, have someone stop the roughing pump and air release the roughing line.
4. As air enters the roughing line, there should be no upward change of rate (loss in vacuum) in the chamber vacuum reading.
5. If the chamber rapidly loses vacuum when you are venting the roughing lines, the roughing valve is leaking.

Foreline Valve

To check the seal integrity of the foreline valve, perform the following steps:

1. Pump down the vacuum chamber to 1,000 microns or less.
2. Press the Process Cycle Stop button to stop the pumping of the furnace.
3. Select the vacuum sensor tube that is reading the vacuum level of the diffusion pump. Normally, this will read somewhere in the range of 20 to 200 microns.
4. While you are watching the vacuum level in the diffusion pump, have someone turn off the roughing pump and air release the roughing lines.
5. As air enters the roughing lines, there should be no upward movement (loss in vacuum) in the diffusion pump's vacuum reading.
6. If the diffusion pump loses vacuum, the foreline valve is leaking.

Holding Valve

Typically, if the oil keeps disappearing from the holding pump and there are no signs of external oil leakage, the holding valve is leaking across its own seal, subsequently pulling the holding pump oil backwards into the diffusion pump.

While there is much more that goes into leak-checking — from knowing how to use and calibrate a helium mass spectrometer to locating inert gas leaks and understanding their causes and effects — being able to correctly determine your linear leak rate and troubleshoot possible causes can save you valuable production time.

You can learn more about finding leaks in your vacuum furnace at IpsenHarold.com.

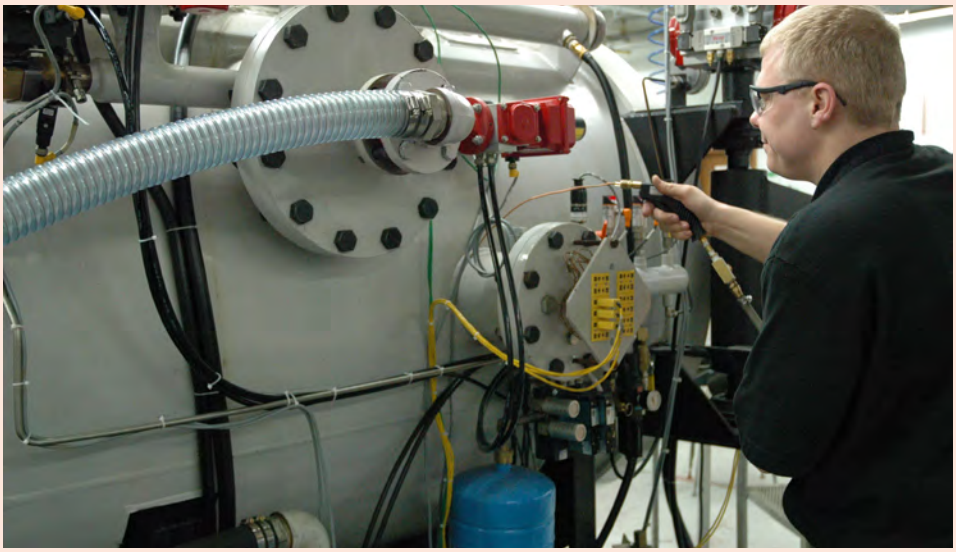

Figure 1: A helium mass spectrometer being used to leak-check a TITAN® vacuum heat-treating system

ABOUT THE AUTHOR: Jim Grann, Ipsen's senior technical manager, started with Ipsen in 1978, and since then, he has held roles in quality control, technical support, and Ipsen U instruction, among others. He is a technical expert who works with support services, furnace orders, inspections, and special processes. His 38 years of experience and interactions with customers around the world allow Grann to provide excellent solutions and support when troubleshooting furnace- and process-related issues.

Wisconsin Oven Corporation

By offering standard and custom-designed ovens to a wide spectrum of industries around the globe, Wisconsin Oven Corporation is a world-class supplier of thermal processing equipment.

By Kenneth Carter

MOST ORDINARY PEOPLE MAY NEVER REALIZE THE IMPACT Wisconsin Oven has on every aspect of their daily lives.

But from the time they pull themselves out of bed in the morning to the time they climb back into it at night, Wisconsin Oven probably has had a hand in almost everything they come in contact with.

Wisconsin Oven, owned by Thermal Product Solutions, was formed in 1973. It is a leading manufacturer of custom industrial ovens used for heat treating, finishing, drying, curing, heat treatment, and many others.

"We like to say you're never more than 10 feet away from something processed in a Wisconsin Oven," said Mike Grande, sales manager and senior application engineer for Wisconsin Oven Corporation.

But almost everything? Hyperbole, right?

Well, maybe not.

"You're lying on your mattress before you even get out of bed; we've supplied ovens to process millions of mattress springs," Grande said. "Every single fully assembled box spring and mattress before the cloth gets put on is tempered at 450 degrees for between 4 and 12 minutes. That gives the spring its springiness."

But that's just the start.

"You go get your clothes on, and in your closet, you grab a pair of pants, and if you wear non-wrinkle pants, the way that's done, it's processed in an oven," Grande said. "They take the fabric, and they embed a certain proprietary chemical in it. It's heated up, and it sets the fabric, so it's more resistant to wrinkles."

And that doorknob you twist to leave the house? It ended up in an oven, too.

"Doorknobs are usually covered with lacquer or some sort of coating, and those are processed in ovens," Grande said. "There's been millions of them processed through Wisconsin Ovens."

HUNDREDS OF USES

The hoses and pistons in a car engine. The interior of the car itself. Office ceiling tiles. Refrigerators. Washing machines. The list goes on. Hundreds of everyday items have seen the inside of a Wisconsin Oven product.

Wisconsin Oven, located in East Troy, Wisconsin, offers a variety of standard ovens that are pre-engineered, but it also has the ability to custom-design ovens for any application, according to Grande.

Its ovens are mostly electric or gas heated, but alternatives such as steam or oil are also available. The ambient temperatures possible with an oven range from about 100 degrees to 1,400 degrees Fahrenheit.

An oven's size can vary as well.

"Hundred-feet-plus long is not unusual as far as the longest dimension you might see," Grande said. "And the smaller ones are maybe as large as your refrigerator at home."

Many of the standard ovens offered by Wisconsin Oven are of the walk-in batch design.

"We sell a high volume of them," Grande said. "It's amazing how many people buy those things."

But when there's not a predesigned oven that can get the job done, Wisconsin Oven will design and construct one that will.

CUSTOM MADE

"We did one for a company that makes tanker trucks," Grande said. "After they weld all that steel to make the tank, they have to temper it, so it doesn't crack over time. The oven itself was 50 feet long to handle a 40-foot load, and it had a huge top load — kind of like a coffin — with a hinged top door. And the whole thing opens up, and they lower this tanker truck tank into the oven, close it up, and run it up to 1,200 degrees."

The oven ended up with a heating chamber 50 feet long, 13 feet wide, and 12 feet high.

"It took 40 weeks — close to a year — to design and build," he said. "And we had to achieve ±10 degrees Fahrenheit temperature uniformity."

Customers often require a tight temperature range in an oven. The tanker oven went through a lot of testing

and a lot of adjusting, according to Grande. The oven had to be certified at 40 points. In order to achieve that, thermocouple probes had to be installed at every 5-foot interval in the oven to verify the temperature stayed between 1,190 degrees and 1,210 degrees Fahrenheit.

"Uniformity is very important," Grande said. "That's what everyone wants — the aerospace, the automotive, the composite people, the wind-power people."

A recent oven designed and created for wind-turbine blades actually achieved a uniformity of ±1 degree Celsius, he said.

"It performed better than they expected," Grande said. "That's the kind of things that people are demanding these days, so we try to accommodate them."

OEM ROOTS

Wisconsin Oven's desire to offer the perfect product goes back to the company's roots where it initially served as an OEM manufacturer.

"We built ovens for other companies with their nameplate, and that was the core of our business for many years," Grande said.

As the years passed, Grande said people would see their ovens in the field with its customers' nameplates on them, and they would discover they were manufactured by Wisconsin Oven.

"We had set high standards, and we had to put good quality processes in place and have quality people, and that really got us off to a good start in the industry," he said.

And now, even the sky isn't a limit to Wisconsin Oven and its products.

AEROSPACE APPLICATIONS

"On the really exciting side, the composite manufacturers, the people who make rockets and aircraft, are really big into curing using ovens," Grande said. "So we manufacture some of the largest ovens in the world that are used for rocket parts."

A 40-foot rocket body with a 5-foot diameter has to be rolled into an oven. Those rockets use the latest technology in composite materials such as carbon fiber or Kevlar.

"Our customers are household names in the field of private space exploration," Grande said.

Those companies invest a lot of money into their products, and, because the parts such as rocket bodies are so expensive to make, they expect to reuse them. So the oven they commission from Wisconsin Oven need to perform flawlessly.

As an example, a part going into a huge oven larger than a building may cost $200,000, according to Grande.

"They spare no expense in making the oven top quality in every possible way to make sure they won't have a failure while they're processing their load, or it'll cost them $200,000," he said.

ADVANCED SYSTEMS

In making sure it is able to offer its customers the latest technological advances,

Wisconsin Oven is constantly updating and advancing its products.

A lot of that advancement is evident in the control systems that run the ovens.

"That's where the technology is getting more advanced," Grande said. "Our clients want more and more sophisticated controls. In the old days, it was kind of considered a new thing where a manufacturing engineer could sit at his desk and check the temperatures on his ovens and make sure they're operating properly from his PC. That's routine now."

Now, an oven's control system is connected by Ethernet to a company's network, according to Grande.

"It allows them to keep an eye on things, and if there's an alarm of some sort or if there's a failure or if something stops, they can get a message or an error signal sent directly to their computers, so they're not down for a long time," he said. "It's pretty common to have messages texted or emailed to the engineer, also."

And, of course, there's an app for that, too.

"The latest thing is there are apps where you can use your smartphone and monitor what's going on that way," Grande said.

Precision equipment and service has helped make a name for Wisconsin Oven in industries that include automotive, aerospace, building construction, plastics, medical, home appliances, weaponry, and military use.

ENERGY SECTOR

Wisconsin Oven products also are used in the oil and gas industry where coatings on the inside of oil pipes are cured to prevent corrosion and shipped all over the world.

The wind-energy industry also has a growing need for Wisconsin Oven.

"They use a lot of ovens to cure the wind-turbine components, heat treat the gearsets, and cure the blades," Grande said. "Last year, we sold 20 ovens for that industry."

Overall, Wisconsin Oven might ship more than 200 ovens a year of varying sizes, he said.

Much of that success is highlighted by a five-year warranty on its standard ovens, the longest in the business, according to Grande.

"We are able to back the equipment with a five-year warranty, which really blows everyone away," he said. "We found we don't lose money on it. Our ovens easily last a lot longer than five years. And it's very much appreciated by our customers. It allows us to impress upon them that we'll always be there for them."

FOR MORE INFORMATION: go to www.wisoven.com

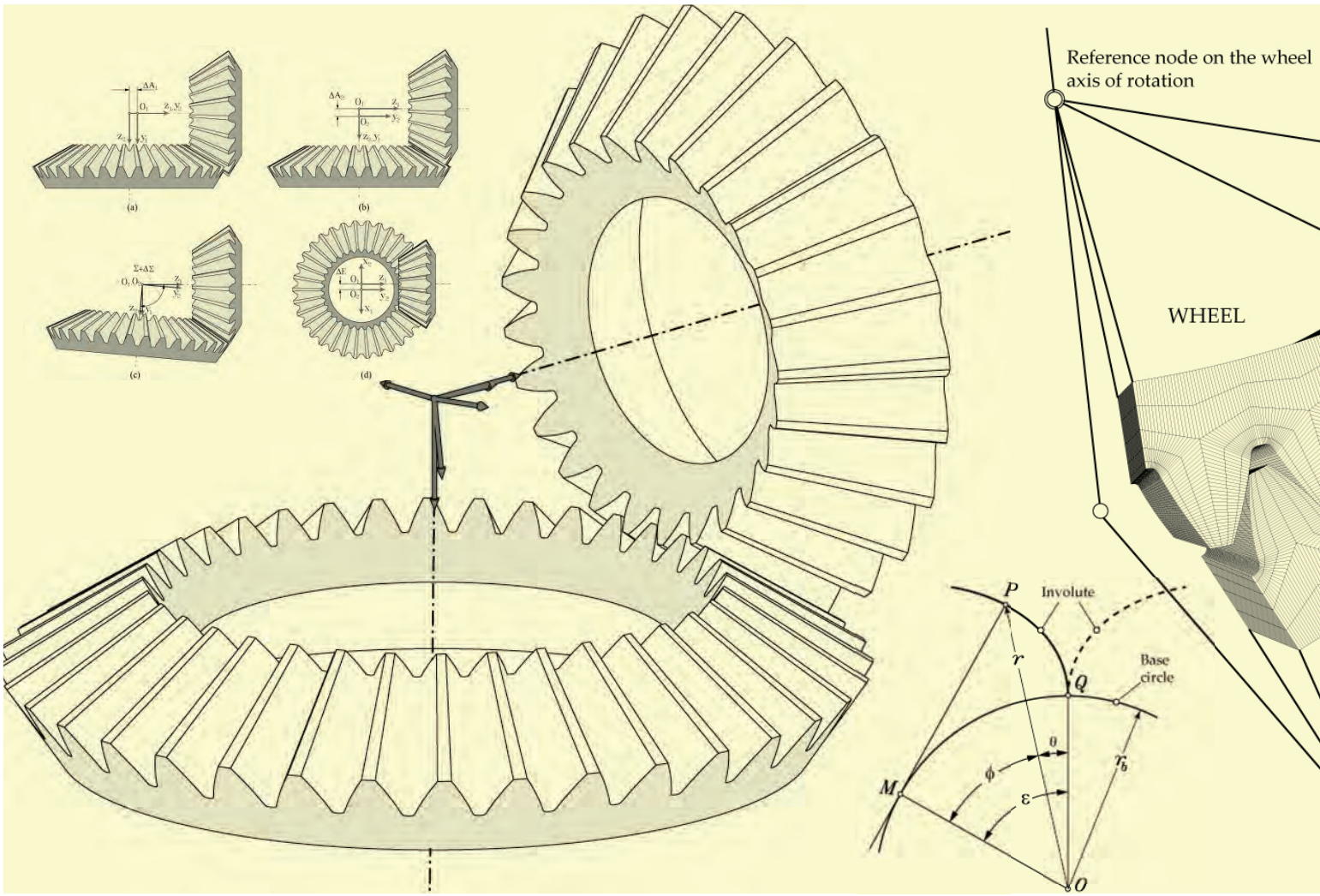

Computerized Design of Straight Bevel Gears with Optimized Profiles for Forging, Molding, or 3D Printing

By Alfonso Fuentes-Aznar, Ignacio Gonzalez-Perez, and Harish K. Pasapula

The computerized generation of straight bevel gears with spherical involute profiles is developed and the advantages of its application investigated. Possible microgeometry modifications of the gear tooth surfaces are proposed to provide stable contact patterns when errors of alignment occur.

Straight-tooth bevel gears are the simplest type of bevel gears that can be used for power transmission between intersecting shafts. They are commonly referred to as straight bevel gears, for brevity. Shafts for power transmission with straight bevel gears are usually mounted at a shaft angle of 90 degrees but can be designed to work at a wide range of shaft angles. They operate with efficiency around 98 percent or even better. They are widely applied in low-speed applications or static loading conditions [1]. The most traditional application of straight bevel gears is in differential drives in which the speed is low and the load type is mainly static.

Straight bevel gears are conical. Their teeth are tapered in both tooth thickness and tooth height [2]. In one end, the tooth height is large, while in the other end, it is small. These gears impose both radial and thrust loads on their bearings.

The great pioneer in the bevel gear field was William Gleason, founder of The Gleason Works in 1865. In 1874, William Gleason invented the first bevel gear planer. That

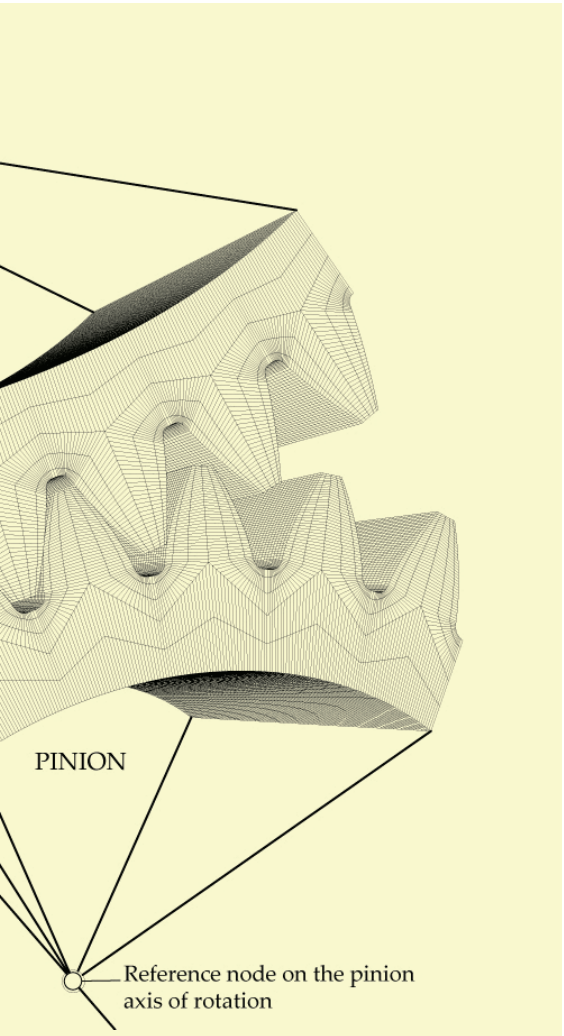

development was the first piece of technology that allowed the bevel gear industry to be created and opened vast new possibilities for the transmission of motive power. However, the first machines to cut straight bevel gears were difficult to set up and time-consuming while cutting gears [3]. Revacycle and Coniflex cutting methods were developed to improve the efficiency of manufacturing straight bevel gears.

Still, in many of today's applications of straight bevel gears, forging or molding manufacturers of bevel gears imitate cut surfaces of Coniflex and Revacycle gears, which is mainly a legacy of the time when forging manufacturers were trying to duplicate cut gears to prove that these gears can also be near-net forged or plastic molded [1]. However, there is no limitation on the geometry that those methods can use as objective geometries. These methods can use potentially any geometry for the gear tooth surfaces because molds are manufactured point by point. This fact opens new possibilities to look for new theoretical geometries for bevel gears.

The involute profile is the most commonly used tooth profile for cylindrical gears. However, for bevel gears, there is no standard reference profile. In this work, the spherical involute profile, considered the counterpart profile of the involute for bevel gears, will be derived and applied for straight-tooth bevel gears. The computerized generation of straight bevel gears with spherical involute profiles will be developed and the advantages of its application investigated. Spherical involute profiles might be applied for bevel gears manufactured by forging, molding, or 3D printing. The spherical involute profile is expected to give the best conditions of meshing and contact for straight bevel gears. Possible microgeometry modifications of the gear tooth surfaces also will be investigated in order to provide stable contact patterns when errors of alignment occur.

THE SPHERICAL INVOLUTE PROFILE

The parametric equations defining the spherical involute profile can be obtained by using two approaches: One is based on spherical trigonometry and will be referred to as the direct definition method. The other method is based on coordinate transformation and will be referred to as the indirect definition of the spherical involute profile.

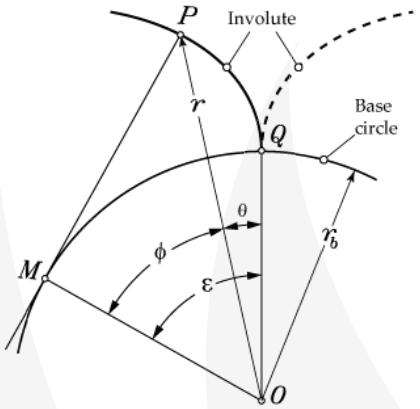

Figure 1: Basic definition of the planar involute profile

Direct Definition

The direct definition of the spherical involute is based on spherical trigonometry and follows the derivations proposed by Al-Daccak et al. [4] and Kolivand et al. [1]. Other works of reference are [5] and [6]. In [5], a practical application of the spherical involute surface to forged straight bevel gears is provided. In [6], the geometrical characteristics and kinematic behavior of spherical involute gears are explained.

The planar involute of a circle is defined as the curve traced by a point P on a taut chord that unwraps from a circle, constituting the base circle of the involute. Figure 1 shows the basic definition of the involute curve and its related design parameters. Point P in Figure 1 is a point of an involute curve traced while it unwraps from base circle of radius r_b. From Figure 1:

$$\tan\phi = \frac{\overline{MP}}{\overline{OM}} = \frac{\widehat{MQ}}{r_b} = \frac{r_b(\phi+\theta)}{r_b} = \phi + \theta \qquad \textbf{Equation 1}$$

so that:

$$\theta = \tan\phi - \phi \qquad \textbf{Equation 2}$$

Equation 2 is the fundamental equation for the planar involute curve. Angle θ is known as the involute polar angle. Angle ε in Figure 1 is the involute roll angle, which is the angle whose arc on the base circle of radius unity equals the tangent of angle ϕ at a selected point on the involute. For the planar involute, angle ϕ equals the pressure angle when point P lies on the pitch circle.

The spherical involute is the 3D counterpart of the planar involute of a circle. Similar to the definition of the planar involute, the spherical involute is defined as a 3D curve traced by a point P on a taut chord $\widehat{MP}$ unwrapping from base circle of radius r_b that lies on sphere S with origin at O_s and radius r_0 (see Figure 2). Point P in Figure 2 is a point of an involute curve traced while it unwraps from base circle of radius r_b, obtained as the intersection between the base cone and the sphere of radius r_0. The spherical involute is traced on the surface of the sphere S while point P unwraps over it from the base circle. Therefore, the arc length of the great circle $\widehat{MP}$ is equal to the arc length of base circle, which is $\widehat{MQ}$, and according to this:

$$r_0\varphi = r_b(\phi+\theta) = r_0\varepsilon\sin\gamma_b \qquad \textbf{Equation 3}$$

Here, similar to the definitions for the planar involute curve, angle θ is the involute polar angle, and angle ε = (ϕ + θ) is the involute roll angle. Simplifying Equation 3:

$$\varphi = \varepsilon\sin\gamma_b \qquad \textbf{Equation 4}$$

Considering again in Equation 4 that ε = (ϕ + θ), and solving for θ, we obtain:

$$\theta = \frac{\varphi}{\sin \gamma_b} - \phi$$ **Equation 5**

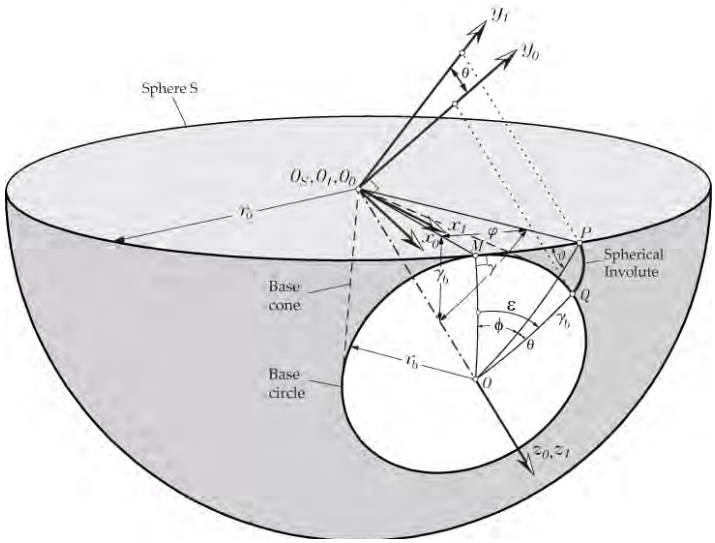

Figure 2: Schematic representation of the spherical involute

that can be considered as the function of the spherical involute. The following derivations will allow us to get angle φ as a function of angles γ_b and ϕ.

According to the principles of spherical trigonometry, arcs are represented by their angles [7]. Therefore, arcs $\widehat{MP}$, $\widehat{OM}$, and $\widehat{OP}$ can be represented by their angles φ, γ_b, and γ, respectively. By applying the law of cosines to the right spherical triangle *OMP* [7], the following relations can be derived:

$$\cos\ \gamma = \cos\varphi \cos\ \gamma_b + \sin\varphi \sin\gamma_b \cos 90° = \cos\varphi \cos\gamma_b$$ **Equation 6**

$$\cos\varphi = \cos\ \gamma_b \cos\gamma + \sin\gamma_b\ \sin\gamma \cos\phi$$ **Equation 7**

Similarly, by applying the spherical law of sine to the right angle spherical triangle *OMP* [7], additional relations can be obtained:

$$\frac{\sin\varphi}{\sin\phi} = \frac{\sin\gamma}{\sin 90^\circ} = \frac{\sin\gamma_b}{\sin\nu}$$ **Equation 8**

that yields the following equation for sin γ,

$$\sin\gamma = \frac{\sin\varphi}{\sin\phi}$$ **Equation 9**

Substituting for cos γ and sin γ in Equation 7, according to Equations 6 and 9, we obtain:

$$\cos\varphi = \cos\varphi \cos^2\gamma_b + \frac{\sin\gamma_b \sin\varphi}{\tan\phi}$$ **Equation 10**

Upon rearranging Equation 10 and collecting terms, we obtain the following equation for angle φ as a function of angles γ_b and ϕ, namely:

$$\tan\varphi = \sin\gamma_b \tan\phi$$ **Equation 11**

Using Equation 4 into Equation 11, we obtain:

$$\tan(\varepsilon \sin\gamma_b) = \sin\gamma_b \tan\phi$$ **Equation 12**

which can be considered the basic equation defining the spherical involute. If we substitute back ε = (ϕ + θ) and rearrange terms, we have:

$$\theta = \frac{\tan^{-1}(\sin\gamma_b \tan\phi)}{\sin\gamma_b} - \phi$$ **Equation 13**

Equation 13, similarly to Equation 5, represents the spherical involute function, relating the polar angle θ with the azimuthal angle ϕ of point *P* by means of the base cone angle γ_b. This equation shows similarity with Equation 2, which defines the planar involute function.

In order to get the curve traced by point *P* on the reference sphere, the coordinates of point *P* are needed. The coordinates of point *P* in coordinate system S_1 (x_1, y_1, z_1) can be derived as a function of angle γ (see Figure 2). Taking the tangent of both terms of Equation 4, we have:

$$\tan\varphi = \tan(\varepsilon \sin\gamma_b)$$ **Equation 14**

The tangent of φ can be obtained by using the values of sin φ and cos φ from Equations 9 and 6, namely:

$$\sin\varphi = \sin\gamma \sin\phi$$ **Equation 15**

$$\cos\varphi = \frac{\cos\gamma}{\cos\gamma_b}$$ **Equation 16**

so that:

$$\tan\varphi = \frac{\sin\varphi}{\cos\varphi} = \frac{\sin\gamma \sin\phi \cos\gamma_b}{\cos\gamma} = \tan\gamma \sin\phi \cos\gamma_b$$ **Equation 17**

Equalizing Equations 14 and 17, the following equation can be obtained:

$$\tan\gamma = \frac{\tan[(\theta+\phi)\sin\gamma_b]}{\sin\phi \cos\gamma_b}$$ **Equation 18**

Position vector of point *P* in coordinate system S_1 (x_1, y_1, z_1) (Figure 2) is given by:

$$\mathbf{r}_1^{(P)} = \begin{bmatrix} 0 \\ r_0 \sin\gamma \\ r_0 \cos\gamma \\ 1 \end{bmatrix}$$ **Equation 19**

The whole spherical involute profile can be drawn in coordinate system S_o (x_o, y_o, z_o) by rotating coordinate system S_1 (x_1, y_1, z_1), around axis z_1 in clockwise direction an angle θ (Figure 2), so that:

$$\mathbf{r}_0^{(P)} = \begin{bmatrix} -r_0 \sin\gamma \sin\theta \\ r_0 \sin\gamma \cos\theta \\ r_0 \cos\gamma \\ 1 \end{bmatrix}$$ **Equation 20**

Equation 20 will represent the right side profile of the straight bevel gear tooth surface. The left side profile of the straight bevel gear tooth surface can be obtained by rotating coordinate system S_1 (x_1, y_1, z_1), around axis z_1 in counterclockwise direction an angle θ, namely:

$$\mathbf{r}_0^{(P)} = \begin{bmatrix} r_0 \sin\gamma \sin\theta \\ r_0 \sin\gamma \cos\theta \\ r_0 \cos\gamma \\ 1 \end{bmatrix}$$ **Equation 21**

Indirect Definition

The indirect method is based on coordinate transformation and follows the works by Figliolini et al. [8] and Lee et al. [9]. By compar-

ing the direct and indirect approaches, a good insight view of both approaches is obtained.

Figure 3 shows the schematic representation of the generation of the spherical involute profile using the coordinate transformation method. A spherical involute curve can be traced by a point P of the great circle C of the fundamental sphere S during the pure-rolling motion of its disk plane Π on the base cone of the bevel gear (Figure 3). By using coordinate transformation from coordinate system $S_o(x_o, y_o, z_o)$, in which the point P is defined, to coordinate system $S_3(x_3, y_3, z_3)$ which axis y_3 is aligned with $\overline{OQ}$, where point Q represents the origin of the involute, lying on the base circle, the spherical involute profile can be obtained.

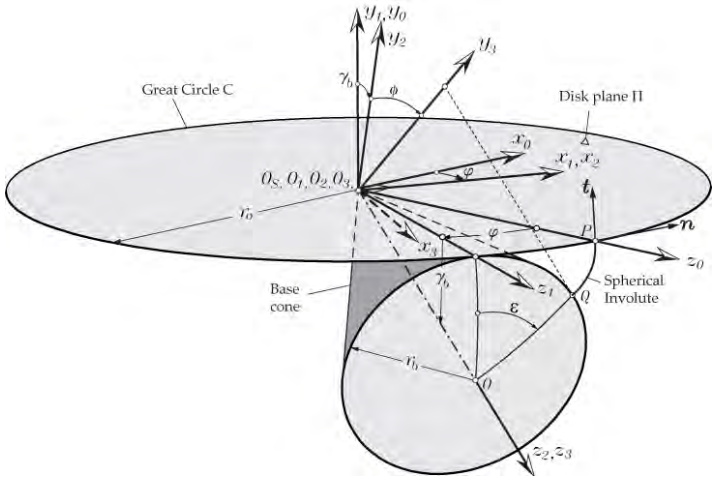

Figure 3: Schematic representation of the generation of the spherical involute profile using the coordinate transformation method

Point P is defined in coordinate system $S_o(x_o, y_o, z_o)$, which axis z_o passes through point P, as follows:

$$\mathbf{r}_0^{(P)} = \begin{bmatrix} 0 \\ 0 \\ r_0 \\ 1 \end{bmatrix} \qquad \textbf{Equation 22}$$

where:

r_0 is the radius of the sphere in which the spherical involute profile is going to be traced.

The coordinate transformation matrices from coordinate system $S_o(x_o, y_o, z_o)$ to coordinate system $S_3(x_3, y_3, z_3)$ are written in the following:

$$\mathbf{M}_{10}(\varphi) = \text{RotationCW}(y_0, \varphi) = \begin{pmatrix} \cos\varphi & 0 & \sin\varphi & 0 \\ 0 & 1 & 0 & 0 \\ -\sin\varphi & 0 & \cos\varphi & 0 \\ 0 & 0 & 0 & 1 \end{pmatrix} \qquad \textbf{Equation 23}$$

Notation "RotationCW(y_0,φ)" means that the transformation matrix corresponds to a rotation of the coordinate system in clockwise direction (CW) around axis y_0 an angle φ. Similarly:

$$\mathbf{M}_{21} = \text{RotationCCW}(x_1, \gamma_b) = \begin{pmatrix} 1 & 0 & 0 & 0 \\ 0 & \cos\gamma_b & \sin\gamma_b & 0 \\ 0 & -\sin\gamma_b & \cos\gamma_b & 0 \\ 0 & 0 & 0 & 1 \end{pmatrix} \qquad \textbf{Equation 24}$$

$$\mathbf{M}_{32}(\varepsilon) = \text{RotationCW}(z_2, \varepsilon) = \begin{pmatrix} \cos\varepsilon & -\sin\varepsilon & 0 & 0 \\ \sin\varepsilon & \cos\varepsilon & 0 & 0 \\ 0 & 0 & 1 & 0 \\ 0 & 0 & 0 & 1 \end{pmatrix} \qquad \textbf{Equation 25}$$

$$\mathbf{r}_3^{(P)}(\varepsilon, \varphi) = \mathbf{M}_{32}(\varepsilon)\mathbf{M}_{21}\mathbf{M}_{10}(\varphi)\mathbf{r}_0^{(P)} = \begin{pmatrix} r_0(\cos\varepsilon\sin\varphi - \sin\varepsilon\cos\varphi\sin\gamma_b) \\ r_0(\sin\varepsilon\sin\varphi + \cos\varepsilon\cos\varphi\sin\gamma_b) \\ r_0(\cos\varphi\cos\gamma_b) \\ 1 \end{pmatrix} \qquad \textbf{Equation 26}$$

By applying the fundamental equation for pure rolling of disk plane Π on the base cone, given by Equation 4, and written here again for clarity:

$$\varphi = \varepsilon \sin\gamma_b \qquad \textbf{Equation 27}$$

together with Equation 26, a point P on the involute will be perfectly defined in coordinate system $S_3(x_3, y_3, z_3)$ for any given angle ε. We recall that γ_b is the cone base angle that will be obtained directly from the initial design data. Equation 26 gives the coordinates of the right side of the spherical involute profile of the gear tooth surfaces at the sphere of radius r_0. To obtain the left side profile, Equations 23 to 25 should be modified accordingly.

Determination of the Normal Vector

One advantage of the indirect method of determination of the spherical involute is that the normal and tangent vectors to the tooth profile can be derived easily. Determination of the normal to the gear tooth surfaces will be needed to perform tooth contact analysis. Figure 3 shows the unit normal and unit tangent vectors in coordinate system S_0. The unit normal in coordinate system S_0 is given by:

$$\mathbf{n}_0^{(P)} = \begin{bmatrix} 1 \\ 0 \\ 0 \end{bmatrix} \qquad \textbf{Equation 28}$$

and the unit tangent vector to the spherical involute profile at point P:

$$\mathbf{t}_0^{(P)} = \begin{bmatrix} 0 \\ 1 \\ 0 \end{bmatrix} \qquad \textbf{Equation 29}$$

Normal and tangent vectors to the spherical involute profile in coordinate system $S_3(x_3, y_3, z_3)$ are obtained by:

$$\mathbf{n}_3^{(P)}(\varepsilon, \varphi) = \mathbf{L}_{32}(\psi)\mathbf{L}_{21}\mathbf{L}_{10}(\varphi)\mathbf{n}_0^{(P)} \qquad \textbf{Equation 30}$$

$$\mathbf{t}_3^{(P)}(\varepsilon, \varphi) = \mathbf{L}_{32}(\psi)\mathbf{L}_{21}\mathbf{L}_{10}(\varphi)\mathbf{t}_0^{(P)} \qquad \textbf{Equation 31}$$

We recall that angles ε and φ are related by Equation 27, representing the condition of pure rolling of disk plane Π on the base cone. Matrices L_{ij} are 3x3 submatrices of the corresponding matrix M_{ij}, obtained by eliminating the last row and the last column. This results from the fact that the vector components (projections on coordinate axes) do not depend on the location of the origin of the coordinate system [10].

DEFINITION OF THE SPHERICAL BEVEL GEAR TOOTH SURFACES

Gear Tooth Thickness

The tooth thickness t_p for the to-be-generated bevel gear is considered as given. The standard tooth thickness is obtained by considering

half of the angular pitch, namely:

$$t_p = \frac{\pi}{N} \qquad \text{Equation 32}$$

where:
N is the number of teeth of the gear.

The required backlash is considered modifying t_p accordingly. Figure 4 shows the additional coordinate transformation to obtain the involute profile in a coordinate system aligned with the center line of the gear tooth.

The transformation for the right side of the tooth profile is:

$$\mathbf{M}_{43} = \text{RotationCCW}(z_3, \xi_p) = \begin{pmatrix} \cos\xi_p & \sin\xi_p & 0 & 0 \\ -\sin\xi_p & \cos\xi_p & 0 & 0 \\ 0 & 0 & 1 & 0 \\ 0 & 0 & 0 & 1 \end{pmatrix} \qquad \text{Equation 33}$$

where:
ξ_p is equal to $(t_p/2)+\theta_p$ as shown in Figure 4.
Angle θ_p is the polar angle when point P lies on the pitch cone.

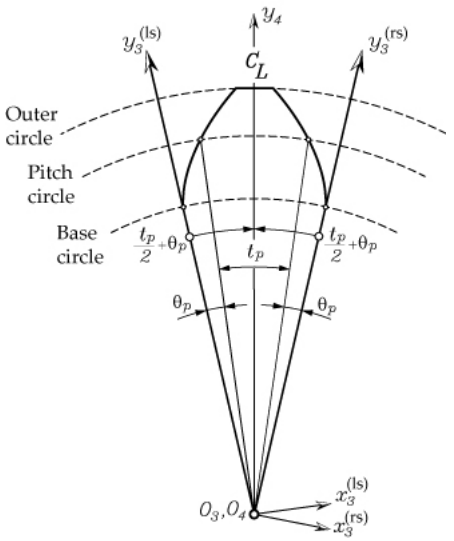

Figure 4: Toward determination of the bevel gear tooth thickness

Similarly, for the left side, the coordinate transformation will be:

$$\mathbf{M}_{43} = \text{RotationCW}(z_3, \xi_p) = \begin{pmatrix} \cos\xi_p & -\sin\xi_p & 0 & 0 \\ \sin\xi_p & \cos\xi_p & 0 & 0 \\ 0 & 0 & 1 & 0 \\ 0 & 0 & 0 & 1 \end{pmatrix} \qquad \text{Equation 34}$$

Determination of the Polar Angle at the Pitch Cone

The polar angle at the pitch cone, θ_p, can be determined by Equation 13, which expresses the polar angle θ as a function of angles γ_b and ϕ. For the planar involute profile, the azimuthal angle ϕ is equal to the pressure angle when P lies on the pitch cylinder. However, that statement cannot be extrapolated to the case of spherical gear when point P lies on the pitch cone. According to previous derivations (see Equation 11):

$$\tan\varphi = \sin\gamma_b \tan\phi \qquad \text{Equation 35}$$

Also, according to previous derivations (see Equation 17):

$$\tan\varphi = \tan\gamma \sin\phi \cos\gamma_b \qquad \text{Equation 36}$$

where $\gamma = \gamma_p$ and $\phi = \phi_p$ when P lies on the pitch cone. Equalizing the previous two equations:

$$\sin\gamma_b \tan\phi_p = \tan\gamma_p \sin\phi_p \cos\gamma_b \qquad \text{Equation 37}$$

$$\sin\gamma_b \frac{\sin\phi_p}{\cos\phi_p} = \tan\gamma_p \sin\phi_p \cos\gamma_b \qquad \text{Equation 38}$$

$$\frac{\sin\gamma_b}{\cos\phi_p} = \tan\gamma_p \cos\gamma_b \qquad \text{Equation 39}$$

$$\cos\phi_p = \frac{\tan\gamma_b}{\tan\gamma_p} \qquad \text{Equation 40}$$

Equation 40 allows the azimuthal angle ϕ_p for point P lying on the pitch cone to be determined as a function of the base cone angle γ_b and the pitch angle γ_p. Once the azimuthal ϕ_p is known, the polar angle at the pitch cone can be obtained by using Equation 13, written here again for clarity, wherein $\phi = \phi_p$.

$$\theta_p = \frac{\tan^{-1}(\sin\gamma_b \tan\phi_p)}{\sin\gamma_b} - \phi_p \qquad \text{Equation 41}$$

Determination of the Base Cone Angle

Figure 5 shows the pinion and the wheel of a spherical gear set in contact at point P_0 located at the pitch cone. Subindex 1 refers to the pinion, and subindex 2 refers to the wheel. However, the relations derived here are valid for pinion and wheel, and the corresponding subindexes will not be included. Applying the spherical law of sine to the right angle spherical triangle O_1MP_0 [7], the following relations can be obtained:

$$\frac{\sin\gamma_b}{\sin(90°-\alpha)} = \frac{\sin\gamma_p}{\sin 90°} \qquad \text{Equation 42}$$

Considering that $\sin(90°-\alpha) = \cos\alpha$ and $\sin 90° = 1$:

$$\sin\gamma_b = \cos\alpha \sin\gamma_p\,, \qquad \gamma_b = \sin^{-1}(\cos\alpha \sin\gamma_p) \qquad \text{Equation 43}$$

where α is the pressure angle.

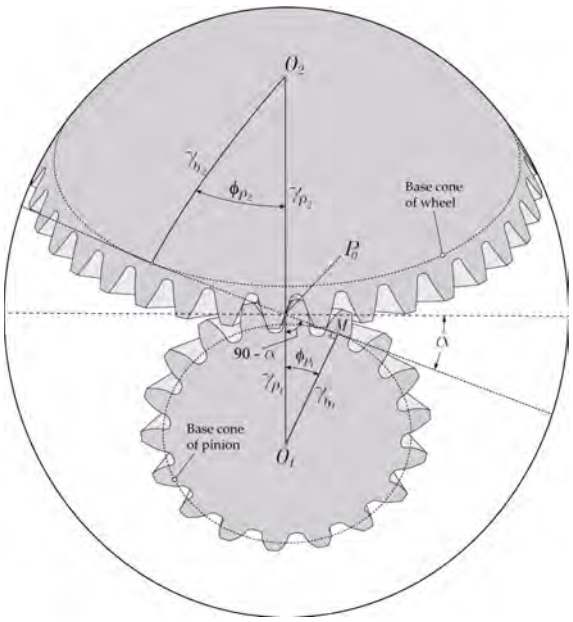

Figure 5: Toward determination of base cone angles

The Spherical Involute Bevel Gear Tooth Surfaces

Figure 6 shows the gear tooth surface generated from the spherical involute profile traced on the outer reference sphere. Points on the spherical involute profile are projected toward the center of the sphere, and in this way, the gear tooth surfaces are generated.

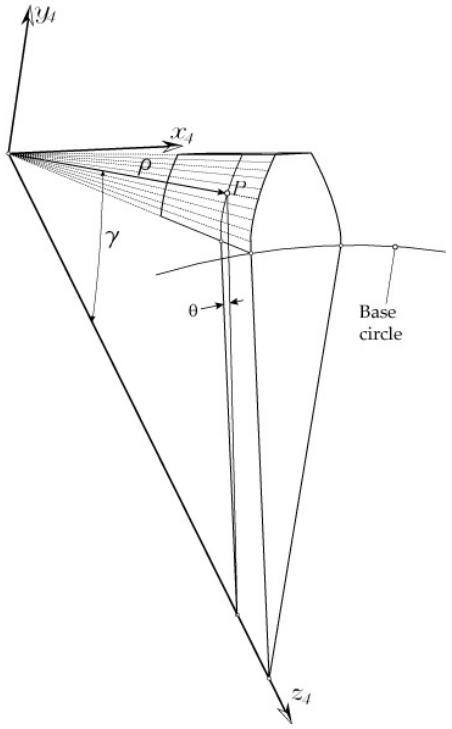

Figure 6: Gear tooth surface generated from the spherical involute profile at the outer reference sphere

The left side gear tooth surface, according to Equation 21, is given in terms of γ and θ as:

$$\mathbf{r}_0^{(P)} = \begin{bmatrix} \rho \sin\gamma \sin\theta \\ \rho \sin\gamma \cos\theta \\ \rho \cos\gamma \\ 1 \end{bmatrix} \qquad \textbf{Equation 44}$$

where:
ρ is the radius of the sphere in which the point lies
γ is the zenith angle that can be determined by Equation 18
Radius ρ will vary between the inner pitch cone distance A_i and the outer pitch cone distance A_0. The outer pitch cone distance is obtained from the pitch radius and pitch angle as:

$$A_0 = \frac{r_p}{\sin\gamma_p} = \frac{m\,N}{2\sin\gamma_p} \qquad \textbf{Equation 45}$$

where:
m is the module
N is the number of teeth
γ_p is the pitch angle of the gear
The inner cone distance A_i is obtained as:

$$A_i = A_0 - F_w \qquad \textbf{Equation 46}$$

where: F_w is the face width of the bevel gear, usually equal approximately to one-third of the outer pitch cone distance A_0.

Face and Root Cone Angles

For spherical involute straight bevel gears, the addendum and dedendum coefficients will be used for determination of the face and root cone angles. The addendum coefficient is denoted here as k_a and the dedendum coefficient as k_d. Those coefficients will determine the addendum and dedendum heights at the outer section of the gear tooth surface by multiplying those values by the module of the gear.

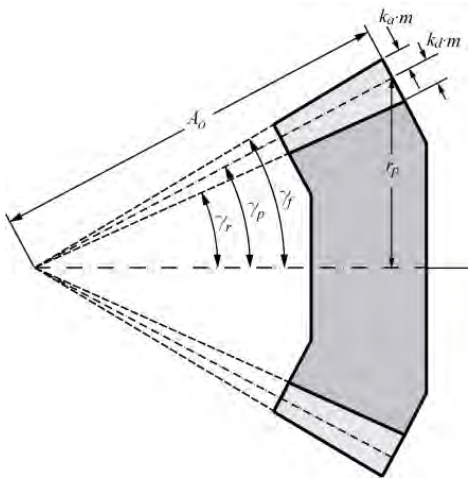

Figure 7: Toward determination of the addendum and dedendum angles

According to Figure 7, the face cone angle γ_f of the spherical involute bevel gear will be determined by:

$$\gamma_f = \gamma_p + \tan^{-1}\left(\frac{k_a m}{A_0}\right) = \gamma_p + \tan^{-1}\left(\frac{2k_a \sin\gamma_p}{N}\right) \qquad \textbf{Equation 47}$$

Similarly, the root cone angle γ_r is given by:

$$\gamma_r = \gamma_p - \tan^{-1}\left(\frac{k_d m}{A_0}\right) = \gamma_p - \tan^{-1}\left(\frac{2k_d \sin\gamma_p}{N}\right) \qquad \textbf{Equation 48}$$

where:
N is the number of teeth of the gear
γ_p is the pitch angle
k_a is the addendum coefficient, usually equal to 1
k_d is the dedendum coefficient, usually equal to 1.25

MODIFIED GEOMETRY FOR LOCALIZATION OF CONTACT

As mentioned before, the indirect definition of the spherical involute profile allows the gear tooth surfaces, their normal, and derivatives to be determined. Based on the indirect definition of the spherical involute profile, microgeometry modifications can be applied to the gear tooth surfaces for localization of contact and predesign of a parabolic function of transmission errors. The proposed gear tooth surface modification is based on changing angle φ in the coordinate transformation matrix given by Equation 23 by modified angle φ' as follows:

$$\varphi' = \varphi - a_p(\varphi - \varphi_p)^2 - a_l\left(\rho - A_0 + \frac{F_w}{2}\right)^2 \qquad \textbf{Equation 49}$$

where:
a_p is the parabola coefficient for profile crowning
a_l is the parabola coefficient for longitudinal crowning
Coefficient a_p influences the maximum level of transmission errors. Coefficient a_l influences the localization of contact. Algorithms to find those coefficients based on the desired level of transmission errors and percentage of face width for contact patterns might be implemented based, for example, on the secant method or the Newton-Raphson algorithm. In this way, those parameters will be determined according to the desired conditions of meshing and contact.

TOOTH CONTACT ANALYSIS OF SPHERICAL INVOLUTE BEVEL GEARS

Computerized simulation of meshing and contact is based on the application of an enhanced algorithm for tooth contact analysis (TCA) and directed to the determination of the contact pattern and function of transmission errors.

The proposed enhanced algorithm for TCA is based on a rigid body hypothesis of contact of mating surfaces. Consequently, no elastic tooth deformation is taken into account for contact pattern determination. Basically, contact path determination is based on the ideas presented in Sheveleva's work [11], according to which the relative position between pairs of contacting tooth surfaces is taken into account and the rotation of one of the members of the gear set is determined until contact is reached. Then, the contact pattern is determined, considering the locus of those points, which are positioned a relative distance between surfaces in contact given by a virtual marking compound thickness, usually equal to 0.0065 mm. Essentially, the described TCA algorithm is independent of the type of bearing contact between mating surfaces (point, line, or edge contact), does not require the solution of any system of nonlinear equations, and takes into account the effect of adjacent pairs of meshing teeth on the contact pattern.

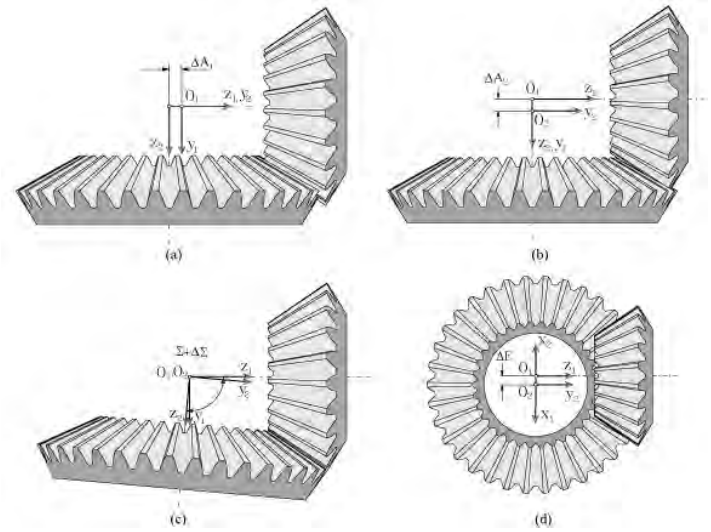

Figure 8: Errors of alignment for simulation of meshing and contact in spherical involute bevel gears: (a) axial displacement of the pinion ΔA_1, (b) axial displacement of the wheel ΔA_2, (c) shaft angle error $\Delta\Sigma$, and (d) minimum distance between axes ΔE

The errors of alignment considered for simulation of meshing and contact are:

- ΔA_1 as the axial displacement of the pinion (Figure 8a)
- ΔA_2 as the axial displacement of the wheel (Figure 8b)
- $\Delta\Sigma$ as the shaft angle error (Figure 8c)
- ΔE as the minimum distance between axes (Figure 8d)

FINITE ELEMENT ANALYSIS

The finite element method has been used to perform stress analysis. Finite element models comprising five pairs of contacting teeth have been employed to avoid influence of the boundary conditions on the results. The model size consists of 190610 elements and 232352 nodes. Figure 9 shows the finite element model of a spherical involute straight bevel gear set. Gear active tooth surfaces have been defined as master surfaces, while pinion active tooth surfaces have been defined as slave surfaces. Three-dimensional solid elements of type C3D8I [12] have been used, being hexahedral first-order elements enhanced by incompatible deformation modes in order to improve their bending behavior. Pinion and gear material is steel defined with an elastic modulus of 210 GPa and Poisson ratio of 0.3.

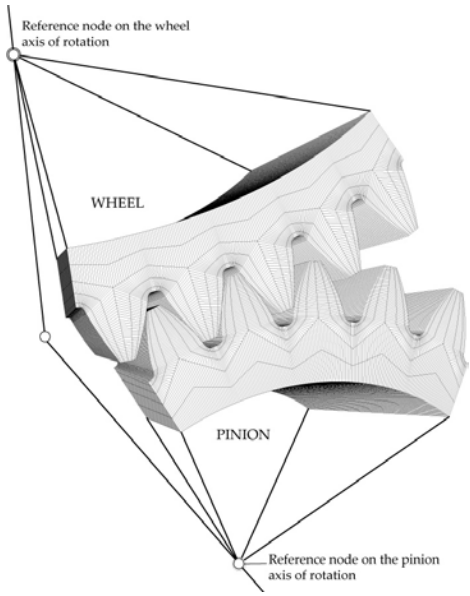

Figure 9: Finite element model of a spherical involute bevel gear with five pairs of contacting teeth

NUMERICAL EXAMPLE

Table 1 shows the general design parameters of a spherical straight bevel gear set that has been used for testing the proposed geometrical approach.

Firstly, Figure 10 shows the contact pattern and function of transmission errors for the case where pinion and gear are perfectly aligned. As expected, the contact pattern covers the whole active tooth surfaces of the pinion and gear, and there are no transmission errors. In this case, pinion and wheel are in lineal contact. This geometry is the perfect candidate for a plastic gear where the contact stresses have to be considerably reduced.

Parameter	[units]	Pinion	Wheel
Number of teeth, N		25	36
Module, m	mm	4	
Shaft angle, Σ	degrees	90	
Pressure angle, α	degrees	25	
Addendum coefficient, k_a		1.00	1.00
Dedendum coefficient, k_d		1.25	1.25
Face width, F_w	mm	29.2	29.2

Table 1: General design parameters of the analyzed spherical involute straight bevel gear

Bevel gear drives with intersecting axes are sensitive to changes of the minimum distance between axes ΔE. Figure 11 shows the contact pattern and function of transmission errors for the case where the minimum distance between the axis of the pinion and wheel pinion is ΔE = 0.075 mm. Although transmission errors are kept low, the contact pattern is shifted to the edge of the tooth surface profile, causing high contact stresses and contributing to the premature failure of the gear drive.

Figure 12 shows the bevel gear drive under an error of alignment $\Delta\Sigma$ =2 degrees, which is a huge error for a gear drive, and Figure 13 shows the contact pattern and function of transmission errors for this case. As shown in Figure 13, the gear drive keeps the lineal contact between pinion and wheel tooth surfaces, and the function of transmission errors is kept equal to zero. Similar to the case of involute cylindrical gears that are not sensitive to center distance error, spherical involute

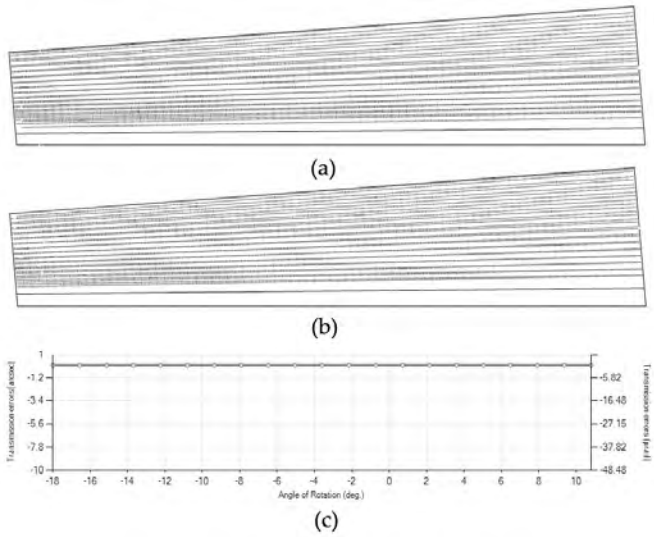

Figure 10: Contact pattern on (a) the pinion tooth surface, (b) wheel tooth surface and (c) function of transmission errors under aligned conditions

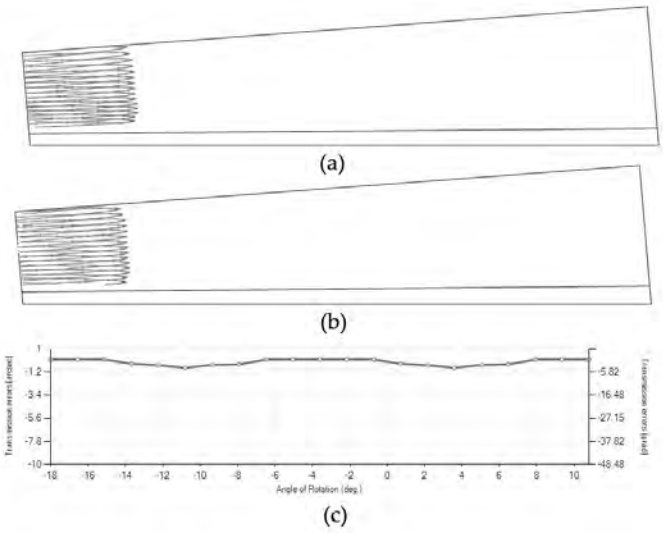

Figure 11: Contact pattern on (a) the pinion tooth surface, (b) wheel tooth surface, and (c) function of transmission errors for an error of alignment ΔE = 0.075 mm

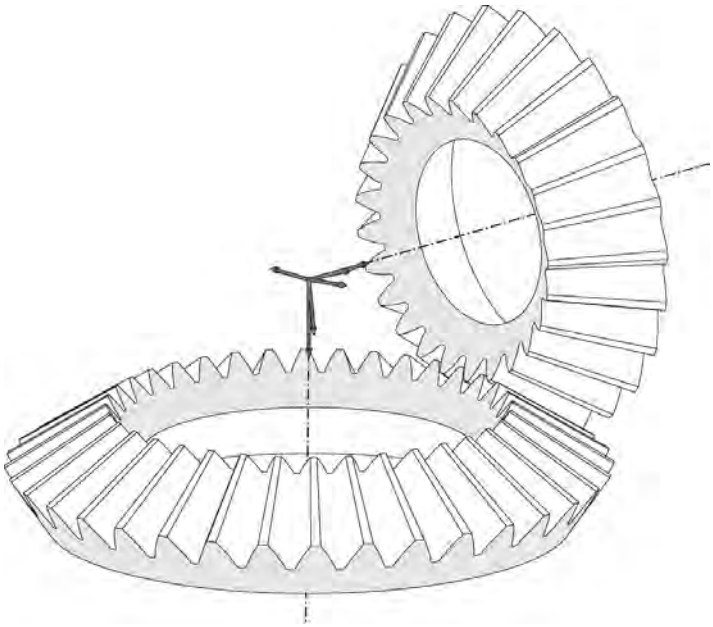

Figure 12: 3D representation of the gear drive under a shaft angle error $\Delta\Sigma$ = 2 degrees

bevel gears are not sensitive to changes in the shaft angle. The limits on changes on the shaft angles are set by the conditions of having positive backlash and a contact ratio higher than 1.

Application of surface modifications according to Equation 49 allows localizing the bearing contact and predesigning a parabolic function of transmission error to minimize the loaded function of transmission errors and provide a low level of noise and vibration of the gear drive. The optimized coefficients for profile crowning a_p and longitudinal crowning a_l in Equation 49 are a_p = 0.01 and a_l = 0.000001. Considering these values, the contact pattern and function of transmission errors shown in Figure 14 are obtained. This contact pattern is good for metal gears because it provides localized contact and a predesigned parabolic function of transmission errors. Profile crowning also helps to provide a smooth procedure of loading and unloading of the gear tooth surfaces in mesh.

Figure 15 shows the contact patterns and function of transmission errors for the case of geometry modification and the influence of an error of alignment ΔE = 0.075 mm. The contact path is still inside the active tooth surface, avoiding, in this way possible, high stresses

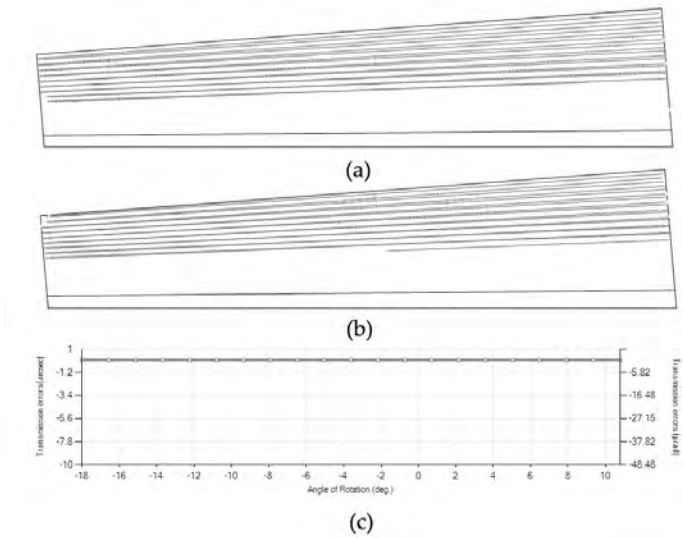

Figure 13: Contact pattern on (a) the pinion tooth surface, (b) wheel tooth surface, and (c) function of transmission errors for non-modified geometry of spherical involute gears under a shaft angle error $\Delta\Sigma$ = 2 degrees

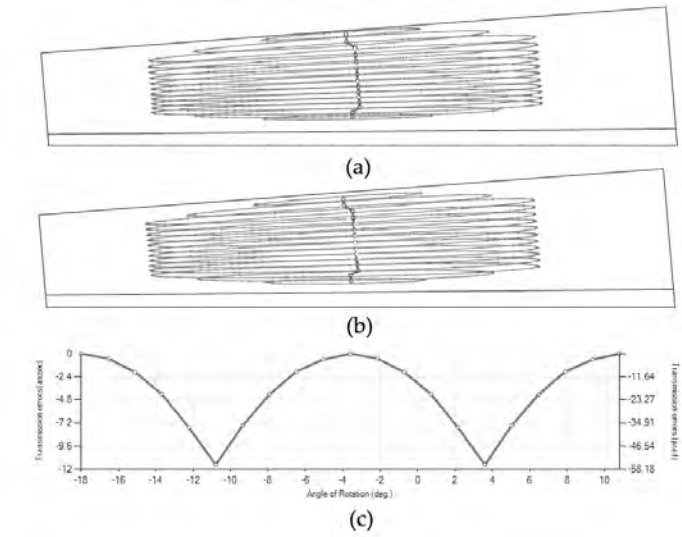

Figure 14: Contact pattern on (a) the pinion tooth surface, (b) wheel tooth surface, and (c) function of transmission errors for modified geometry of spherical involute gears under aligned conditions

due to contacts all over the edge of the surfaces. Finite element analysis will give more information on the mechanical behavior of all cases of design analyzed.

A torque of 500 Nm has been considered for stress analysis. The previous four cases studied from the TCA point-of-view will be compared from the stress analysis point-of-view. The four cases of design are summarized in Table 2.

Figure 16 shows the evolution of maximum contact stresses on (a) the pinion and (b) the wheel tooth surfaces along two cycles of meshing for all cases shown in Table 2. The lowest contact stresses are obtained for Case 1 where no surface modifications and no errors of alignment are being considered. However, when errors of alignment occur and no surface modifications are provided (Case 2), contact stresses are high, and the failure of the gear drive may occur. Modification of the surfaces to localize the bearing contact slightly increment contact stresses along the cycle of meshing (Case 3) with respect to the case with no surface modification, but when errors of alignment occur (Case 4), contact stresses only experience a slight increase (see Figure 16). Here, all finite element models have been kept with the same number of elements and boundary conditions for all cases analyzed to cancel those errors, physical and numerical, associated with the finite element method among the considered cases of design and thus allowing the focus on the difference of stress levels.

Figure 17 shows the evolution of bending stresses in the fillet of the pinion and wheel tooth surfaces along a cycle of meshing for all cases shown in Table 2. Again, the lower bending stresses are obtained for Case 1 with lineal contact and no errors of alignment. Higher bending stresses are obtained for Case 2 with lineal contact (no surface modification) and errors of alignment. Cases 3 and 4 show higher bending stresses than for Case 1 but always smaller stresses than Case 2, demonstrating that modification of geometry contributes effectively to making the gear drive not sensitive to errors of alignment and keeping the stresses low.

Case	Geometry	Errors of alignment
1	Non-modified	No errors
2	Non-modified	$\Delta E = 0.075$ mm
3	Modified ($a_p = 0.01, a_l = 0.000001$)	No errors
4	Modified ($a_p = 0.01, a_l = 0.000001$)	$\Delta E = 0.075$ mm

Table 2: Brief description of cases investigated

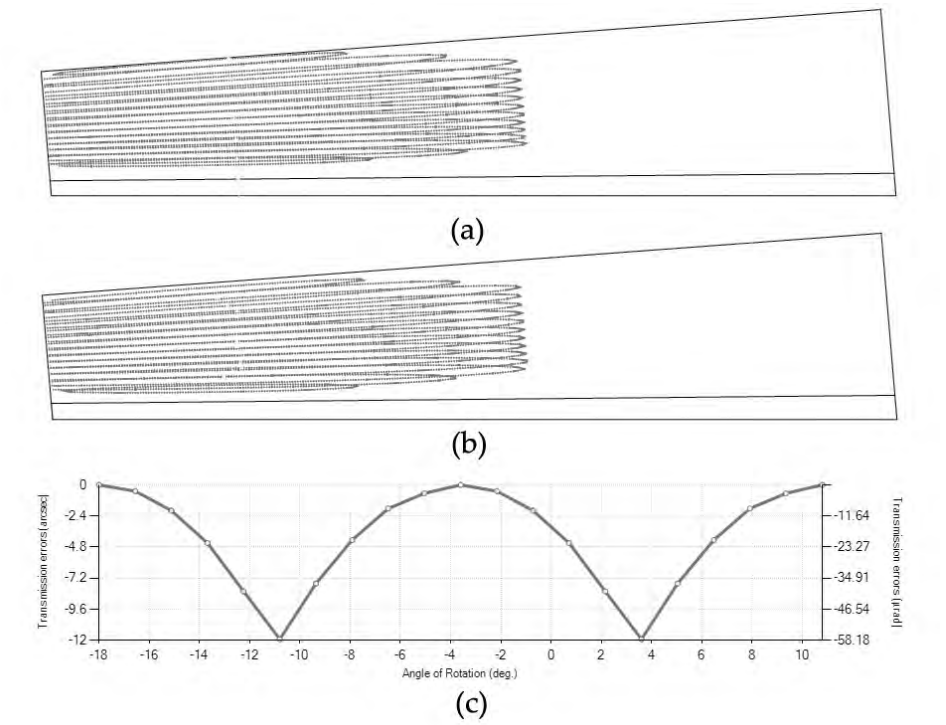

Figure 15: Contact pattern on (a) the pinion tooth surface, (b) wheel tooth surface, and (c) function of transmission errors for modified geometry of spherical involute gears under error of alignment ΔE = 0.075 mm

CONCLUSIONS

Based on the performed research work, the following conclusions can be drawn:

- The spherical involute profile, when considered as reference geometry for straight bevel gears, is providing excellent conditions of meshing and contact for plastic gears because it provides lineal contact between gear tooth surfaces and contributes to reduce contact stresses. Moreover, there are no transmission errors during the action of meshing.
- Straight bevel gears with spherical involute are not sensitive to changes in the shaft angle. The limits on variations of the shaft angle are set by the conditions of having positive backlash and a contact ratio higher than 1.
- An efficient way to incorporate microgeometry modifications into the design of spherical involute bevel gears has been proposed. When applied, microgeometry modifications, parabolic functions of transmission errors, can be predesigned and the contact localized, providing good conditions of meshing under the presence of errors of alignment.

REFERENCES

1. Kolivand, M. and Ligata, H. and Steyer, G. and Benedict, D. K. and Chen, J., 2015, "Actual Tooth Contact Analysis of Straight Bevel Gears," Journal of Mechanical Design, 137(9).
2. Radzevich, S. P., 2015, Dudley's Handbook of Practical Gear Design and Manufacture, 2nd Ed., CRC Press, 2015.
3. Stadtfeld, H. J., 2010, "Coniflex Straight Bevel Gear Manufacturing," Gear Solutions, Aug., pp.40–55.
4. Al-Daccak, M. J. and Angeles, J. and Gonzalez-Palacios, M. A., 1994, "Modeling of bevel gears using the exact spherical involute," Journal of Mechanical Design, 116(2), pp. 364–368.
5. Ligata, H. and Zhang, H. H., 2012, "Geometry Definition and Contact Analysis of Spherical Involute Straight Bevel Gears," International Journal of Industrial Engineering and Production Research, 23(2), pp.101–111.
6. Park, N. G., and Lee, H. W., 2011, "The Spherical Involute Bevel Gear; Its Geometry, Kinematic Behaviour and Standardization," Journal of Mechanical Science and Technology, 25(4), pp.1023–1034.
7. Harris, J. W. and Stocker, H., 1998, Handbook of Mathematic and Computational Science, Springer-Verlag.

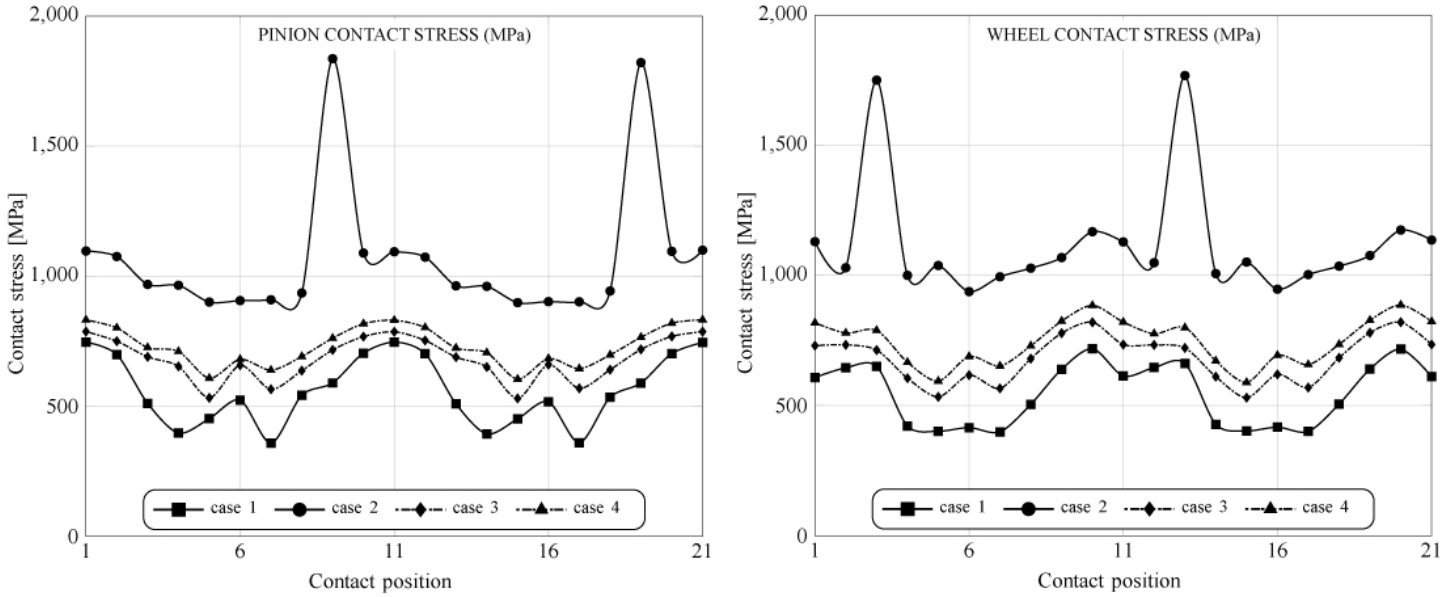

Figure 16: Evolution of maximum contact stresses on the pinion and wheel tooth surfaces along two cycles of meshing

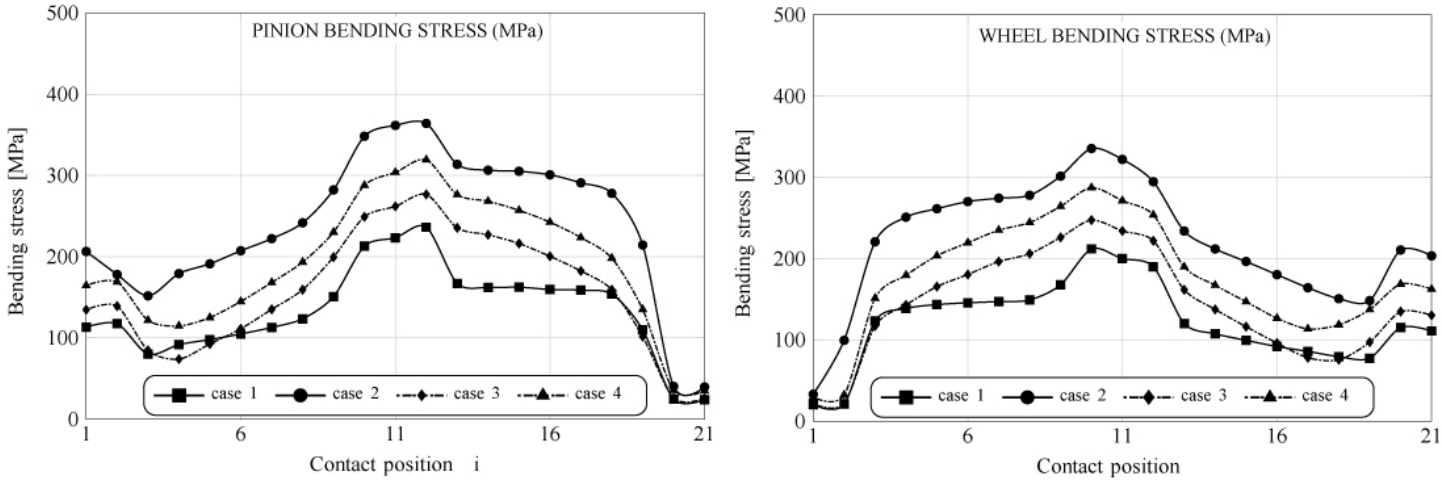

Figure 17: Evolution of bending stresses in the fillet of the pinion and wheel tooth surfaces

8. Figliolini, G. and Angeles, J., 2015, "Algorithms for Involute and Octoidal Bevel Gear Generation," Journal of Mechanical Design, 127(4), pp.664–672.
9. Lee, H. W. and Lee, K. O. and Chung, D. H., 2010, "A Kinematic Investigation of a Spherical Involute Bevel Geared System," Proceedings of the Institutiion of Mechanical Engineers, Part C: Journal of Mechanical Engineering Science, 224(6), pp.1335–1348.
10. Litvin, F. L. and Fuentes, A., 2004, Gear Geometry and Applied Theory, 2nd Edition, Cambridge Univeristy Press, New York.
11. Sheveleva, G. I. and Volkov, A. E. and Medvedev, V. I., 2007, "Algorithms for analysis of meshing and contact of spiral bevel gears", Mechanism and Machine Theory, 42(2), pp.198–215.
12. ABAQUS/Standard User's Manual, 2016, Providence, Rhode Island 02909-2499.

ABOUT THE AUTHORS: Alfonso Fuentes joined the Department of Mechanical Engineering at the Rochester Institute of Technology (RIT) as an associate professor in 2015. Prior to joining RIT, Dr. Fuentes was a full professor of Mechanical Engineering at the Polytechnic University of Cartagena (UPCT) in Spain and head of the Department of Mechanical Engineering. Dr. Fuentes' research focuses on the development of improved gear transmissions applied to helicopters, marine applications, and the automotive industry, development of enhanced design technologies for all types of gear drives, and development of IGD — Integrated Gear Design computer program as the ultimate tool for advanced gear design, analysis, and simulation of any type of gear drive. He is the author of more than 80 publications, including journal articles, conference papers, and technical reports. He is subject editor for gears and cams for the Journal Mechanism and Machine Theory.

Ignacio Gonzalez-Perez has been an associate professor at the Polytechnic University of Cartagena (UPCT) in Spain since 2009 and head of the Department of Mechanical Engineering since 2015. Dr. Gonzalez-Perez has been an active collaborator of Dr. Fuentes for more than 15 years. Both have participated in research projects involving the development of enhanced design technologies for all types of gear drives and in the development of IGD — Integrated Gear Design computer program. Dr. Gonzalez-Perez is currently the principal investigator of the Enhanced Gear Drives Research Group of the Polytechnic University of Cartagena and author of more than 40 publications.

Harish K. Pasapula graduated from Rochester Institute of Technology in 2016 with a master's degree in mechanical engineering. Shortly after, he started working as transmission design engineer at Honda R&D Americas, Inc., in Ohio. He is responsible for optimizing the design of gears, shafts, and bearings and working with different groups to improve the industry standards.

Gas Nitriding of Titanium

By Donald Jordan and Virginia Osterman

This preliminary study examines the effect of the partial pressure of nitrogen on case characteristics when gas nitriding titanium in a vacuum furnace.

Interest in solution gas nitriding and diffusion of nitrogen into the surface of titanium alloys as a means to inhibit adhesive wear (galling) while replacing heavier steel machinery parts has been increasing in applications involving moving components. The use of vacuum furnaces with partial-pressure nitrogen atmospheres provides a practical and economical means for titanium nitride case hardening. The need to establish a consistent, quality process requires knowledge of the specific vacuum furnace used and the effect of partial-pressure nitrogen, temperature, and time. This current study looks at the effect of partial pressure on the case hardness, depth, and surface chemistry of titanium alloy Ti-6Al-4V. Note: This study is ongoing, and more complete conclusions are planned to be published following further work.

INTRODUCTION

For all of the known benefits of using titanium alloys, including high strength-to-weight ratios and excellent corrosion resistance, titanium, unfortunately, is known to exhibit poor tribological properties. That is, it has a high coefficient of friction (COF) when in moving contact with many mating materials, resulting in poor sliding and adhesive wear resistance that leads to failure by galling. Owing to this, metal-to-metal applications encountering friction and wear considerations require a surface treatment for adequate serviceability. This is increasingly a topic of investigation as various segments of industry are searching to reduce moving mass in machinery components [1, 2].

One treatment for enhancing the tribological properties of titanium that has been researched for years is nitriding, which is performed by plasma or gas processes [3]. Nitrogen has great affinity and solid solubility in alpha titanium, which greatly increases hardness and strength [1, 3]. Gas nitriding, the topic of this study, is classified as a diffusion process whereby nitrogen gas dissociates and nascent nitrogen is adsorbed and diffused into the titanium matrix. This nitriding process is not a "coating"; it is a thermochemical heat treatment where nitrogen becomes an integral part of the titanium matrix. So unlike a coating, it does not have to initially bond well to function well; the case will not peel or flake away from the base metal.

The titanium/nitrogen phase diagram in Reference [3] shows that higher levels of nitrogen will form compounds of titanium and nitrogen that can be thought of as a hard ceramic. Provided the compound layer is not too thick and depending on its chemical makeup and service application, it can provide greatly enhanced wear performance. Below the surface compound layer is a diffusion zone that is solid solution strengthened by nitrogen. This adds support to the surface for sustaining higher application loads, and like other diffusion processes, the depth of the diffusion zone is dependent on the time and pressure of the treatment.

Titanium has an even stronger affinity for oxygen than nitrogen, making the purity of the nitriding atmosphere highly influential to the end results [1, 3]. Investigation into the formation of oxygen-enriched surfaces (at high levels forming alpha case) in vacuum heat treating titanium using a graphite-insulated vacuum furnace revealed that even at good commercial vacuum levels of 5 x 10^{-4} Torr, titanium became surface enriched with oxygen during heating to 1,450°F [4]. The study of the "gettering effect" of titanium indicates that oxygen may be a constituent of the case structure when gas nitriding titanium in commercial vacuum furnaces. Depending on the amount present, oxygen in the nitride case is not necessarily a detriment. Oxygen interstitially strengthens titanium like nitrogen, and at a certain level, may contribute to enhanced wear performance in a given application. Ti-6Al-4V has been purposely thermally oxidized to increase wear properties and reportedly performed comparatively well in a wear test study involving numerous surface engineering treatments [2].

Solar Atmospheres is developing processes for gas nitriding titanium in a vacuum furnace using partial-pressure nitrogen gas at elevated temperatures. Of interest are the effects of partial pressure on the case hardness, case depth, and the surface chemistry/crystalline phases of titanium alloy Ti-6Al-4V.

EXPERIMENTAL DETAILS

Ti-6Al-4V sheet was cut into approximately 1.5-inch squares. The surface of the coupons was used as-received following a rigorous alcohol wipe; no surface blasting or polishing was performed prior to processing.

An all-metal (molybdenum) vacuum furnace with a cylindrical, vertical hot zone, 10" diameter x 18" high, was used for this study. Three titanium coupons used for each run were hung on separate molybdenum wires attached to the lid of the furnace. All cycles began after an initial pump down to 2 x 10^{-5} Torr to assure vacuum integrity. The parts were heated in a vacuum to 854°C (1,570°F), and partial-pressure nitrogen was introduced at 70 microns, 1 Torr (1,000 microns), and 630 Torr. Nitriding time was 10 hours for each pressure.

Hardness profiles for each run were measured using a Struers DuraScan and 25-gram load. Specimens were etched using 2-percent HF for metallographic analysis and total optical case depth measurement. The RJ Lee Group in Monroeville, Pennsylvania, performed surface analyses using X-ray photoelectron spectroscopy (XPS) and X-ray diffraction (XRD). The intent of this study was to determine the influence of pressure selection as a means to control the formation of TiN, Ti_2N, and Ti oxide.

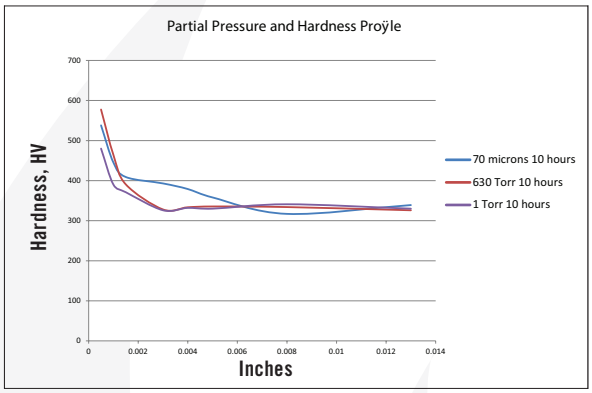

Figure 1: Average hardness profile for Ti-6Al-4V nitrided for 10 hours at 70 microns, 1 Torr (1,000 microns), and 630 Torr at 854°C

RESULTS AND DISCUSSION

The hardness profiles for the three pressures evaluated are presented in Figure 1. This shows that the hardness of the diffusion zone drops off sharply for the 630 Torr (A) and 1 Torr (B) nitrided specimens. The 70-micron (C) results are comparable to the near surface hardness (0.0005 inches or 12.7 µm) of the 630 Torr (A) results, but show a deeper, more gently sloping diffusion zone hardness. Note that the diamond indenter of the DuraScan is too large for the thin compound layers (10 µm range) to be accurately measured. (A nano-indenter hardness tester is needed and will be used in further study along with scratch hardness testing.)

After etching to reveal the microstructure, optical measurements were performed for each pressure, and the results are presented in Table 1. Tests A and B have comparable case depths, while Test C has a case depth about 60 percent deeper. The photomicrographs revealing the total case depths are shown in Figure 2. Higher magnification micrographs of Figure 3 show the thickness of the compound layer. The compound layer

Test	Test Pressure	Time hours	Total Case Depth Inches (µm)	Compound Layer Inches (µm)	Diffusion Zone Inches (µm)
A	630 Torr	10	0.002695 (68.45µm)	0.000371 (9.42 µm)	0.002324 (59.03)
B	1 Torr	10	0.002878 (73.10 µm)	0.000405 (10.29 µm)	0.002473 (62.81)
C	70 microns	10	0.004560 (115.82 µm)	0.000461 (11.71 µm)	0.004099 (104.11)

Table 1

was comparable for all three pressures, yet the total case depth was deepest for the lowest pressure, corroborating the microhardness profile results.

Based on prior investigations of the heat treatment of titanium alloys [4], it was surmised that the deeper case at the lowest pressure may be attributable to a higher presence of residual water vapor in the hot zone, owing to a "stale atmosphere" (relatively poor quality vacuum). This would result in oxygen enrichment within the case when water vapor adsorbs and dissociates on the titanium surfaces. To confirm this hypothesis, surface analyses using X-ray photoelectron spectroscopy (XPS) and X-ray diffraction (XRD) were performed [5]. The main crystalline phases detected with the XRD scans at each pressure are listed in Table 2. Oxygen is present on the surface as the titanium suboxide, Ti_2O.

Normalized X-ray counts, see Table 3, can be used to determine the relative ratios of the compounds TiN, Ti_2N, and Ti_2O. This reveals that the compound layer of sample C, processed at the lowest pressure, has the highest oxide concentration, 33 percent, of the three samples. The oxide concentration of sample A is 14 percent and 11 percent for sample B.

When processing at a low pressure of 70 microns, very little nitrogen flow is pumped through the furnace. Water vapor is inherently adsorbed in the hot-zone insulation and thus the low nitrogen flow becomes concentrated with water vapor upon heating. Further, 70-micron flow results in low furnace volume turnover. This ultimately results in higher levels of oxygen in the case. This result supports the hypothesis.

Samples A (14 percent) and B (11 percent) oxygen concentrations are comparable, owing to increased nitrogen pressures and gas flow rates resulting in greater dilution of water vapor by nitrogen. In order to maintain a pressure of 630 Torr (A), however, an almost completely closed vacuum at times leads to a decrease in the volume turnover at the highest pressure. This results in somewhat higher oxygen concentration at 630 Torr compared to 1 Torr.

CONCLUSIONS

This preliminary study revealed that the partial pressure of nitrogen when gas nitriding Ti-6Al-4V in a vacuum furnace can have a significant effect on the nitrided case characteristics. Processing with low partial pressure of 70 microns resulted in a considerably higher amount of surface oxides being present in the compound layer compared to processing at higher pressures of 1 Torr and 630 Torr. The pressure and gas flow/turnover rate of nitrogen influences the "gettering ability" of titanium for oxygen during the nitriding process. The lowest pressure process resulted in a higher hardness profile and total case depth. This is considered attributable to oxygen being an interstitial strengthening element in titanium — just as it is nitrogen's purpose in diffusion zone strengthening of the case.

Phase	Composition
Titanium (cubic structure)	Ti
Titanium Nitride	Ti_2N
Titanium (hexagonal structure)	Ti
Titanium Oxide	Ti_2O
Titanium Nitride	TiN

Table 2

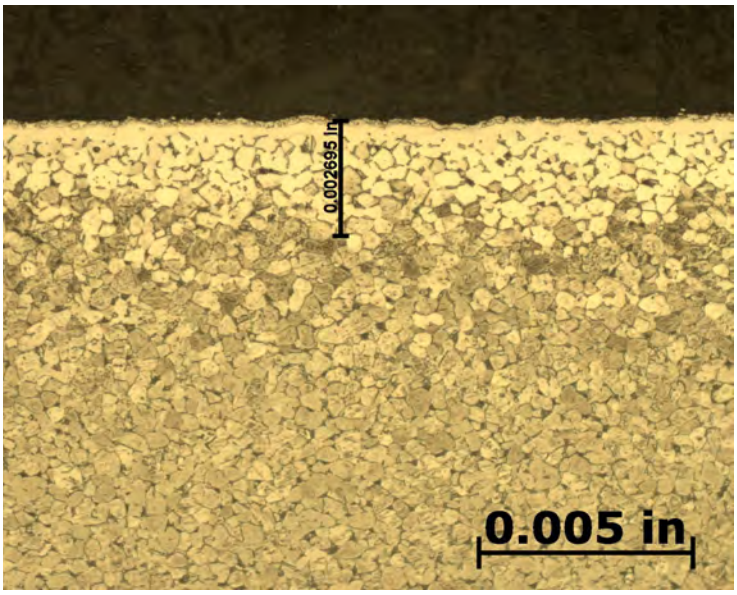

Figure 2a: Micrograph for 630 Torr (A) at 200X showing a total case depth of 0.002695 inches (68.45 µm)

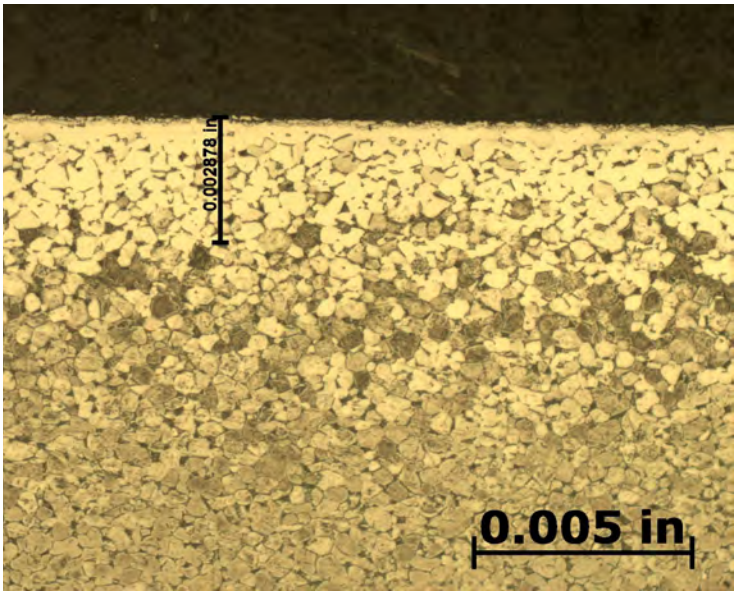

Figure 2b: Micrograph for 1 Torr (B) at 200X showing a total case depth of 0.002878 inches (73.10 µm)

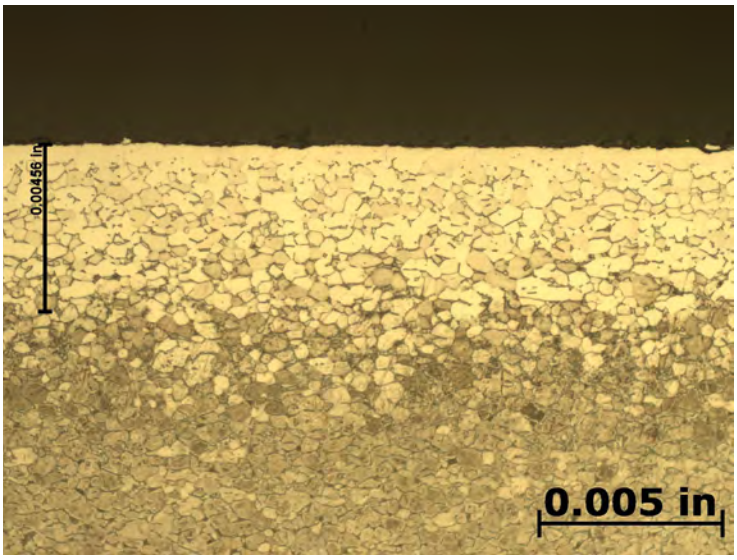

Figure 2c: Micrograph for 70 microns (C) at 200X showing a total case depth of 0.00456 inches (115.82 µm)

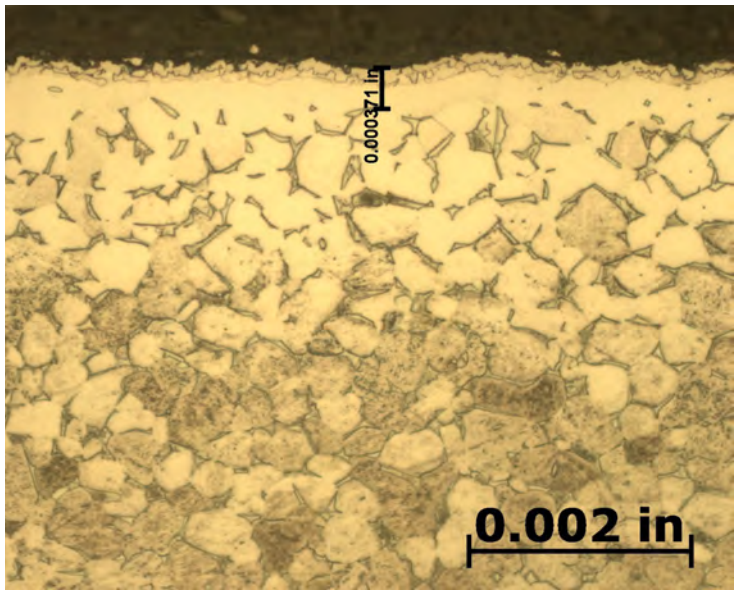

Figure 3a: Micrograph for 630 Torr (A) at 500X showing a compound layer of 0.000371 inches (9.42 µm)

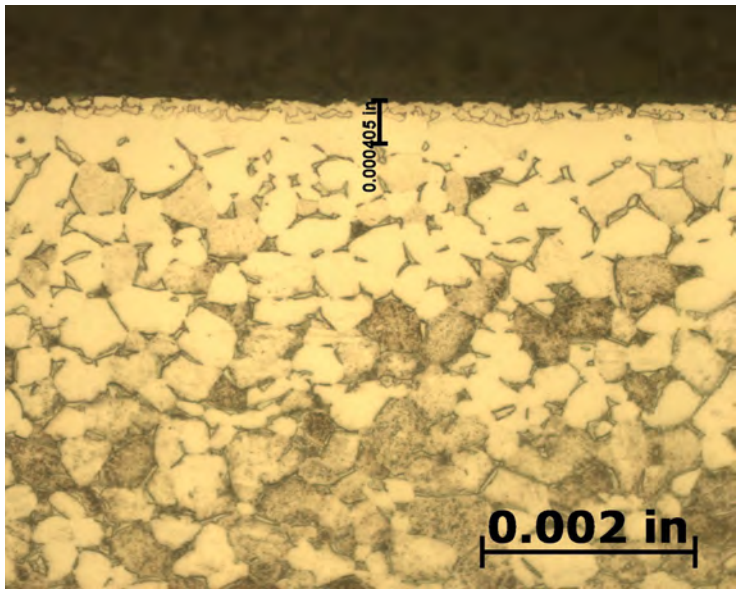

Figure 3b: Micrograph for 1 Torr (B) at 500X showing a compound layer of 0.000405 inches (10.29 µm)

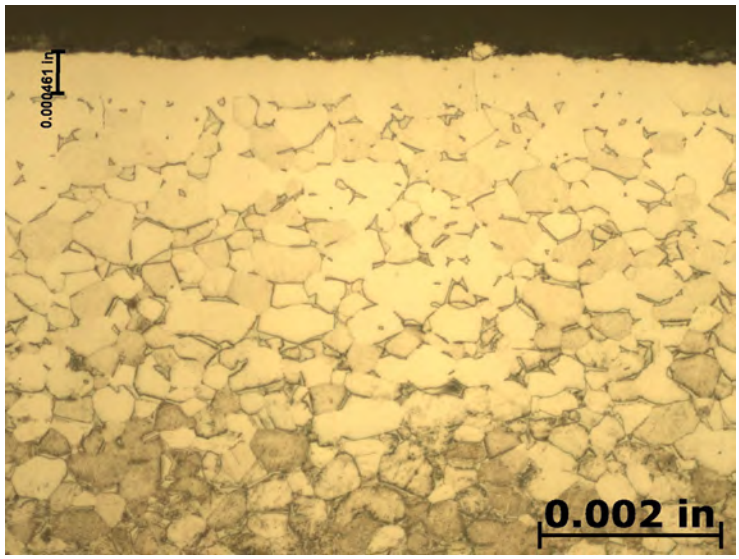

Figure 3c: Micrograph for 70 microns (C) at 500X showing a compound layer of 0.000461 inches (11.71 µm)

Maximum peak counts associated with phases identified in the sample							
Phase	~2θ°	Sample A		Sample B		Sample C	
		Counts	Normalized Counts**	Counts	Normalized Counts**	Counts	Normalized Counts**
Ti–Cubic	38.2	496	--	683	--	2429	--
Ti_2N	39.3	2525	2.2	3222	3.1	395	0.1
Ti-Hexagonal	40.2	634	--	370	--	1501	--
Ti_2O	40.5	416	0.4	429	0.4	228	0.1
TiN	42.6	294	0.3	175	0.2	251	0.1
Ti phases combined*	--	1130	1.0	1053	1.0	3930	1.0

*Counts for both Ti-Cubic and Ti-Hexagonal were added together
**Counts were normalized by dividing by the Ti-combined numbers

Table 3

At this point in the investigation, it is unknown to what extent oxygen may enhance or detract from the wear performance of the nitrided case. Wear requirements for a product tend to be application-specific, but some standardized wear tests are planned for further study of vacuum nitrided Ti-6Al-4V. Reference [3] mentions nitriding of race car steering racks (rack and pinion gearing) as well as engine valves and spring retainers. Solar Atmospheres has nitrided titanium alloy engine valves and spring retainers, in addition to gears designed for the next Mars expedition land rover. This latter application is germane to the gear industry, and the hope is that there is an increasing focus on reducing moving mass in machinery components, including gears.

REFERENCES

1. Bloyce, A., Morton P.H., Bell T.; Surface Engineering of Titanium and Titanium Alloys, ASM Handbook Volume 5, Materials Park, OH, 1994; 835-851.
2. Bansal, D.G., Eryilmaz, O.L., Blau, P.J.; Surface Engineering to Improve the Durability of Ti-6Al-4V Alloy, Wear 271 (2011); 2006-2015.
3. Rolinski, Ed; Nitriding of Titanium Alloys, ASM Handbook 4E, Materials Park, OH, 2016; 604-621.
4. Jordan, D. and Osterman V.; Minimizing Alpha Case during Vacuum Furnace Heat Treating, HTPro, Advanced Materials and Processes, March 2016; 46-48.
5. RJ Lee Group, XRD Analysis of Nitrided Titanium Report presented to Don Jordan, July 15, 2016.

ABOUT THE AUTHORS: Donald Jordan, FASM, is corporate metallurgist for Solar Atmospheres and heads an R&D group that develops vacuum heat treatment processes. The group has focused on thermochemical surface enhancement treatments and has developed processes for low-pressure carburizing and vacuum purge gas nitriding. Solar is recognized as an authority on vacuum heat treatment and vacuum furnace technology. For more information, email Jordan at don@solaratm.com or visit www.solaratm.com.

Virginia Osterman is a senior scientist at Solar Atmospheres. She has a Ph.D. in chemistry and more than 20 years of professional experience in materials and materials processing. Her work in the Solar R&D group includes responsibility for design and improvement of vacuum heating processes for Solar Atmospheres and its customers. She has focused on raw material processing, most prominently, hydriding and dehydriding of titanium, tantalum, and niobium. She has developed and currently teaches an ASM course in vacuum heat treating, geared toward operators and non-scientists, offered at ASM headquarters twice a year. For more information, email Osterman at ginny@solaratm.com or visit www.solaratm.com.

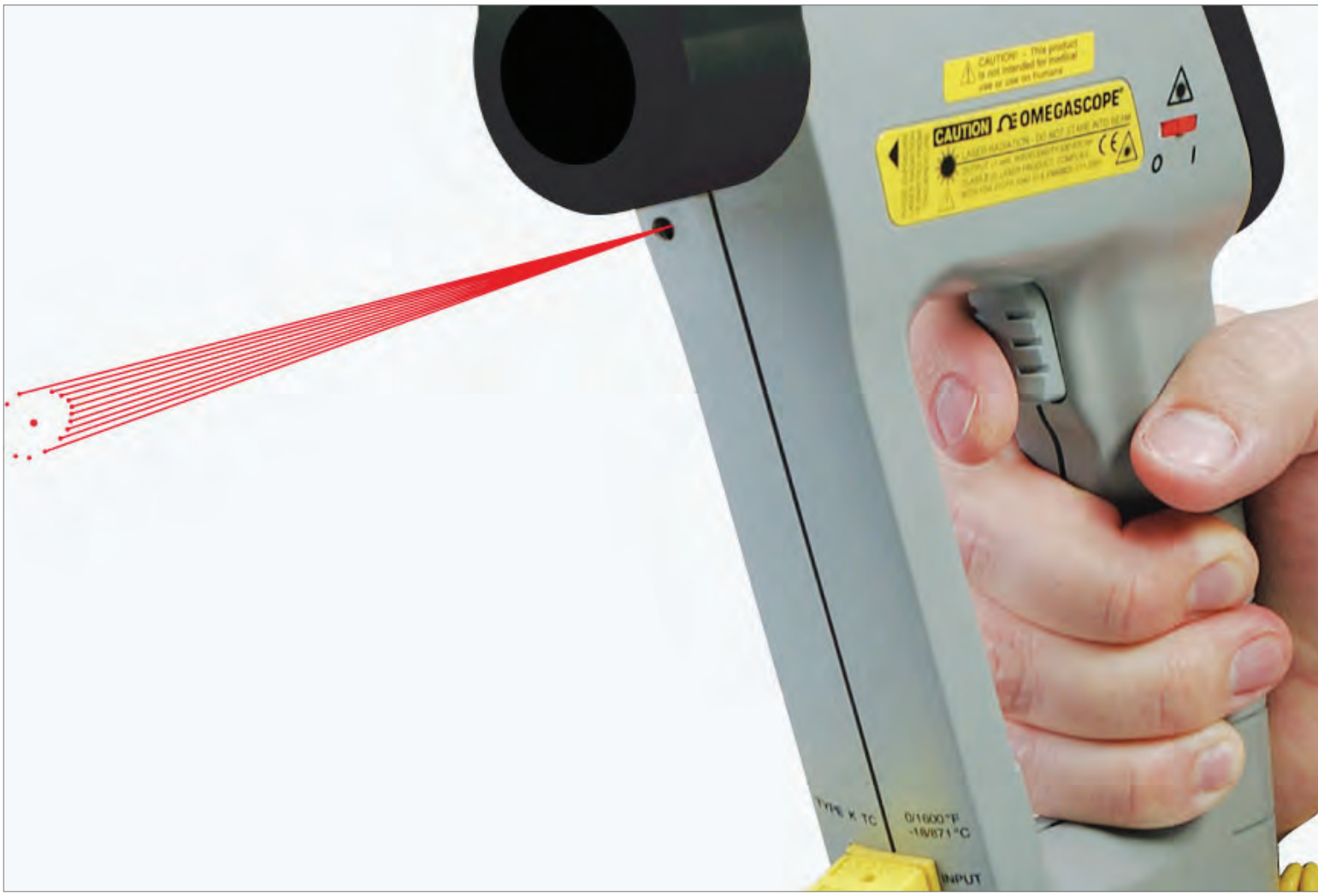

Infrared Temperature Measurement Theory and Application

By John Merchant

Infrared thermometers for non-contact temperature measurement are highly developed sensors that have widespread application in industrial processing and research. This paper describes, in non-mathematical terms, the theory of measurement technology and how it's used with the variety of application parameters.

An infrared thermometer measures temperature by detecting the infrared energy emitted by all materials at temperatures above absolute zero, (zero degrees Kelvin). The most basic design consists of a lens to focus the infrared (IR) energy onto a detector, which converts the energy to an electrical signal that can be displayed in units of temperature after being compensated for ambient temperature variation. This configuration facilitates temperature measurement from a distance without contact with the object to be measured.

As such, the infrared thermometer is useful for measuring temperature under circumstances where thermocouples or other probe-type sensors cannot be used or do not produce accurate data for a variety of reasons. Some typical circumstances are where the object to be measured is moving; where the object is surrounded by an EM field, as in induction heating; where the object is contained in a vacuum or other controlled atmosphere; or in applications where a fast response is required.

Designs for an infrared thermometer (IRT) have existed since the late 19th century, and various concepts were featured by Charles A. Darling [1] in his 1911 book "Pyrometry." However, it was not until the 1930s that the technology was available to turn these concepts into practical measuring instruments. Since that time, there has been considerable evolution in the design, and a large amount of measurement and application expertise has accrued. At the present time, the technique is well-accepted and is widely used in the industry and in research.

MEASUREMENT PRINCIPLES

As previously stated, IR energy is emitted by all materials above zero degrees K. Infrared radiation is part of the electromagnetic spectrum and occupies frequencies

between visible light and radio waves. The IR part of the spectrum spans wavelengths from 0.7 micrometers to 1,000 micrometers (microns). See Figure 1. Within this wave band, only frequencies of 0.7 microns to 20 microns are used for practical, everyday temperature measurement. This is because the IR detectors available to the industry are not sensitive enough to detect the small amounts of energy available at wavelengths beyond 20 microns.

Though IR radiation is not visible to the human eye, it is helpful to imagine it as being visible when dealing with the principles of measurement and when considering applications. Because, in many respects, it behaves the same way as visible light. IR energy travels in straight lines from the source and can be reflected and absorbed by material surfaces in its path. In the case of most solid objects opaque to the human eye, part of the IR energy striking the object's surface will be absorbed, and part will be reflected. Of the energy absorbed by the object, a proportion will be re-emitted, and part will be reflected internally. This will also apply to materials transparent to the eye, such as glass, gases, and thin, clear plastics. But in addition, some of the IR energy also will pass through the object (illustrated in Figure 2). These phenomena collectively contribute to what is referred to as the emissivity of the object or material.

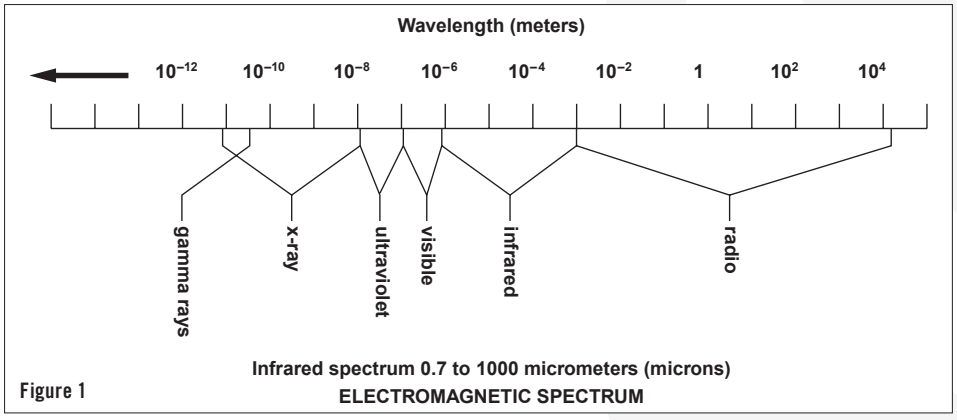

Infrared spectrum 0.7 to 1000 micrometers (microns)

Figure 1 ELECTROMAGNETIC SPECTRUM

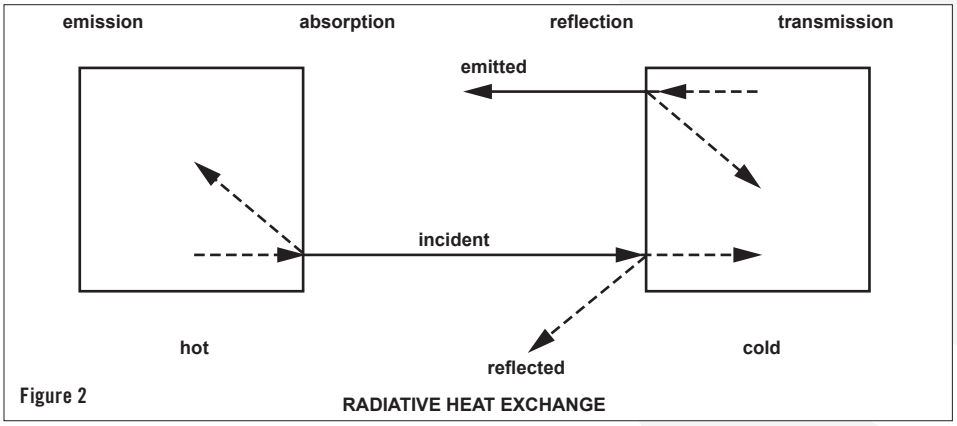

Figure 2 RADIATIVE HEAT EXCHANGE

Materials that do not reflect or transmit any IR energy are known as blackbodies and are not known to exist naturally. However, for the purpose of theoretical calculation, a true blackbody is given a value of 1.0. The closest approximation to a blackbody emissivity of 1.0, which can be achieved in real life, is an IR opaque, spherical cavity with a small tubular entry (see Figure 3). The inner surface of such a sphere will have an emissivity of 0.998.

Different kinds of materials and gases have different emissivities and will emit IR at different intensities for a given temperature. The emissivity of a material or gas is a function of its molecular structure and surface characteristics. It is not generally a function of color unless the source of the color is a radically different substance to the main body of material. A practical example of this is metallic paints with significant amounts of aluminum. Most paints have the same emissivity irrespective of color, but aluminum has a different emissivity that will modify the emissivity of metallized paints.

Just as is the case with visible light, the more highly polished some surfaces are, the more IR energy the surface will reflect. Therefore, the surface characteristics of a material also will influence its emissivity. In temperature measurement, this is most significant in the case of infrared opaque materials with an inherently low emissivity. Thus, a highly polished piece of stainless steel will have a much lower emissivity than the same piece with a rough, machined surface. This is because the grooves created by the machining prevent much of the IR energy from being reflected. In addition to molecular structure and surface condition, a third factor affecting the apparent emissivity of a material or gas is the wavelength sensitivity of the sensor, known as the sensor's spectral response. As stated earlier, only IR wavelengths between 0.7 microns and 20 microns are used for practical temperature measurement. Within this overall band, individual sensors may operate in only a narrow part of the band, such as 0.78 to 1.06, or 4.8 to 5.2 microns. These reasons will be explained later.

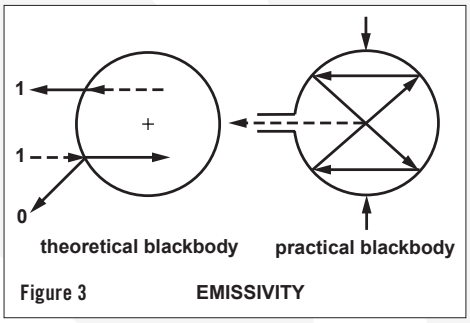

Figure 3 EMISSIVITY

THEORETICAL BASIS FOR IR TEMPERATURE MEASUREMENT

The formulas that infrared temperature measurement is based on are old, established, and well-proven. It is unlikely most IRT users will need to make use of the formulas, but knowledge of them will provide an appreciation of the interdependency of certain variables and serve to clarify the aforementioned. The important formulas include:

- Kirchoff's Law: When an object is at thermal equilibrium, the amount of absorption will equal the amount of emission.
- Stephan Boltzmann Law: The hotter an object becomes, the more infrared energy it emits.
- Wien's Displacement Law: The wavelength at which the maximum amount of energy is emitted becomes shorter as the temperature increases.
- Planck's Equation: Describes the relationship between spectral emissivity, temperature, and radiant energy.

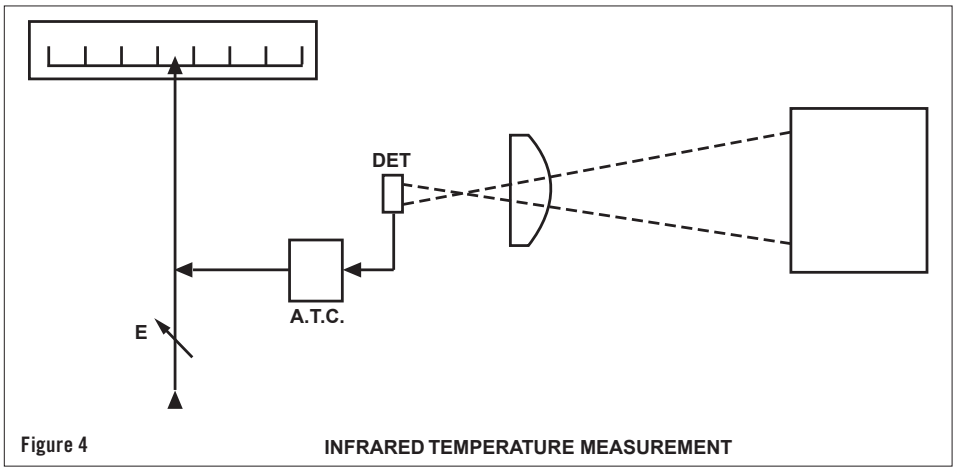

Figure 4 INFRARED TEMPERATURE MEASUREMENT

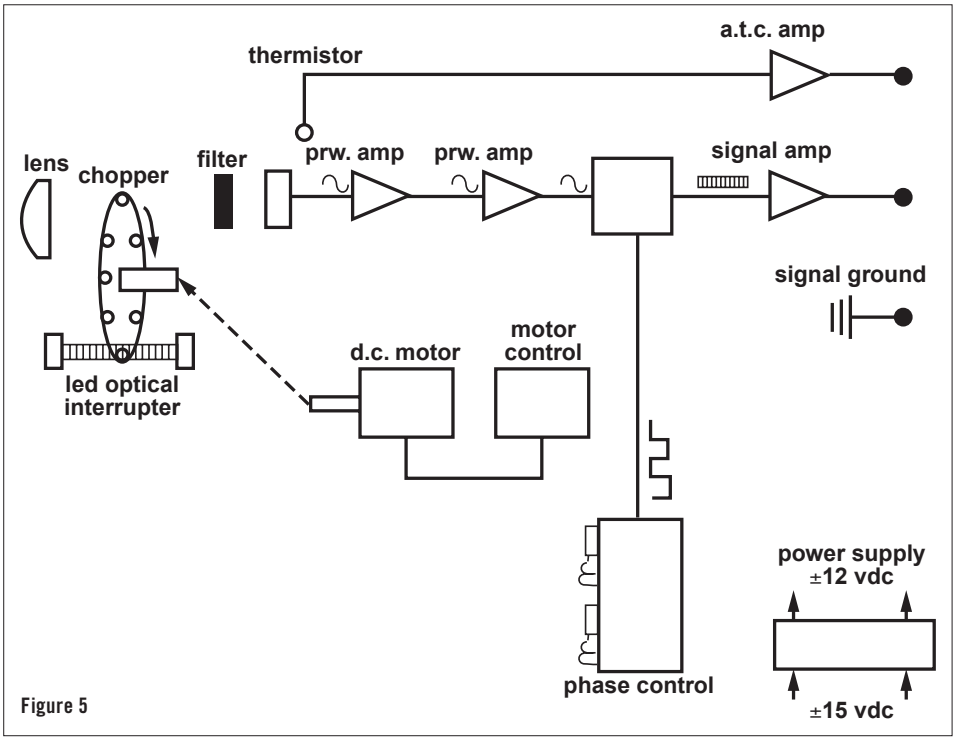

Figure 5

INFRARED THERMOMETER DESIGN AND CONSTRUCTION

A basic infrared thermometer (IRT) design is comprised of a lens to collect the energy emitted by the target; a detector to convert the energy to an electrical signal; an emissivity adjustment to match the IRT calibration to the emitting characteristics of the object being measured; and an ambient temperature compensation circuit to ensure temperature variations within the IRT, due to ambient changes, are not transferred to the final output.

For many years, the majority of commercially available IRTs followed this concept. They were extremely limited in application and, in retrospect, did not measure satisfactorily in most circumstances, though they were durable and adequate for the standards of the time (see concept illustrated in Figure 4).

The modern IRT is founded on this concept, but it is more technologically sophisticated to widen the scope of its application. The major differences are found in the use of a greater variety of detectors; selective filtering of the IR signal; linearization and amplification of the detector output; and provision of standard, final outputs such as 4-20 mA, 0-10 Vdc, etc. Figure 5 shows a schematic representation of a typical contemporary IRT. Probably the most important advance in infrared thermometry has been the introduction of selective filtering of the incoming IR signal — made possible by the availability of more sensitive detectors and more stable signal amplifiers. Whereas the early IRTs required a broad spectral band of IR to obtain a workable detector output, modern IRTs routinely have spectral responses of only 1 micron. The need to have selected and narrow spectral responses arises because it is often necessary to either see through some form of atmospheric or other interference in the sight path or to obtain a measurement of a gas or other substance that is transparent to a broad band of IR energy.

Some common examples of selective spectral responses are 8-14 microns, which avoids interference from atmospheric moisture over long path measurements; 7.9 microns, which is used for the measurement of some thin film plastics; and 3.86 microns, which avoids interference from CO2 and H2O vapor in flames and combustion gases. The choice between a shorter or longer wavelength spectral response also is dictated by the temperature range because, as Planck's Equation shows, the peak energy shifts toward shorter wavelengths as the temperature increases. The graph in Figure 6 illustrates this phenomenon. Applications that do not demand selective filtering for the previously stated reasons often may benefit from a narrow spectral response as close to 0.7 microns as possible. This is because the effective emissivity of a material is highest at shorter wavelengths and the accuracy of sensors with narrow spectral responses is less affected by changes in target surface emissivity.

It will be apparent from the foregoing information that emissivity is an important factor in infrared temperature measurement. Unless the emissivity of the material being measured is known and incorporated into the measurement, it is unlikely that accurate data will be obtained. There are two methods for obtaining the emissivity of a material:

1. Referring to published tables.
2. Comparing the IRT measurement with a simultaneous measurement obtained by a thermocouple or resistance thermometer, and adjusting the emissivity setting until the IRT reads the same.

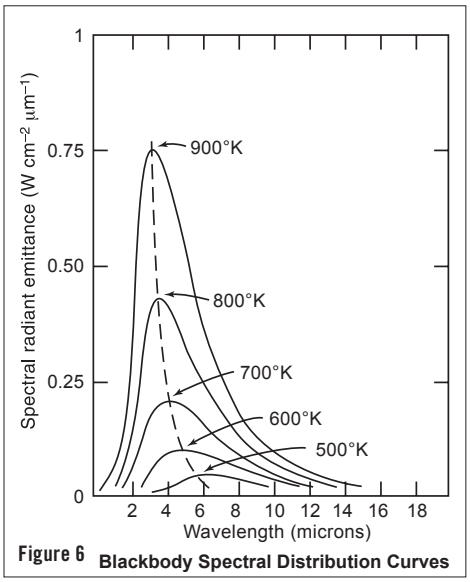

Figure 6 Blackbody Spectral Distribution Curves

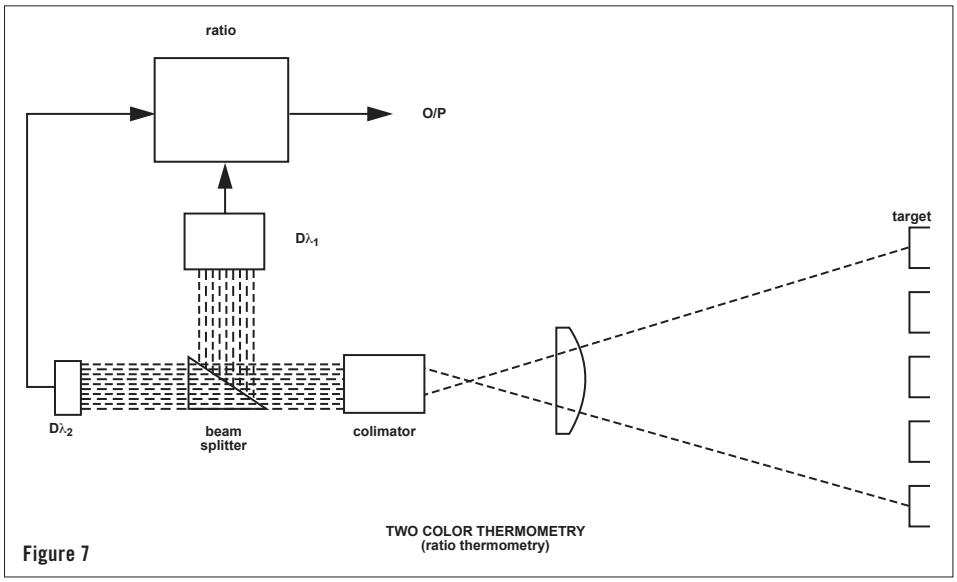

Figure 7

Fortunately, the published data available from the IRT manufacturers and some research organizations is extensive, so it is seldom necessary to experiment. As a rule of thumb, most opaque, non-metallic materials have a high and stable emissivity in the 0.85 to 9.0 range, and most un-oxidized, metallic materials have a low to medium emissivity from 0.2 to 0.5, with the exception of gold, silver, and aluminum, which have emissivities in the order of 0.02 to 0.04 and are, as a result, difficult to measure with an IRT. While it is almost always possible to establish the emissivity of the basic material being measured, a complication arises in the case of materials that have emissivities that change with temperature, such as most metals, and other materials such as silicon and high-purity, single-crystal ceramics. Some applications that exhibit this phenomenon can be solved using the two-color ratio method.

TWO-COLOR RATIO THERMOMETRY

Given that emissivity plays such a vital role in obtaining accurate temperature data from infrared thermometers, it is not surprising that attempts have been made to design sensors that would measure independently of this variable. The best known and most commonly applied of these designs is the two-color ratio thermometer. This technique is not dissimilar to the infrared thermometers described so far, but it measures the ratio of infrared energy emitted from the material at two wavelengths, rather than the absolute energy at one wavelength or wave band. The use of the word "color" in this context is somewhat outdated, but nevertheless has not been superseded. It originates in the old practice of relating visible color to temperature, hence "color temperature."

The basis for the effectiveness of two-color thermometry is that any changes in either the emitting property of the material surface being measured or in the sight path between the sensor and the material will be "seen" identically by the two detectors, and thus the ratio and therefore the sensor output will not change as a result. Figure 7 shows a schematic representation of a simplified two-color thermometer.

Because the ratio method will, under prescribed circumstances, avoid inaccuracies resulting from changing or unknown emissivity, obscuration in the sight path, and the measurement of objects that do not fill the field of view, it is useful for solving some difficult application problems. Among these are the rapid induction heating of metals, cement kiln burning zone temperature, and measurements through windows that become progressively obscured, such as vacuum melting of metals. It should be noted, however, that these dynamic changes must be "seen" identically by the sensor at the two wavelengths used for the ratio, and this is not always the case. The emissivity of all materials does not change equally at two different wavelengths. Those materials that do are called "greybodies." The ones that do not are called "non-greybodies." Not all forms of sight-path obscuration attenuate the ratio wavelengths equally either. The predominance of particulates in the sight path that are the same micron size as one of the wavelengths being used will obviously unbalance the ratio.

Phenomena that are non-dynamic in nature, such as "non-greybody" material, can be dealt with by biasing the ratio — an adjustment referred to as "slope." However, the appropriate slope setting must generally be arrived at experimentally. Despite these limitations, the ratio method works well in a number of well-established applications, and in others, is the best, if not the most preferred, solution.

CONCLUSION

Infrared thermometry is a mature but dynamic technology that has gained the respect of many industries and institutions. It is an indispensable technique for many temperature measurement applications and the preferred method for some others. When the user adequately understands the technology and all the relevant application parameters are properly considered, a successful application will usually result, providing the equipment is carefully installed. Careful installation means ensuring the sensor is operated within its specified environmental limits and adequate measures are taken to keep the optics clean and free from obstructions. When choosing a manufacturer, a factor in the selection process should be the availability of protective and installation accessories and the extent in which these accessories allow rapid removal and replacement of the sensor for maintenance. If these guidelines are followed, the modern infrared thermometer will operate more reliably than thermocouples or resistance thermometers in many cases.

REFERENCES

1. Darling, Charles R.; "Pyrometry. A Practical Treatise on the Measurement of High Temperatures." Published by E.&F.N. Spon Ltd. London. 1911.

ABOUT THE AUTHOR: John Merchant is a sales manager for Mikron Instrument Company Inc. For more information, go to www.omega.com.

Effects of the Composition of Ca-Rich Inclusions on Tool Wear Mechanisms During the Hard-Turning of Steels for Transmission Components

By Niclas Ånmark and Thomas Bjö k

Comparing a Ca-treated carburizing steel grade to a standard steel grade, the role of non-metallic inclusions on the tool wear and PCBN cutting tool life in fine machining of carburizing steel grades is investigated.

This study describes the influence of the steel characteristics of Ca-treated carburizing steel grades during hard part turning of synchronizing rings in gearbox production. The main focus was on the chemical composition of the non-metallic inclusions in the evaluated workpieces and their effect on the PCBN tool wear. In addition, a Ca-treated carburizing steel grade was compared to a standard steel grade. Machining tests were performed at the transmission machining site at Scania in order to evaluate the PCBN cutting tool life as defined by the generated surface roughness during actual production. The progression of flank and crater wear was evaluated by using a scanning electron microscope (SEM) equipped with an energy dispersive X-ray spectrometer (EDS) and a secondary electron (SE) detector.

The Ca-treated steel showed a more than doubled tool life than that of the standard steel grade. The superior machinability was linked to the formation of a Ca-enriched slag barrier composed of (Mn,Ca)S and (Ca,Al)(O,S). It is believed that the stability of the protective deposits is essential to minimize diffusion-induced chemical wear of the PCBN tool.

BACKGROUND

Gearbox production of synchromesh rings, shafts, crown wheels, and pinions, among others, constitutes a number of manufacturing processes that are aligned in leveled and balanced flows. Typically, the flows are divided into soft machining, heat treatment, and hard machining. Examples of machining processes in a production line are turning, hob-milling, and drilling. Other common

machining operations are deburring, grinding, and honing. A major challenge in transmission machining is to combine a high operating production efficiency, a high quality of the finished parts, a low tooling cost, and a robust production [1–5]. Therefore, the cutting tools and the workpiece materials used in transmission machining must be carefully adapted to the machining process and the workpiece specification.

Hard part turning is often the last machining process in a production line, and it aims at removing the final layers of the metal from the workpiece in order to produce the predetermined surface and geometry. The most frequent alternative to hard part turning is grinding, which is costly and leads to a reduced operating production efficiency. Moreover, cutting tools made of polycrystalline cubic boron nitride (PCBN) have been developed decades ago to machine hardened steel. In general, the PCBN is described as a super hard material, which gives an extreme yield strength also at high temperature [6]. The precise performance of a PCBN cutting tool in a defined machining process is given by the CBN composition, the CBN grain size, and the tool edge preparation [7-9]. In general, a high-PCBN cutting tool is composed of 70-90 vol% CBN, while a low-PCBN cutting tool has 50-70 vol% of CBN [10]. The remaining part is balanced by a metallic or a ceramic binder, like cobalt (Co) or titanium carbon nitride (TiCN), respectively. Previous research has shown that low-PCBN cutting tools have a longer service life than high-PCBN cutting tools [11, 12]. At the same time, low-PCBN cutting tools have been found to have a lower hardness and fracture toughness compared to high-PCBN cutting tools [10]. These contradictory results were explained by the interaction between the binder phase and the steel constituents of the workpiece, which resulted in CBN grain pluck-out and subsequent abrasive wear [13]. Another explanation is that the longer tool life of low-PCBN is attributed to its large bonding strength [14] and low thermal conductivity [15]. Thus, the heat generated at the tool edge-chip interface is transferred to the produced chips. At the same time, high-PCBN tools have a higher hardness and brittleness than low-PCBN tools. Thus, they are more prone to the elevated loads at the cutting edge [16].

In addition, it has been shown that a smaller average CBN grain size is beneficial for the resistance to an abrasive wear of PCBN cutting tools. It is due to an increased hardness and rupture strength of fine CBN grains. However, many research results are published on continuous hard machining, often at a laboratory scale, while less research is reported on intermittent machining, especially for production conditions. Even though there may be similarities, the machining conditions are different, which can effect the active tool wear mechanisms. Typically, the wear mechanisms of PCBN cutting tools are of an abrasive [17-19], an adhesive [20], a chemical [11], or a diffusive [21] nature. Frequently reported wear patterns are a flank and a crater wear, a micro-chipping, an edge fracture, and a nose wear.

Carburizing steel grades are widely used in automotive production because of their excellent resistance to fatigue and due to their ability to carry high loads. In addition, carburized steel components have a typical surface hardness of 60 ±2 HRC, which levels out at 550 HV (~52.4 HRC) within a depth of 1 mm. Due to the risk for inclusion-induced fatigue of gearbox components at elevated stress values, the level of the steels' cleanliness is of utmost importance. Thus, it must be secured to ensure a high-performance steel. Therefore, carburizing steel grades for gearboxes and diesel engines at Scania are classified into three levels, A, B, and C, based on their cleanliness level (see Table 1). Level A refers to high-performance steels, while Level B refers to a default level. Steel grades of Level C are rarely used and are solely selected if there is a low risk of an inclusion-induced fatigue. Additional requirements may be used to ensure a certain quality of a steel grade. For example, vacuum degassing, electromagnetic stirring, method of casting, reduction ratio, austenitizing temperature, hardenability, microstructure, and delivery state may be specified as a requirement for a specific steel grade.

Although the high-cleanliness steels have excellent mechanical strengths, the advantage has come at the expense of a reduced tool life and a more difficult chip breakage. In many applications, where a default type of steel is selected, a high production rate is the objective. For that purpose, many steel manufacturers have developed steels with improved machinability. High sulphur content as well as Ca-treatment are common means. Additions of calcium during deoxidation of liquid steel transforms hard Al_2O_3 inclusions into Ca-aluminates, which are softer and less likely to cause a cutting tool wear [22-27]. In addition, it should be pointed out that MnS and CaS inclusions are completely soluble with each other at the temperatures of a molten steel production [28]. Thus, it enables the formation of (Mn,Ca)S inclusions, which have a higher hot-hardness than pure MnS [29] inclusions. Therefore, complex (Mn,Ca)S inclusions are believed to be more abrasive than pure MnS inclusions. However, a successful Ca-treatment leading to a Ca-content of about 40 ppm requires a certain level of

Cleanliness level	Intended for	Sulphur content	Oxygen content
Level A	Components with high risk of inclusion induced fatigue	150–250 ppm	≤ 15 ppm
Level B	Most components, default level	200–400 ppm	≤ 50 ppm
Level C	Components with low risk of inclusion induced fatigue	200–400 ppm	≤ 80 ppm

Table 1: Classification of carburizing steel grades that are used in automotive production.

Des.	C	Si	Mn	Cr	Ni	Mo	Cu	Al	V	N	S	O	Ca
R	0.23	0.33	1.56	0.18	0.13	0.06	0.14	0.028	0.09	110	260	11	11
M	0.18	0.32	1.44	0.38	0.13	0.03	0.22	0.020	0.09	110	280	16	53

Table 2: Chemical composition of carburizing steels used for machining tests, in wt%*

***Contents of N, S, O, and Ca are given in ppm.**

sulphur, typically around 300 ppm. Such machinability-improved, Ca-treated steel grades are fitted into the Level B of the steel qualities presented in Table 1. Therefore, they can be used to increase the production rate.

This work extends from a previous study where the influence of inclusion composition was linked to the tool wear during hard part turning of carburized steel by using a PCBN cutting tool [30]. It was found that Ca-treated steel showed a superior machinability in comparison to standard and clean steel. In addition, the machinability-improving effect of the Ca-treated steel was linked to the formation of protective slag deposits of (Mn,Ca)S and (Ca,Al) (O,S) that form on the rake face crater of the cutting tool. This study aims at clarifying the link between steel characteristics of the carburizing steels and the influence on the wear mechanisms and the cutting tool life in hard part turning of synchromesh rings during a gearbox production. In addition, the tool wear morphologies at different cutting speeds and frequencies of interruption were investigated. Here, a Ca-treated, machinability-improved steel grade was compared to a standard steel.

EXPERIMENT

Work Materials and Cutting Tools

Middle cones for a synchromesh gearbox were made of two carburizing steel grades. A standard carburizing grade of type EN 19MnVS6 was used as reference (R). See Table 2. The machinability-improved steel (M) was also of the type EN 19MnVS6. In addition to a relatively high sulphur content, the M-steel is Ca-treated to reach a 53 ppm calcium content. The two grades fit into the same classification with respect to the steel cleanliness standard of Scania.

Middle cones (see Figure 1) of 170 mm in diameter were heat-treated as follows:

1. Carburizing at 930°C for 3.4 h.
2. Quenching in oil.
3. Tempering at 195°C for 2 h.

Hardness profiles including surface hardness and case hardening depth were measured using the Vickers hardness method (HV1).

A SECO PCBN cutting tool with designation CCGW09T308S-01030-L1WZB, CBN150, was used in this work. The grade is made of a 0.45 volume fraction of CBN mixed with a ceramic binder composed of TiCN and Al_2O_3 and having an average grain size below 1 μm. The cutting tool has a 30° chamfer of width of 0.1 mm and a nose radius of r_ε = 0.8 mm (see Figure 2). In addition, it has a wiper geometry that is suitable for high feeding rates. At the current cutting speed of 166 m/min., the hard part machining engagement of each middle cone is about 11 s, which corresponds to a chip cut length (CCL) of 30 m.

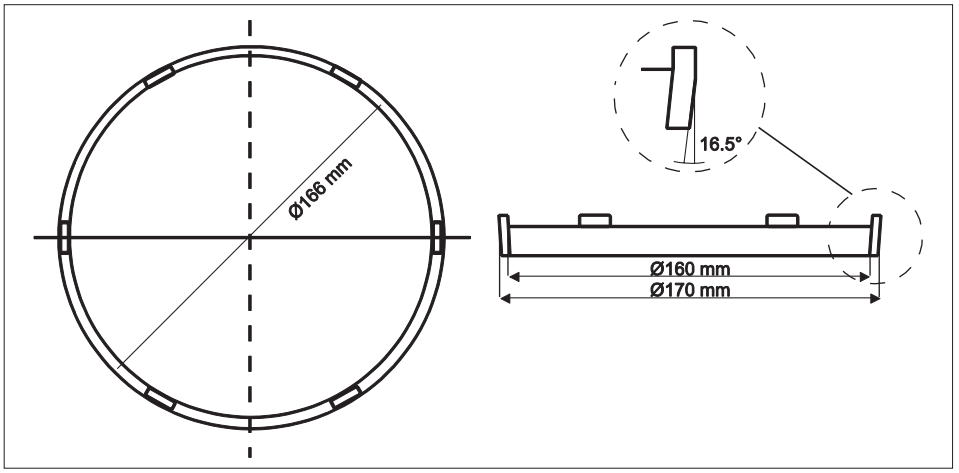

Figure 1: A schematic of the workpiece

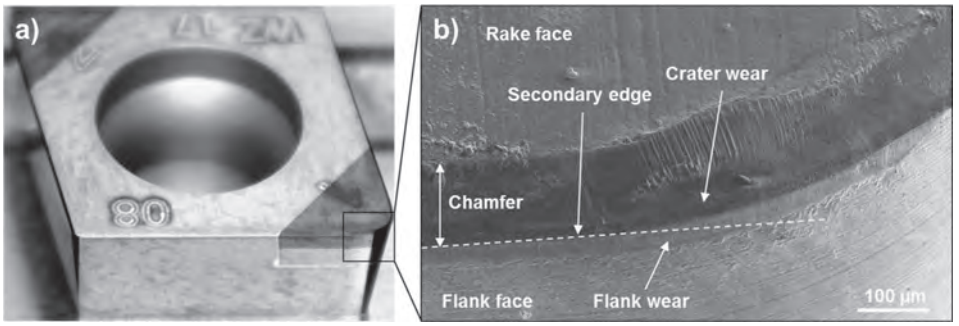

Figure 2: Overview of (a) a PCBN edge and (b) a tool wear together with the corresponding key terms (LOM, SEM-SE)

Machining Tests and Tool Wear Monitoring

The machining tests were performed in an EMAG turning lathe under dry conditions. Tool life tests were performed by using a feed rate f_n = 0.24 mm/rev., a radial depth of cut of a_p = 0.15 mm, and cutting speeds of v_c = 166-300 m/min. Most attention was paid to the tests at 166 m/min., which is the current cutting speed used in production. Three consecutive machining tests were included, which used both R and M-steel grades. The additional machining tests were made with an interruption prior to tool life aiming at studies of the initial wear mechanisms, as seen in Table 3. The tests duration corresponded to about 1/12 of their respective tool life. The test times were 7.5 and 16 minutes the R and M-steels, respectively. The corresponding chip cut lengths (CCL) were 1230 m and 2590 m, respectively.

The tool life criterion was defined as the surface roughness Ra ≥ 0.7 μm of the machined component or at a cutting edge failure. The surface roughness of the middle cone was recorded after completion of each machined component using a Mahr Perthometer S2. Therefore, a detailed tool wear analysis was conducted by using SEM with secondary electron (SE) imaging.

Analysis of Test Specimens

An inclusion analysis was undertaken by using scanning electron microscopy (SEM) in combination with energy dispersive X-ray spectroscopy (EDS). A back-scattered electrons detector was used with the SEM. Moreover, the investigated non-metallic

Steel	v_c (m/min)	t (min)	CCL (m)
R	166	7.5	1230
M	166	16	2590

Table 3: Test matrix for interrupted cutting tests

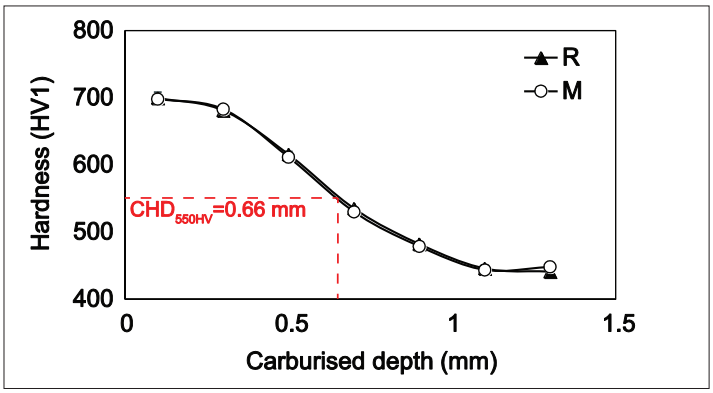

Figure 3: Hardness profiles of the tested steels as a function of the carburized depth

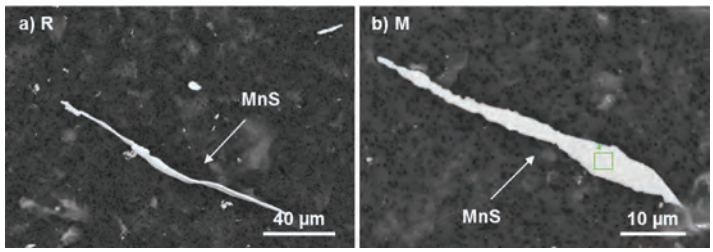

Figure 4: Typical MnS inclusions observed in the steel samples of the R and M grades

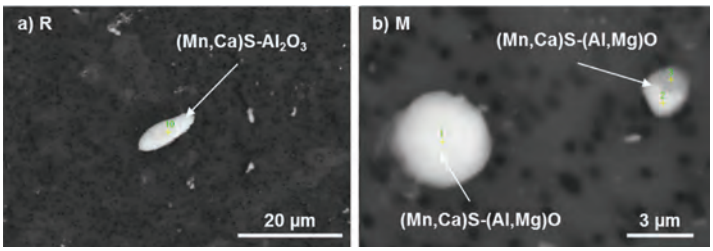

Figure 5: Typical oxy-sulphide inclusions observed in the steel samples of the R and M grades

inclusions were precipitated on a film filter surface after a completed electrolytic extraction of the steel specimens. The steel was dissolved by using a 10% acetyleacetone electrolyte and using an electric current of 40-60 mA.

RESULTS

Hardness Profiles

The surface hardness of steel R and M was 698 ±4 HV (60.1 ±0.2 HRC), and the carburizing depth was 0.66 mm, as seen in Figure 3.

Inclusion Characteristics of the Evaluated Steels

The reference steel grade R is characterized by MnS inclusions, which elongates during rolling to lengths greater than 100 µm (Figure 4a). Also, it contains less elongated (Mn,Ca)S-Al_2O_3 oxy-sulphides, which had a plate-like shape (Figure 5a) with a typical diameter of 10 µm. Similarly to the R-steel, the Ca-treated (modified M) steel grade contains elongated MnS inclusions with lengths of up to 100 µm (Figure 4b). In addition, the M-steel contains many fine and globular (Mn,Ca)S-(Al,Mg)O oxy-sulphides with a typical equivalent circular diameter smaller than 10 µm (Figure 5b).

PCBN Cutting Tool Life and Tool Wear

The M-steel shows a superior machinability compared to the R-steel; the corresponding tool life was 38 min. (CCL = 6300 m) and 18 (CCL = 3000 m), respectively, (see Figure 6a) for a cutting speed of 166 m/min. The tool life criterion of $R_a > 0.7$ mm was reached for the reference steel grade, while the test with the M-steel were halted due to distortions of the machined workpiece and chipping of the tool. The surface roughness (R_a) measurements indicate a smaller scatter when machining in the R-steel than in the M-steel (Figure 6b). Furthermore, the distinct difference between the two steel grades is that the generated surface roughness of the M-steel leveled out at about 0.5 µm, while the generated surface roughness of the R-steel displayed a progressive growth. The chip formation of both steel grades was acceptable. The chips were short and had an arc-like shape.

Although the R-steel and the M-steel generates an edge chipping at the end of the tool life, the tested PCBN edges have a well-balanced wear morphology consisting of a flank and a crater wear (Figure 7). However, note that the PCBN flank wear had progressed further at the end of the tool life of the M-steel (V_B = 64 ±10 µm) in comparison to the R-steel (V_B = 44 ±8 µm). This follows the more than doubled service life of M. Typically, the R-steel generated chipping wear at an earlier stage, yet with significant scatter, as well as larger chippings, as compared to M, (Figures 7 and 8). Moreover, a ridge formation was observed on the upper side of the rake face crater after a completed hard part turning of the steels. Also, the ridge formation was more pronounced after machining an R-steel than after machining an M-steel (Figure 7).

An investigation of increased cutting speeds showed that the cutting speeds of 200, 250, and 300 m/min. could be used with the M-steel with surface roughness below the $R_a \geq 0.7$ µm criterion for 31, 11, and 6 min., respectively. The corresponding chip cut lengths were 6200, 2750, and 1800 m, respectively. In fact, only the test with the M-steel at 300 m/min. was stopped after 10 min. following

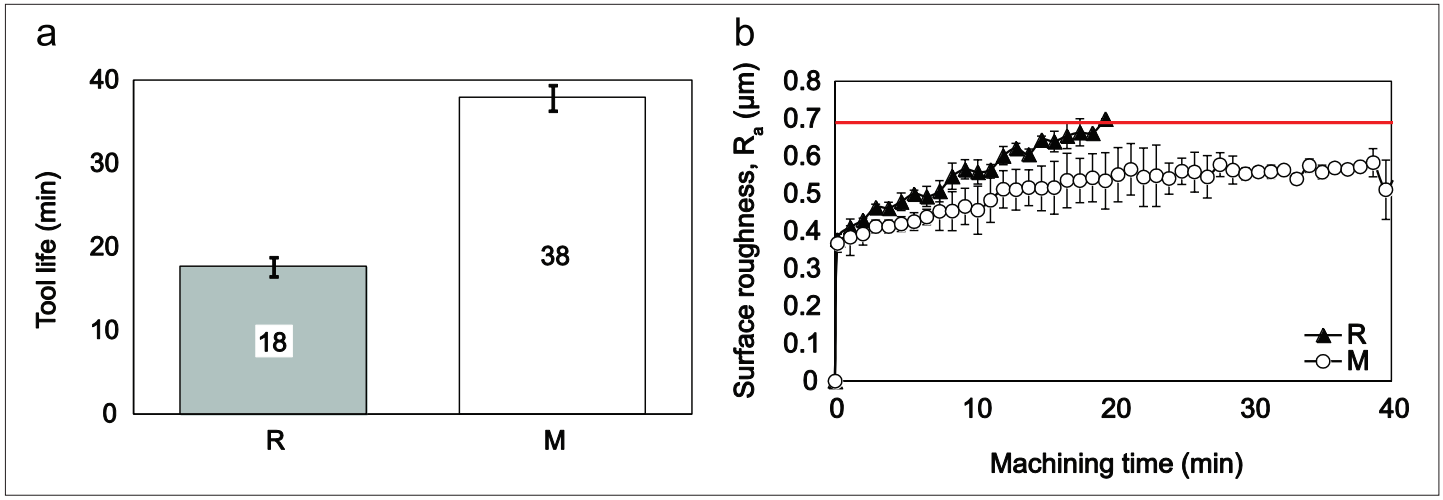

Figure 6: Tool life of the tested steels (a) and the generated surface roughness (b) at f_n = 0.24 mm/rev., a_p = 0.15 mm, and v_c = 166 m/min.

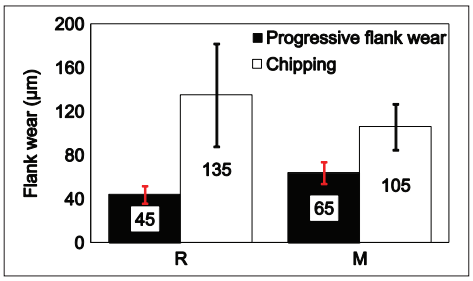

Figure 8: Progressive and chipping flank wear of tool life tested cutting edges at v_c = 166 m/min, f_n = 0.24 mm/rev, and a_p = 0.15 mm

the $R_a \geq 0.7$ µm criteria. The tests at 200 m/min. and 250 m/min. did not exceed Ra ≥ 0.6 µm. Instead, they were stopped due to a shape change. On the contrary, it was only possible to machine the reference steel grade R not more than a 200 m/min. rate, which resulted in a tool life of about 8 min. (Figure 9). The cutting speeds of 250 and 300 m/min. resulted in an instant edge fracture when machining the R-steels. In addition, a more distinct ridge formation was observed in the rake face crater after a machining of the steels at the higher cutting speeds of 200-300 m/min. (Figure 10).

Additional machining tests were undertaken and stopped prior to reaching the tool life. Tests were stopped at 7.5 min. (1230 m) and 16 min. (2590 m) for the R and M-steels, (see Figure 11). All cutting edges displayed a well-balanced flank and rake face wear, and no indication of chipping wear was found. However, a somewhat more advanced rake face wear was observed on the cutting tool tested with the R-steel in comparison to the M-steel. The flank wear progression was very similar in these tests. Moreover, the same tendency of a ridge formation on the upper part of the tool-chip contact zone on the rake face was observed with the R-steel (see Figures 7 and 10).

Workpiece Material Adhered to the Cutting Edge

Transferred workpiece material was observed in the chip exit part of the rake face, after machining the R-steels (see Figure 12a). On the contrary, machining in the M-steel with a PCBN edge resulted in a minimum of material transfer to the rake face. Only small remnants of workpiece burr was found on the cutting edges, as given by Fe signals of the EDS analysis after machining both the R and the M-steels (Figure 12b).

EDS of the M-steel crater indicated the presence of the slag elements Mn, S, Ca, Al, and O (see Figure 13). The segment rich in Mn and S has an elongated shape, parallel to the edge line. The elements Al and O were enriched in the ridges of the rake face crater and had a less elongated shape. Also, a low and even concentration of Ca is revealed in the crater (Figure 13c). Except for Al and O, much less slag deposits was found in the rake face crater for the R-steel compared to the M-steel, Figure 14.

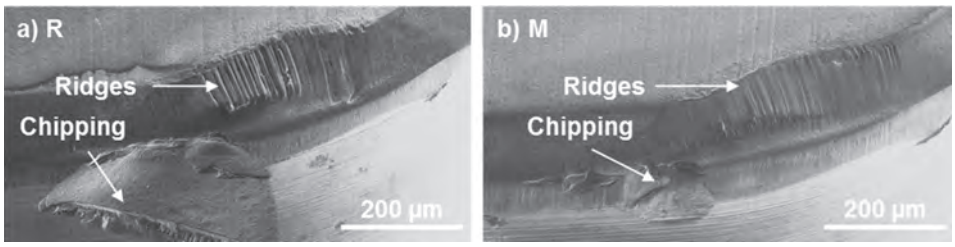

Figure 7: The PCBN edges imaged by SEM after having reached their tool life: (a) R (t = 18 min.), (b) M (t = 38 min.); the edges were etched prior to imaging

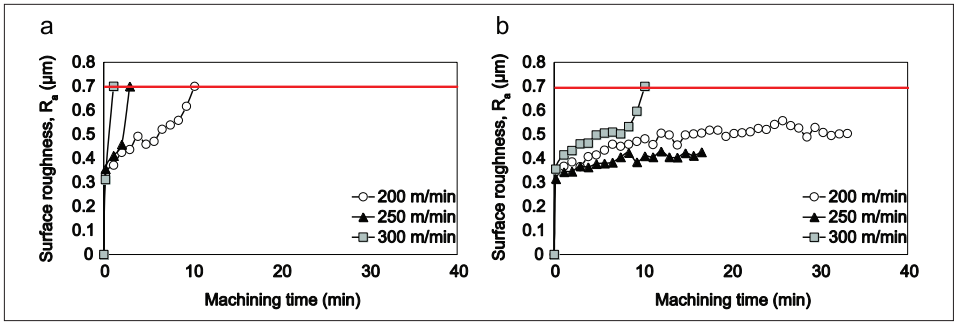

Figure 9: Progression of the generated surface roughness of steel (a) R and (b) M recorded at the tool life tests with higher cutting speeds (f_n = 0.1 mm/rev, a_p = 0.1 mm, and v_c = 200–300 m/min.

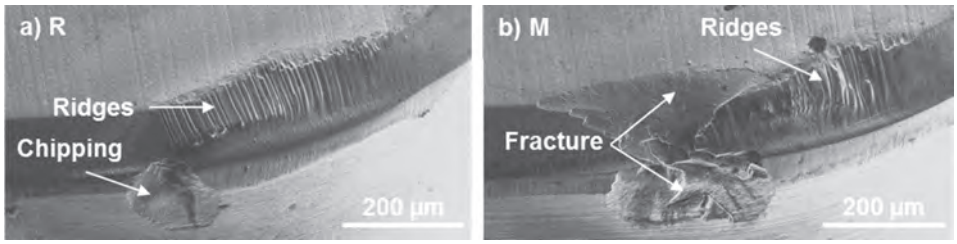

Figure 10: SEM micrographs of the PCBN edges interrupted at 56 parts after a cutting test at (a) 200 m/min. (8 min.) and (b) 300 m/min. (6 min.); the edges were etched prior to imaging

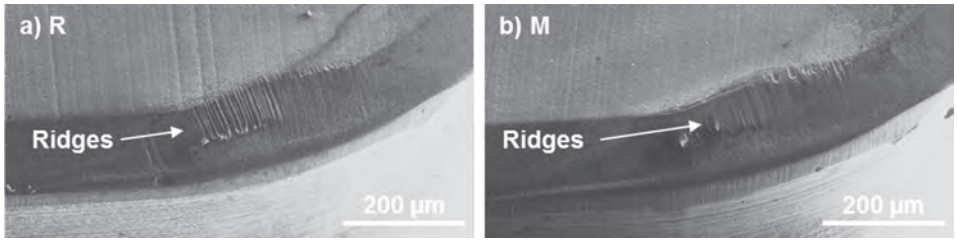

Figure 11: SEM micrographs of the PCBN edges after the cutting tests at v_c = 166 m/min. interrupted at (a) 41 parts (7.5 min.) and (b) 86 parts (16 min.); the edges were etched prior to imaging

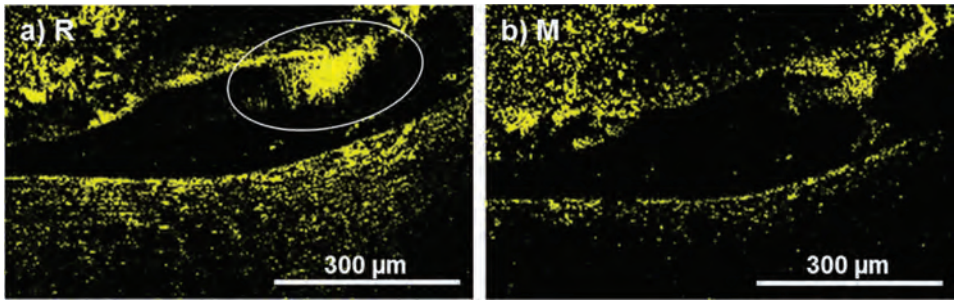

Figure 12: EDS-maps of Fe in the crater and the edge region after turning tests, which were interrupted at 41 (7.5 min.) and 86 parts (16 min.), respectively; obtained from the edges in Figure 11

Economic Impact

The annual production rate of middle cones at the manufacturing site is about 200,000 parts. The tested cutting tools from SECO have a listing price of about 42€ each. At the same time, the cutting tool life of the tested

PCBN edges raised with about 110 percent at the evaluated cutting speed of 166 m/min. and the feed rate of 0.24 mm/rev. In total, this results in a reduced annual tooling cost saving of 50 percent, from 40,000 to 20,000€ (see Figure 15).

DISCUSSION

The economic impact of an improved PCBN cutting tool life on gearbox production at Scania and purchase strategy: The more than doubled service life of the PCBN cutting tool in hard part turning of middle cones for gearboxes with the M-treated, machinability-improved steel enables an attractive annual tooling cost saving of about 50 percent, as compared to the R-steel, (Figures 6 and 15). Moreover, even with the cutting speed increased from 166 to 200 m/min., the PCBN tool life with the M-steel was 31 minutes, as compared to 18 min. for the R-steel at 166 m/min. (Figures 6 and 9). This corresponds to an increased service life of about 70 percent with the M-steel in terms of machining time, and actually about the doubled in terms of cut chip length. Consequently, the M-steel allows a significantly increased production rate.

The machinability-improved steel (M) corresponds to a Level B type of steel with respect to the cleanliness, (Table 1). The level B class is by far the most widespread cleanliness category used in transmission parts at Scania. Therefore, to introduce the M-steel on a wider range of components would lead to a significantly reduced manufacturing cost per produced component. In addition, the implementation of M-steels also has the potential to markedly increase the standard performance of the operating production efficiency and the production capability.

Tool life limiting wear modes: The surface roughness above the threshold value of Ra ≥ 0.7 µm was used as the tool life criterion in this study. In the reference turning operation of an R-steel at a 166 m/min. rate, the progressive flank wear had expanded to 44 ±8 µm, as based on three cutting edges analyzed. However, the flank wear given by the maximum extension of the edge chipping was 135 ±47 mm. Studies of the secondary edge showed that the chipping was actually located near the surface generating point on the secondary cutting edge, typically 150-200 µm from the nose. Therefore, the pronounced tool chipping tendency with the R-steel is believed to affect the generation of the workpiece surface significantly and consequently the tool life. The progressive flank face wear rate with the M-steel was lower than that of the R-steel, which indicates on a more easy-to-machine type of steel grade. However, the most valuable benefit with the M-steel in this study is the reduced expansion of the chipping on the flank face of the secondary cutting edge. The significantly reduced chipping wear made the R_a-value level out at 0.5 µm with the M-steel (see Figure 6b), i.e., below the tool life criterion. Consequently, the use of M-steels enables a significantly more robust machining process.

The general effect of non-metallic inclusions and the degradation mechanisms of

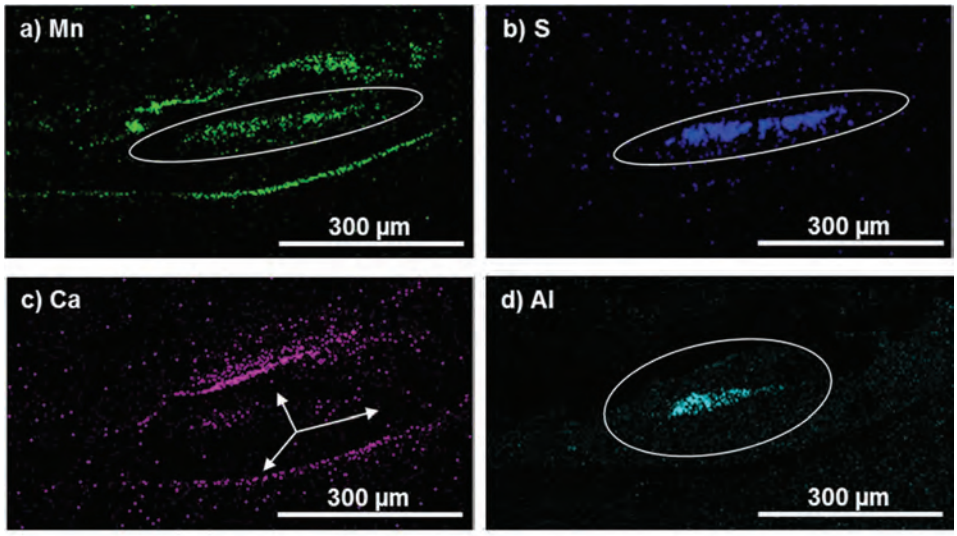

Figure 13: EDS-maps of Mn, S, Ca, Al, and O, respectively, in the crater and edge region of the M-steel after the cutting tests, which were interrupted at 86 parts (16 min.)

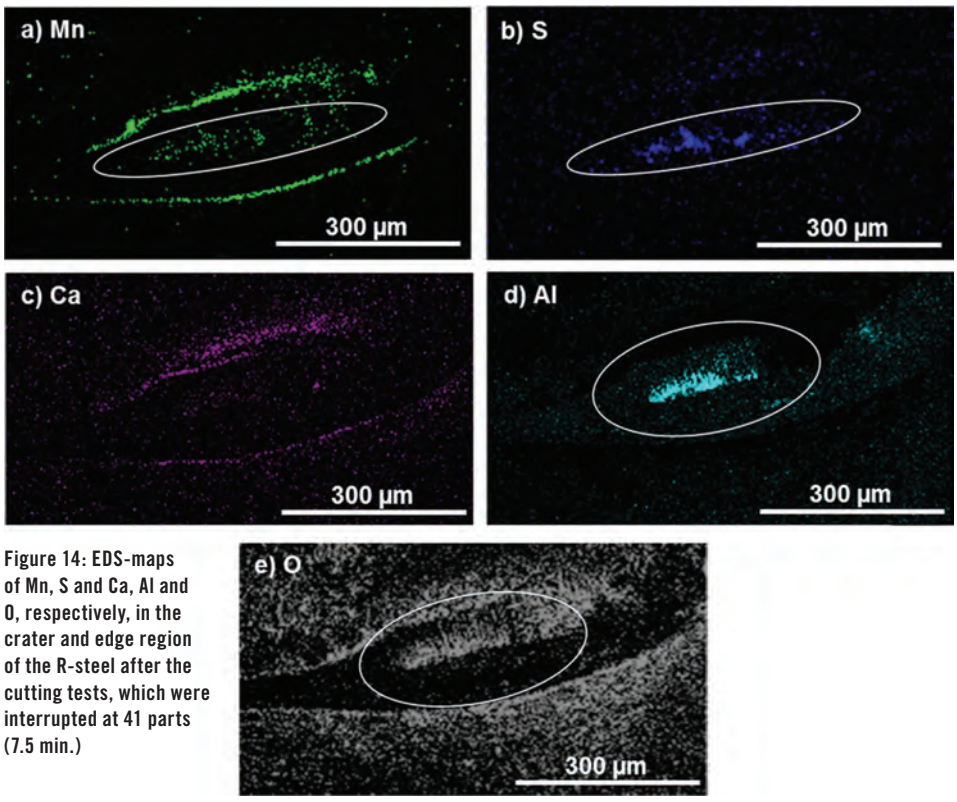

Figure 14: EDS-maps of Mn, S and Ca, Al and O, respectively, in the crater and edge region of the R-steel after the cutting tests, which were interrupted at 41 parts (7.5 min.)

low-PCBN cutting tool at hard part turning: PCBN tool wear in interrupted hard machining was studied during the gearbox production. It was found that the low-PCBN cutting tool (45 vol% CBN) failed, primarily due to an edge chipping and due to a crater wear during hard part turning of middle cones. Furthermore, this work shows that the PCBN cutting tool life during hard part turning depends on the formation and stability of the lubricating slag layers that acts as a barrier between the tool edge and the workpiece. It is relatively established in soft turning that calcium is enriched on the tool rake face and thereby has the ability to reduce the tool wear progression [31]. Furthermore, the analogous effect of the reduced wear on the rake face is obtained also during hard part turning, as shown recently by Ånmark et al. [30].

The current study confirms the strong positive effect of the Ca-based slag deposits formed on the tool edge and how they reduce the chemical degradation of the tool rake face. Moreover, the current study shows how the chipping wear can be significantly reduced by using a Ca-treated steel. It is proposed that the slag deposits detected on the rake face exist also on the edge line. However, the limitation of EDS analysis is of about 0.5 µm layer thickness; this does not show with this technique. It is proposed that slag deposits form also on the tool edge line and that they reduce adhesion and burr formation that may be the origin of the premature chipping behavior of the tests with the R-steel. This is of utmost importance for the tool life as it is defined by the component surface roughness. Since chipping wear is characterized by discrete and stochastic events, the reduced chipping is extremely important for the production robustness.

It is believed that the Ca-enriched barrier of slag deposits protects the tool against wear induced by a diffusion phenomenon in the tool-chip contact on the rake face of the PCBN cutting tool. Thus, this minimizes the material transfer to the PCBN edge. These findings agree with the EDS investigation, which only indicated a minor material transfer to the PCBN cutting edge after the machining of the R-steel and none after the machining of the M-steels. Without the lubricating slag layer, a higher friction between the tool edge and the chip flow is expected, which means a higher temperature at the tool-chip interface. Therefore, Fe-rich compounds from the chip flow may penetrate the tool surface and attack the CBN grains. It is easy to imagine an edge chipping of the PCBN tool if the CBN is depleted and replaced by Fe-rich compounds near the tool edge surface [13]. This phenomenon is believed to be promoted by a high temperature at the cutting edge, which is governed by an increased cutting speed [32]. The depletion of PCBN-cutting tools by Fe-rich compounds correlate well to the findings in a previous study where clean steels with a low content of non-metallic inclusions generated a significant amount of workpiece material (Fe) transfer to the PCBN cutting edge, coming from the chip flow and caused an edge chipping and a severe crater wear [30].

Distribution of slag deposits and the effect of calcium on the mechanism of ridge formation in the PCBN rake face crater: The improved machinability of the M-steel is linked to the Ca-enriched barrier of (Mn,Ca)S and (Ca, Al)(O,S) phases that are built up on the PCBN rake face crater (see Figures 13 and 14) during hard part turning. Moreover, the EDS analysis showed that the steel constituents were transferred into different zones of the PCBN cutting edge as shown schematically in Figure 16. In Zone A, which represents the cutting edge, foremost the Fe and O contents are pronounced, especially when cutting in the

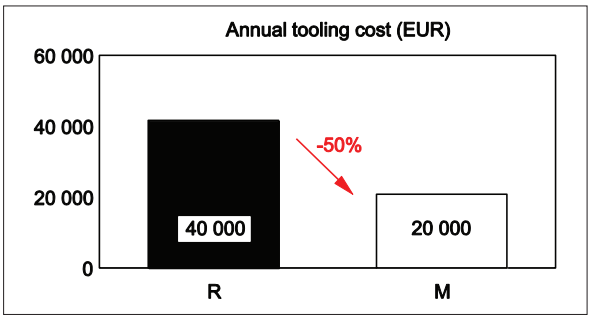

Figure 15: A cost-save calculation based on the prolonged service lifetime of the M-steel

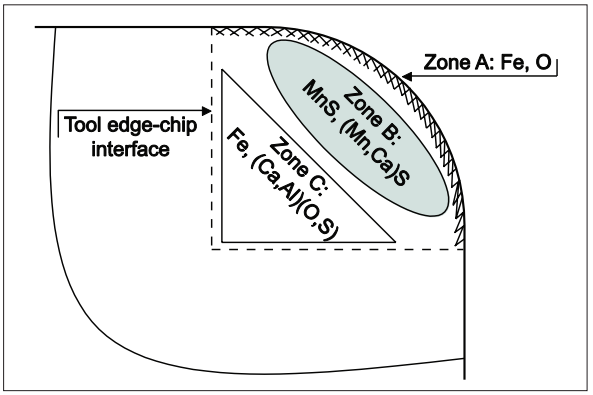

Figure 16: Closeup micrographs of the PCBN edges after an interrupted machining operation of (a) R and (b) M at a 166 m/min. rate for 18 and 38 min., respectively; the edges were etched prior to imaging

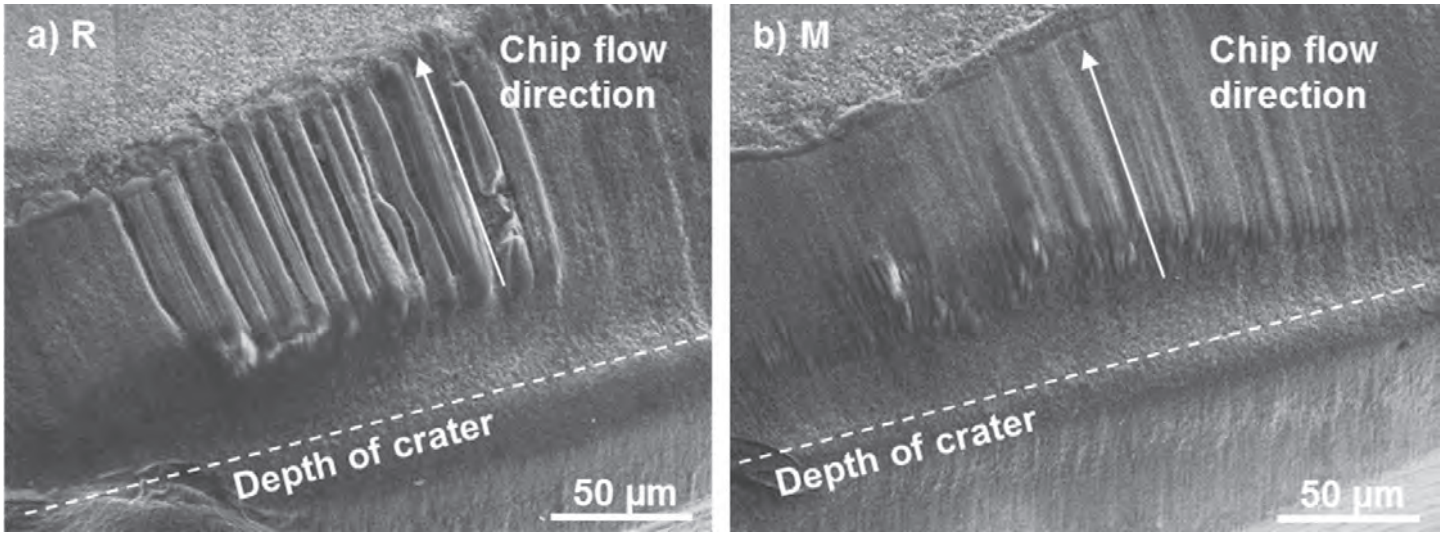

Figure 17: Schematic drawing of the tool edge-chip contact zone and the distribution of the transferred Fe, O, Al, Mn, Ca, and S elements from the workpiece

R-steel. Zone B and C indicate the presence of Ca-enriched slag deposits. In Zone B, layers of MnS and (Mn,Ca)S phases were found. Typically, they had an elongated shape parallel to the edge line. In Zone C, a transferred layer of (Ca, Al)(O,S) was found together with Fe. The presence of (Mn,Ca)S and (Ca,Al)(O,S) phases in Zone C, at the rake face crater of the PCBN edge, is linked to the characteristic wear pattern of the ridges, as seen in Figures 7, 10, and 11 and the closeup picture in Figure 17. Similar results were obtained by Brion et al. in a previous study, where Fe and O were enriched in Zone A and C while Mn and S were more dominant in Zone B [33]. Without the Ca-treatment, no formation of the protective non-metallic inclusions will occur. This may lead to a faster degradation of the PCBN cutting tool as a consequence of a diffusion-induced chemical wear. Furthermore, it is believed that the PCBN ridges develop continuously during the intermittent machining operation and that the wear morphology becomes more apparent at higher cutting speeds. This is due to an increased interaction between the PCBN cutting edge and the chip flow.

Outlook on industrial use of Ca-treated steels: A large scale implementation of Ca-treated steels aiming at improved machinability requires extensive studies of how the material behaves through the complete manufacturing route, including rough turning, gear hobbing and drilling, heat treatment, distortion, hard machining, and grinding, etc. Positive results from studies of this scope make it possible to replace the current standard steels. These types of studies are dedicated for future work. Moreover, there is a multi-source requirement of steel suppliers that can offer Ca-treated steels with the desired steel quality.

The current study indicates that the use of a Ca-treated steel enables new possibilities in the optimization of productivity and robustness. The combination of a significantly reduced chipping wear on the flank face and the minimal crater wear on the rake face obtained with the M-steel in this study indicates that a higher CBN content tool grade can be used with this steel. High CBN content PCBN grades are often considered tougher, yet more susceptible to wear by chemical dissolution than that of the tool grade used in this study. An option with the M-steel would therefore be to not increase the tool life but to further reduce the risk of chippings and edge fractures. These phenomena are stochastic to their nature and undesired from a robust production point-of-view.

However, prior to a full-scale introduction of the Ca-treated steel two aspects must be dealt with: 1. The modified metallurgy of Ca-treatment must be verified with respect to the fatigue strength in component tests and compared to available data of the reference steel and specification. 2. There is a multi-source requirement of steel suppliers that can offer Ca-treated steels with the desired steel quality. Guaranteed deliveries from several suppliers and with repeatable properties is necessary to make use of the improved machinability of the M-steel.

CONCLUSIONS

The role of non-metallic inclusions on the tool wear and PCBN cutting tool life in fine machining of carburizing steel grades was investigated. A Ca-treated carburizing steel grade was compared to a standard steel grade. Furthermore, tool life tests were conducted in order to study the active degradation mechanisms at the end of the tool life. Also, additional machining tests were made with an interruption prior to the tool life aiming at studies of the initial wear mechanisms. From the findings in this work, the following conclusions can be made:

The hard part machinability of a standard carburizing steel (reference R) was improved by 110 percent by the Ca-treatment (modified M-steel). The improved machinability corresponds to a reduced tooling cost of 50 percent at the middle cone production of gearboxes at Scania. Therefore, to implement the M-steel on a wider range of components would be economically beneficial for the gearbox production at Scania. This can lead to a significantly reduced cost per produced component.

The most valuable benefit of the M-steel in this study is the reduced expansion of the chipping on the flank face of the secondary cutting edge and the more controlled progressive flank wear. Consequently, the M-steel enables a more robust machining process than the R-steel.

Thanks to its beneficial tool wear characteristics, a Ca-treated steel can be combined with a higher CBN content tool grade in hard part turning to further minimize the risk of stochastic chippings and edge fractures, thereby promoting the production robustness. It is believed that the Ca-enriched barrier of slag deposits protects the tool against a diffusion-induced wear at the rake face of the PCBN cutting tool. Thus, this would minimize the material transfer to the PCBN edge. In addition, without the lubricating slag layer, a higher friction between the tool edge and the chip flow is expected. This, in turn, means a higher temperature at the tool-chip interface. Therefore, Fe-rich compounds from the chip flow may penetrate the tool surface and attack the CBN grains, which will result in an edge chipping. It is also believed that the extremely thin slag deposits form also on the edge line and on the flank face. These films reduce the affinity of the tool-chip contact, and they impede transfer of workpiece material on to the cutting edge line, thereby explaining the reduced chipping wear in the machining tests with the M-steel.

The improved machinability of the M-steel is linked to the Ca-enriched barrier of (Mn,Ca)S and (Ca,Al)(O,S) non-metallic inclusions that is built up on the PCBN rake face crater during hard part turning. The presence of (Mn,Ca)S and (Ca,Al)(O,S) phases at the rake face crater of the PCBN edge generates a characteristic wear pattern of ridges. Without the Ca-treatment, no formation of the protective non-metallic inclusions will occur, which may lead to a faster degradation of the PCBN cutting tool as a consequence of a diffusion-induced chemical wear.

ACKNOWLEDGMENTS

This work was funded by the unit of transmission machining at Scania CV AB.

REFERENCES

1. F. Klocke, E. Brinksmeier, K. Weinert, Capability profile of hard cutting and grinding processes, CIRP Ann. Manuf. Technol. 54 (2005) 22–45, http://dx.doi. org/10.1016/S0007-8506(07)60018-3.
2. K.K.B. Hon, Performance and evaluation of manufacturing systems, CIRP Ann. Manuf. Technol. 54 (2005) 139–154, http://dx.doi.org/10.1016/S0007-8506(07) 60023-7.
3. N. Stricker, G. Lanza, The concept of robustness in production systems and its correlation to disturbances, Procedia CIRP 19 (2014) 87–92, http://dx.doi.org/ 10.1016/j.procir.2014.04.078.

4. N. Stricker, A. Pfeiffer, E. Moser, B. Kadar, G. Lanza, L. Monostori, Supporting multi-level and robust production planning and execution, CIRP Ann. Manuf. Technol. 64 (2015) 415–418, http://dx.doi.org/10.1016/j.cirp.2015.04.115.
5. H.G. Beyer, B. Sendhoff, Robust optimization - a comprehensive survey, Comput. Methods Appl. Mech. Eng. 196 (2007) 3190–3218, http://dx.doi.org/ 10.1016/j.cma.2007.03.003.
6. P.J. Heath, Ultra-hard materials, Eur. J. Eng. Educ. 12 (1987) 5–20, http://dx.doi. org/10.1080/03043798708939332.
7. J. Fulemova, Z. Janda, Influence of the cutting edge radius and the cutting edge preparation on tool life and cutting forces at inserts with wiper geometry, Procedia Eng. 69 (2014) 565–573, http://dx.doi.org/10.1016/j.proeng.2014.03.027.
8. B. Denkena, A. Lucas, E. Bassett, Effects of the cutting edge microgeometry on tool wear and its thermo-mechanical load, CIRP Ann. Manuf. Technol. 60 (2011) 73–76, http://dx.doi.org/10.1016/j.cirp.2011.03.098.
9. B. Denkena, D. Biermann, Cutting edge geometries, CIRP Ann. Manuf. Technol. 63 (2014) 631–653, http://dx.doi.org/10.1016/j.cirp.2014.05.009.
10. Y.K. Chou, C.J. Evans, M.M. Barash, Experimental investigation on cubic boron nitride turning of hardened AISI 52100 steel, J. Mater. Process. Technol. 134 (2003) 1–9, http://dx.doi.org/10.1016/S0924-0136(02)00070-5.
11. J. Barry, G. Byrne, Cutting tool wear in the machining of hardened steels Part II: cubic boron nitride cutting tool wear, Wear 247 (2001) 152–160, http://dx.doi. org/10.1016/S0043-1648(00)00528-7.
12. Y. Huang, Y.K. Chou, S.Y. Liang, CBN tool wear in hard turning: a survey on research progresses, Int. J. Adv. Manuf. Technol. 35 (2006) 443–453, http://dx. doi.org/10.1007/s00170-006-0737-6.
13. J. Angseryd, E. Olsson, H.-O. Andrén, Effect of workpiece sulphur content on the degradation of a PCBN tool material, Int. J. Refract. Met. Hard Mater. 29 (2011) 674–680, http://dx.doi.org/10.1016/j.ijrmhm.2011.04.016.
14. W.Y.H. Liew, B.K.A. Ngoi, Y.G. Lu, Wear characteristics of PCBN tools in the ultra-precision machining of stainless steel at low speeds, Wear 254 (2003) 265–277, http://dx.doi.org/10.1016/S0043-1648(03)00002-4.
15. K. Bouacha, M.A. Yallese, S. Khamel, S. Belhadi, Analysis and optimization of hard turning operation using cubic boron nitride tool, Int. J. Refract. Met. Hard Mater. 45 (2014) 160–178, http://dx.doi.org/10.1016/j.ijrmhm.2014.04.014.
16. A. McKie, J. Winzer, I. Sigalas, M. Herrmann, L. Weiler, J. Rödel, N. Can, Mechanical properties of cBN–Al composite materials, Ceram. Int. 37 (2011) 1–8, http://dx.doi.org/10.1016/j.ceramint.2010.07.034.
17. S.Y. Luo, Y.S. Liao, Y.Y. Tsai, Wear characteristics in turning high hardness alloy steel by ceramic and CBN tools, J. Mater. Process. Technol. 88 (1999) 114–121, http://dx.doi.org/10.1016/S0924-0136(98)00376-8.
18. M.A. Davies, Y. Chou, C.J. Evans, On chip morphology, tool wear and cutting mechanics in finish hard turning, CIRP Ann. Manuf. Technol. 45 (1996) 77–82, http://dx.doi.org/10.1016/S0007-8506(07)63020-0.
19. G. Poulachon, B.P. Bandyopadhyay, I.S. Jawahir, S. Pheulpin, E. Seguin, Wear behavior of CBN tools while turning various hardened steels, Wear 256 (2004) 302–310, http://dx.doi.org/10.1016/S0043-1648(03)00414-9.
20. Z.N. Farhat, Wear mechanism of CBN cutting tool during high-speed machining of mold steel, Mater. Sci. Eng. A. 361 (2003) 100–110, http://dx. doi.org/10.1016/S0921-5093(03)00503-3.
21. M. Zimmermann, M. Lahres, D.V. Viens, B.L. Laube, Investigations of the wear of cubic boron nitride cutting tools using Auger electron spectroscopy and X- ray analysis by EPMA, Wear 209 (1997) 241–246, http://dx.doi.org/10.1016/ S0043-1648(96)07488-1.
22. R.V. Väinölä, L.E.K. Holappa, P.H.J. Karvonen, Modern steelmaking technology for special steels, J. Mater. Process. Technol. 53 (1996) 453–465, http://dx.doi. org/10.1016/0924-0136(95)02002-4.
23. L.E.K. Holappa, A.S. Helle, Inclusion control in high-performance steels, J. Mater. Process. Technol. 53 (1995) 177–186, http://dx.doi.org/10.1016/ 0924-0136(95)01974-J.
24. N. Ånmark, A. Karasev, P. Jönsson, The effect of different non-metallic inclu- sions on the machinability of steels, Materials 8 (2015) 751–783, http://dx.doi. org/10.3390/ma8020751.
25. N. Ånmark, Inclusion Characteristics and Their Link to Tool Wear in Metal Cutting of Clean Steels Suitable for Automotive Applications, KTH Royal Institute of Technology, Stockholm (2015) http://dx.doi.org/10.13140/ RG.2.1.1958.3524.
26. A. Nordgren, Tool Wear and Inclusion Behaviour During Machining of Ca- treated Steels, KTH - The Royal Institute of Technology, Stockholm, 1993.
27. A. Nordgren, A. Melander, Deformation behaviour of different types of inclusion during chip formation in turning of quenched and tempered steels, J. Mater. Sci. Technol. 5 (1989) 940–951, http://dx.doi.org/10.1179/mst.1989.5.9.940.
28. C.-H. Leung, L.H. Vlack, Solubility Limits in Binary (Ca,Mn) Chalcogenides, J. Am. Ceram. Soc. 62 (1979) 613–616, http://dx.doi.org/10.1111/j.1151-2916.1979. tb12743.x.
29. C.-H. Leung, L.H. Vlack, Solution and precipitation hardening in (Ca, Mn) sul- fides and selenides, Metall. Trans. A 12 (1981) 987–991, http://dx.doi.org/ 10.1007/BF02643479.
30. N. Ånmark, T. Björk, A. Ganea, P. Ölund, S. Hogmark, A. Karasev, P. Göran Jönsson, The effect of inclusion composition on tool wear in hard part turning using PCBN cutting tools, Wear 334–335 (2015) 13–22, http://dx.doi.org/ 10.1016/j.wear.2015.04.008.
31. A. Larsson, S. Ruppi, Structure and composition of built-up layers on coated tools during turning of Ca-treated steel, Mater. Sci. Eng. A. 313 (2001) 160–169, http://dx.doi.org/10.1016/S0921-5093(01)00964-9.
32. H.M. Lin, Y.S. Liao, C.C. Wei, Wear behavior in turning high hardness alloy steel by CBN tool, Wear. 264, 2008), pp. 679–684, http://dx.doi.org/10.1016/j.wear. 2007.06.006.
33. J.M. Brion, B. Sander, G. Pierson, J. Lepage, J. Von Stebut, Mechanisms of built- up layer formation on turning tools: Influence of tool and workpiece, Wear 154 (1992) 225–239, http://dx.doi.org/10.1016/0043-1648(92)90156-3.

ABOUT THE AUTHORS: Niclas Ånmark is with the Department of Advanced Engineering Transmission Production, Scania CV AB, Sweden. Thomas Björk works in the Department of Materials and Manufacturing, Swerea KIMAB, Sweden.

AISTech.org

STEEL'S PREMIER TECHNOLOGY EVENT

AISTech® 2017

The Iron & Steel Technology Conference and Exposition

8–11 May 2017 | Nashville, Tenn., USA | Music City Center

Registration Now Open!

GLOBAL EVENT SPONSOR

THE SYSTEMS GROUP

AIST ASSOCIATION FOR IRON & STEEL TECHNOLOGY

EQUIPMENT | CONTACT *THERMAL PROCESSING* AT 800-366-2185 TO LIST YOUR EQUIPMENT.

Heat Treat Equipment – REF #101
Phone: 734-331-3939 • Fax: 734-331-3915
Email: john@heattreatequip.com
Website: www.heattreatequip.com

Premier Furnace/BeaverMatic Inc. – REF #102
23850 Freeway Park Drive
Farmington Hills, Michigan 48335
Phone: 248-596-9000 • Fax: 248-596-9001
Email: sales@premierfurnace.com

The W.H. Kay Company – REF #103
30925 Aurora Road, Cleveland, OH 44139
Phone: 440-519-3800 • Fax: 440-519-1455
Email: sales@whkay.com
Website: www.whkay.com

Park Thermal – REF #104
257 Elmwood Ave #300, Buffalo, NY 14222
Phone: 905-877-5254 • Fax: 905-877-6205
Email: jmistry@parkthermal.com
Website: www.parkthermal.com

BATCH OVENS & BOX TEMPERING FURNACES
54" wide x 72" long x 84" high, Despatch Walk-In Oven Gas, 500 F. ..... REF #102
8" 18" 8" Lucifer Elec. 1250 F. ..... REF #103
12" 16" 18" Lindberg Elec. 1200 F. ..... REF #103
12" 16" 18" Lindberg (3) Elec. 1250 F. ..... REF #103
30" 48" 22" Dow Elec. 1250 F. ..... REF #103
34" 19" 33" Poll.Ctrls Burnoff Gas 900 F. ..... REF #103
36" 36" 35" Despatch Elec. 400 F. ..... REF #103
36" 36" 120" Steelman Elec. 450 F. ..... REF #103
36" 48" 36" Grieve Elec. 350 F. ..... REF #103
36" 60" 36" CEC (2) Elec. 650 F. ..... REF #103
37" 19" 25" Despatch Elec. 500 F. ..... REF #103
37" 25" 37" Despatch Elec. 850 F. ..... REF #103
37" 25" 50" Despatch Elec. 500 F. ..... REF #103
38" 20" 24" Blue-M Elec. 1200 F. ..... REF #103
38" 26" 38" Grieve Elec. 1000 F. ..... REF #103
48" 24" 48" Blue-M Elec. 600 F. ..... REF #103
48" 30" 42" Despatch Gas 850 F. ..... REF #103
48" 48" 48" CEC (N2) Elec. 1000 F. ..... REF #103
48" 48" 60" Gasmac Burnoff (2) Gas 850 F. ..... REF #103
48" 48" 72" Despatch (2) Elec. 500 F. ..... REF #103
48" 48" 72" Lydon Elec. 500 F. ..... REF #103
54" 108" 72" Despatch Elec. 500 F. ..... REF #103
56" 30" 60" Gruenberg Elec. 450 F. ..... REF #103

BOX FURNACES
J.L. Becker Slot Forge Furnace, 1986, Brand New, Never Used ..... REF #101
L & L Special Furnace Electrically Heated Box Furnace, 1991 ..... REF #101
J.L. Becker Box Temper Furnace, 1989 ..... REF #101
Sunbeam Electric Box Furnace, good running condition REF #101
Surface 30-48-30 Electric Temper Furnace, good/ very good condition ..... REF #101
Atmosphere Furnace Co. 36-48-30 Electric Temper Furnace, good/ very good condition ..... REF #101
Atmosphere Furnace Co. 36-48-30 Electric Temper Furnace, good/ very good condition ..... REF #101
Surface Combustion 30-48-30 Gas Fired Temper Furnace, good/ very good condition ..... REF #101
Surface 30-48-30 Gas Fired Temper Furnace, good/ very good condition ..... REF #101
24" wide x 48" long x 18" high, Lindberg batch temper, Gas, 1400 F. ..... REF #102
30" wide x 48" long x 26" high, BeaverMatic batch temper, Gas, 1400 F. ..... REF #102
8" 18" 8" Blue-M Elec. 2000 F. ..... REF #103
12" 24" 8" Lucifer-Up/Down (Retort) Elec. 2150/1400 F. ..... REF #103
12" 24" 8" C.I. Hayes (Atmos) Elec. 1800 F. ..... REF #103
12" 24" 12" Hevi-Duty (2) Elec. 1950 F. ..... REF #103
12" 24" 12" Lucifer-Up/Down Elec. 2400/1400 F. ..... REF #103
3" 24" 12" Electra-Up/Down Elec. 2000/1200 F. ..... REF #103
15" 30" 12" Lindberg (Atmos) - Retort Elec. 2000 F. ..... REF #103
17" 14.5" 12" L & L (New) Elec. 2350 F. ..... REF #103
22" 36" 17.5" Lindberg (Atmos) Elec. 2050 F. ..... REF #103
24" 36" 18" Thermnlyne (2) - Unused Elec. 1800 F. ..... REF #103
36" 48" 24" Sunbeam (N2) Elec. 1950 F. ..... REF #103
36" 72" 42" Eisenmann Kiln (Car) Gas 3100 F. ..... REF #103
60" 48" 48" Recco (1998) Gas 2000 F. ..... REF #103
60" 96" 60" Park Thermal Elec. 1850/2200 F. ..... REF #103
126" 420" 72" Drever "Lift Off"-Atmos (2 Avail) Gas 1450 F. ..... REF #103
13" 14" 12" ELECTRIC 1300°F ..... REF #104
10" 10" 18" ELECTRIC 2000°F ..... REF #104
22" 36" 22" ELECTRIC 1600°F ..... REF #104
12" 6" 8" ELECTRIC 2000°F ..... REF #104
12" 8" 18" ELECTRIC 2800°F ..... REF #104
20" 13" 36" ELECTRIC 1850°F ..... REF #104
12" 18" 18" ELECTRIC 1250°F ..... REF #104
4" 10" 4" ELECTRIC 2000°F ..... REF #104
22" 10" 8" ELECTRIC - C/W STAND 1250-2000°F ..... REF #104
15" 8" 30" ELECTRIC - ATMOSPHERE 1950°F ..... REF #104
11" 11" 17" ELECTRIC - CABINET 2000°F ..... REF #104
33" 40" 48" ELECTRIC 500°F ..... REF #104
18" 18" 30" ELECTRIC - GLO BAR 2900°F ..... REF #104
30" 30" 54" ELECTRIC - AGING 500°F ..... REF #104
30" 30" 54" R ELECTRIC - AGING 500°F ..... REF #104
30" 30" 54" ELECTRIC 500°F ..... REF #104
24" 18" 24" NATURAL GAS - BATCH FURNACE ..... REF #104
24" 18" 24" NATURAL GAS - BATCH FURNACE ..... REF #104
36" 30" 84" ELECTRIC 1200°F ..... REF #104
24" 24" 24" ELECTRIC 2000°F ..... REF #104
29" 22" 36" NATURAL GAS 1250°F ..... REF #104
12" 11" 24" ELECTRIC - BOX 2000°F ..... REF #104
24" 24" 24" ELECTRIC - GAS MAC 850°F ..... REF #104
18" 12" 12" ELECTRIC 2100°F ..... REF #104
48" 30" 36" ELECTRIC - ATMOSPHERE TEMPERING ..... REF #104
50" 24" 29" NATURAL GAS 1250°F ..... REF #104
36" 18" 24" ELECTRIC 1250°F ..... REF #104
17" 17" 36" NATURAL GAS 1250°F ..... REF #104
15" 6" 10" ELECTRIC 1850°F ..... REF #104
6" DIA 48" ELECTRIC - TUBE FURNACE 1200°C ..... REF #104
7" 4" 14" GAS ..... REF #104
10" DIA 18" GAS - FORGE FURNACE ..... REF #104
9" 6" 15" GAS - FORGE FURNACE ..... REF #104
6" 6" 15" GAS - FORGE FURNACE ..... REF #104
12" 10" 20" ELECTRIC - SPEEDY MELT FURNACE 2000°F ..... REF #104
12" 9" 18" ELECTRIC ..... REF #104
12" 12" 18" NATURAL GAS 1250°F ..... REF #104
14" 14" 18" ELECTRIC - GLOBAR 2500°F ..... REF #104
17" 17" 17" ELECTRIC - HITEMP KILN 2200°F ..... REF #104
35" 24" 60" ELECTRIC 1430°F ..... REF #104
10" 9" 14" ELECTRIC - FRONT DOOR LOADING 2000°F ..... REF #104
12" 12" 24" ELECTRIC - 13KW 2300°F ..... REF #104
12" 12" 24" ELECTRIC - 20KW 2000°F ..... REF #104
18" 12" 24" ELECTRIC 2000°F ..... REF #104
36" 24" 56" ELECTRIC 800°F ..... REF #104
24" 24" 36" ELECTRIC - CYCLONE 1250°F ..... REF #104
24" 36" 30" ELECTRIC RE-CIRC. BOX FURNACE 2000°F ..... REF #104
18" 20" 45" ELECT. RE-CIRC. W/ FLAME CURTAIN & BASKET 2000°F ..... REF #104
12" 12" 18" ELECT. RE-CIRC. BATCH (MATCH PAIR WITH I3958) 1250°F ..... REF #104
12" 12" 18" ELECT. RE-CIRC. BATCH (MATCH PAIR WITH I3957.) 1250°F ..... REF #104

CAR BOTTOM FURNACES
Holcroft 48-144-48 Car Bottom Furnace ..... REF #101
Sauder 48-144-48 Car Bottom Furnace ..... REF #101
48" 48" 72" GAS FIRED CAR BOTTOM 2000°F ..... REF #104
130" 72" 216" GAS FIRED CAR BOTTOM 2000°F ..... REF #104
130" 72" 215" GAS FIRED CAR BOTTOM 2400°F ..... REF #104
108" 36" 192" GAS FIRED CAR BOTTOM 2400°F ..... REF #104
72" 48" 216" GAS FIRED CAR BOTTOM 2000°F ..... REF #104

CHARGE CARS
Surface Combustion 30-48 Charge Car (Double Ended), fairly good condition ..... REF #101
Atmosphere Furnace Company 36-48 Charge Car (Double Ended) ..... REF #101
Surface Combustion 30-48 Charge Car (Double Ended) REF #101

CONTINUOUS ANNEALING FURNACES
Wellman Continuous Mesh Belt Annealing Furnace ..... REF #101
Aichelin-Stahl Continuous Roller Hearth Furnace & Conveying System, 1996 ..... REF #101
Park Thermal Continuous Mesh Belt Furnace, 2005, Excellent Condition – New – Never been used ..... REF #101

CONTINUOUS HQT FURNACES
Tokyo Gasden Ro Continuous Mesh Belt HQWT Furnace Line, 1989 ..... REF #101

CONTINUOUS TEMPERING FURNACES
Surface Combustion Mesh Belt Temper Furnace ..... REF #101
J.L. Becker Conveyor-Type Temper Furnace with Ambient Air Cool Continuous Belt, 1997 IQ Furnaces ..... REF #101
Surface Combustion 30-48-30 Pro-Electric IQ Furnace REF #101
AFC 36-48-30 IQ Furnace with Top Cool ..... REF #101
AFC 36-48-30 IQ Furnace ..... REF #101
Surface Combustion 30-48-30 IQ with Top Cool, Excellent Condition, 2000 ..... REF #101
Surface Combustion 30-48-30 IQ Furnace, Excellent Condition ..... REF #101

DRAW TEMPER FURNACES
24" wide x 48" long x 18" high, Lindberg batch temper, Gas, 1400 F ..... REF #102
30" wide x 48" long x 26" high, BeaverMatic batch temper, Gas, 1400 F (NEW) ..... REF #102
18" 12" 30" ELECTRIC 1250°F ..... REF #104
16" 15" 12" ELECTRIC - BOX DRAW 1250°F ..... REF #104
36" 16" 24" ELECTRIC - BOX DRAW 1250°F ..... REF #104
12" 18" 16" ELECTRIC - BOX DRAW 1400°F ..... REF #104
30" 20" 48" ELECTRIC - BOX DRAW 1250°F ..... REF #104
24" 18" 36" NATURAL GAS ROLLER DRAW 1400°F ..... REF #104
30" 30" 48" NATURAL GAS 1200°F ..... REF #104
60" 40" 60" NATURAL GAS - DRAW FURNACE 800°F ..... REF #104
29" 16" 36" ELECTRIC - DRAW/TEMPER 1400°F ..... REF #104
54" 54" 150" ELECTRIC 900°F ..... REF #104
24" 18" 10 FEET ELECTRIC 500°F ..... REF #104
30" 24" 72" GAS - GRAVITY FEED DRAW 1350°F ..... REF #104
12" 14" 12" ELECTRIC - WATER COOLED FAN 1200°F ..... REF #104

ENDOTHERMIC GAS GENERATORS

Lindberg 1500 CFH Endothermic Gas Generator, 1992, good condition ..... **REF #101**
Lindberg 1500 CFH Endothermic Gas Generator, 1996, excellent condition ..... **REF #101**
Surface Combustion 5600 CFH Endo. Gas Generator ... **REF #101**
Surface Combustion 5600 CFH Endo. Gas Generator ... **REF #101**
Surface Combustion 5600 CFH Endo. Gas Generator ... **REF #101**
Surface Combustion 5600 CFH Endo. Gas Generator ... **REF #101**
Rolock Inc. 2000 CFH Endothermic Gas Generator..... **REF #102**

EXOTHERMIC GAS GENERATORS

J.L. Becker 12,000 CFH Exothermic Gas Generator w/ Dryer, w ..... **REF #101**
Thermal Transfer 30,000 CFH Exothermic Gas Generator, 1994, excellent condition ..... **REF #101**
Seco Warwick 2000 CFH Exothermic Gas Generator..... **REF #102**
Sunbeam 2000 CFH Exothermic Gas Generator ..... **REF #102**
Alhern 6000 CFH Exothermic Gas generator ..... **REF #102**
J L Becker 6000 CFH Exothermic Gas Generator..... **REF #102**
JL Becker 6000 CFH Exothermic Gas Generator..... **REF #102**

FLUIDIZING BED FURNACE

14" 30 DIA 5" ELECTRIC 1600°F ..... **REF #104**

FREEZERS

Webber 36-48-36 Chamber Freezer, 1980 ..... **REF #101**
Cincinnati Sub Zero 36-48-36 Chamber Freezer, 1995 . **REF #101**

MESH BELT FURNACES

17" 8" 10' ELECTRIC 600°F ..... **REF #104**
23" 4" 10' NATURAL GAS 1250°F ..... **REF #104**
24" 12" 96" ELECTRIC 500°F ..... **REF #104**

MESH BELT BRAZING FURNACES

Lindberg Continuous Mesh Belt Brazing Furnace ..... **REF #101**
J.L. Becker 26" Mesh Belt Brazing Annealing Furnace, 2007 ..... **REF #101**
10" J.L. Becker Mesh Belt Furnace with Muffle, 1988 . **REF #101**
24" J.L. Becker Mesh Belt Furnace ..... **REF #101**
Premier Furnace 14" wide mesh belt Aluminum Brazing Furnace 1400 F..... **REF #102**
Alhern 20" wide mesh belt Copper Brazing, Annealing Furnace 2100 F..... **REF #102**
J L Becker 20" wide mesh belt Copper Brazing, Annealing Furnace 2100 F. ..... **REF #102**
JL Becker 20" wide mesh belt Copper Brazing, Annealing Furnace 2100 F. ..... **REF #102**
Alhern 28" wide mesh belt Copper Brazing, Annealing Furnace 2100F. ..... **REF #102**

MISC. EQUIPMENT

Atmosphere Furnace Co. 36-48 Stationary Holding Stations, 1987, 36"W x 48"L work area ..... **REF #101**
Atmosphere Furnace Co. 36-48 Stationary Holding Stations, 1987, 36"W x 48"L work area ..... **REF #101**
Atmosphere Furnace Co. 36-48 Stationary Holding Stations, 1987, 36"W x 48"L work area ..... **REF #101**
Atmosphere Furnace Co. 36-48 Scissors Lift Holding Stations, 1987, 36"W x 48"L work area ..... **REF #101**
Atmosphere Furnace Co. 36-48 Scissors Lift Holding Stations, 1987, 36"W x 48"L work area ..... **REF #101**
Surface Combustion 30-96 Stationary Load Tables, 96-inch rail length, 15-inch rail centers ..... **REF #101**
Surface Combustion 30-96 Stationary Load Tables, 96-inch rail length, 15-inch rail centers ..... **REF #101**
Surface Combustion 30-96 Stationary Load Tables, 96-inch rail length, 15-inch rail centers ..... **REF #101**
Surface Combustion 30-48 Scissors Lift Table, 48-inch rail length ..... **REF #101**
Airco Flo meter panel# 1 ..... **REF #102**
Airco Flo meter panel# 2 ..... **REF #102**
Smart Skim unit..... **REF #102**
8xxx 2.400 CFH 12 oz (2) North American 1/3HP ..... **REF #103**
8xxx 3.000 CFH 12 oz (3) North American 1/2HP ..... **REF #103**
8xxx 5.400 CFH 4 oz North American 1/3HP ..... **REF #103**
8236 12.000 CFH 12oz (3) North American 1/2HP ..... **REF #103**
8712 15.600 CFH 37 oz, North American 5HP ..... **REF #103**
8193 19.500 CFH 32 oz, Spencer 5HP ..... **REF #103**
8245 23.400 CFH 8 oz. North American 1,5HP ..... **REF #103**
8185 24.000 CFH 24 oz. Buffalo Forge 7.5HP ..... **REF #103**
8251 45.600 CFH 16 oz. Spencer 5HP ..... **REF #103**
8252 66.000 CFH 24 oz . Snencer(New) 10HP ..... **REF #103**
8253 66.000 CFH 24 oz. Spencer 10HP ..... **REF #103**
8250 150.000 CFH 16 oz. Hauck 15HP ..... **REF #103**

OVER - UNDER FURNACES

12" 11" 48" GLO BAR ELECTRIC 3000°F ..... **REF #104**
9.5" 9.5" 18" COILED ELEMENTS ELECTRIC 2300°F . **REF #104**
22" 11" 14" COILED ELEMENTS ELECTRIC 2200°F ... **REF #104**
12" 7" 30" ELECTRIC - CRESS ..... **REF #104**
18" 12" 24" ELECTRIC 2100/1250°F ..... **REF #104**
12" 12" 36" ELECTRIC 2300/1250°F ..... **REF #104**

PARTS WASHERS

J.L.Becker Gas-Fired Tub Washer ..... **REF #101**
48-72-48 Gas Fired Spray Washer ..... **REF #101**
Dow Furnace Co. 30-48-30 Electrically Heated Spray, Dunk & Agitate Washer ..... **REF #101**
Atmosphere Furnace Co. 36-48-30 Spray/Dunk Washer **REF #101**
Atmosphere Furnace Co. 36-48-30 Spray/Dunk Washer **REF #101**
Surface Combustion 30-48-30 Electrically Heated Spray Dunk/ Dunk Washer ..... **REF #101**
Surface Combustion 30-48-30 Electrically Heated Washer ..... **REF #101**

PIT FURNACES

Lindberg 28" x 28" Pit-Type Temper Furnace ..... **REF #101**
14" 60" Procedyne - Fluidised Bed Elec. 1850 F. ..... **REF #103**
16" 20" Lindberg Elec. 1250 F. ..... **REF #103**
22" 26" L & N Elec. 1200 F. ..... **REF #103**
28" 48" Lindberg Elec. 1400 F. ..... **REF #103**
38" 48" Lindberg Elec. 1400 F. ..... **REF #103**
40" 60" L & N -Steam/N2 Elec. 1400 F. ..... **REF #103**
40" 60" Wellman-Steam/N2 Elec. 1400 F. ..... **REF #103**
48" 48" Lindberg (Atmos) - Fan Elec. 1850 F. ..... **REF #103**
20" 48" ELECTRIC 1200°F ..... **REF #104**
30" 36" NATURAL GAS 1250°F ..... **REF #104**
24" 30" ELECTRIC 1400°F ..... **REF #104**
16" 18" GAS - CYCLONE 1300°F ..... **REF #104**
28" 96" NATURAL GAS 1400°F ..... **REF #104**
24" 28" ELECTRIC - HOMO CARBURIZING 1400°F ..... **REF #104**
16" 30" ELECTRIC SALT POT 1650°F ..... **REF #104**
22" 36" 22" ELECTRIC SQUARE PIT 1600°F ..... **REF #104**
6" 4" 16" ELECTRIC VACUUM PIT 2400°F ..... **REF #104**
24" 24" ELECTRIC 1400°F ..... **REF #104**
12" dia 18" ELECTRIC - HOMO PIT 1200°F ..... **REF #104**
30" 30" 30" ELECTRIC 800°F ..... **REF #104**
30" DIA 30" ELECTRIC - PIT CYCLONE 1250°F ..... **REF #104**
12" 20" ELECTRIC - KEYHOLE 1250°F ..... **REF #104**
4.5" 24" 4" ELECTRIC - SQUARE PIT ..... **REF #104**
24" 48" 24" ELECTRIC - SQUARE PIT 1200°F ..... **REF #104**
18" 18" 18" ELECTRIC - TOP LOAD 2000°F ..... **REF #104**
16" Dia. 20" ELECTRIC - CYCLONE 1250°F ..... **REF #104**
22" Dia 26" ELECTRIC - CYCLONE 1250°F ..... **REF #104**
22"Dia 26" ELECTRIC 1250°F ..... **REF #104**
8"dia 9"deep ELECTRIC - TEMPERING 1250°F ..... **REF #104**
35" 60" GAS ..... **REF #104**
28"DIA 28" ELECTRIC - CYCLONE PIT 1250°F ..... **REF #104**

VACUUM FURNACES

Brew/Thermal Technology Vacuum Furnace ..... **REF #101**
Abar Ipsen 2-Bar Vacuum Furnace, 1986, good condition ..... **REF #101**
24"W x 36"D x 18"H Hayes (Oil Quench) Elec. 2400 F. . **REF #103**
48" Dia 60" High Ipsen (Bottom Load) Elec. 2400 F. .. **REF #103**

ATMOSPHERE GENERATORS

750 CFH Endothermic Dow Elec. ..... **REF #103**
750 CFH Endothermic Insen Gas ..... **REF #103**
1000 CFH Exothermic Gas Atmosphere ..... **REF #103**
1000 CFH Ammonia Dissociator Lindberg Elec. ..... **REF #103**
1000 CFH Ammonia Dissociator Drever Elec. ..... **REF #103**
1500 CFH Endothermic (Air Cooled) Ipsen Elec. ..... **REF #103**
1500 CFH Endothermic Ipsen Gas ..... **REF #103**
3000 CFH Endothermic air Cooled) Lindberg Gas ..... **REF #103**
3000 CFH Endothermic (Air Cooled) Lindberg (2) Gas .. **REF #103**
3000 CFH Endothermic (Air Cooled) Lindhera Gas ..... **REF #103**
3600 CFH Fnclothermic (Air Cooled) Surface (2) Gas ... **REF #103**
3600 CFH Endothermic Surface Gas ..... **REF #103**
5600 CFH Endothermic Surface (3) Gas ..... **REF #103**
6000 CFH Nitrogen Generator (2000) Gas Atmospheres Gas ..... **REF #103**
10 000 CFH Exothermic Seco-Warwick Gas ..... **REF #103**

INTERNAL QUENCH FURNACES

24 inch wide, 48 inch long, 18 inch high, Lindberg, Gas, 1850 F..... **REF #102**
24"W 36"D 18"H Dow (Slow Cool) Line Elec. 2000 F. . **REF #103**
24"W 36"D 1 8"H Ispen T-4 - Air Cooled Gas 1850 F. . **REF #103**
24"W 36"D 18"H Ispen T-4 - Air Cooled Gas 1850 F. .. **REF #103**
24"W 36"D 18"H Isoen T-4 - Air Cooled Gas 1850 F. .. **REF #103**
24"W 36"D 18"H Ispen T-4 - Air Cooled Gas 1850 F ... **REF #103**
30"W 48"D 30"H Surface Allcase Elec. 1750 F. ..... **REF #103**
30" 30" 48" NATURAL GAS 1750°F ..... **REF #104**
12" 10" 24" ELECTRIC - BABY PACEMAKER 1850°F .. **REF #104**
45" 40" 72" ELECTRIC - ALUMINUM QUENCH 1250°F **REF #104**
12" 9" 18" IPSEN 2000°F ..... **REF #104**
87" 36" 87" SURFACE COMBUSTION W/ 12,500G. QUENCH 1850°F ..... **REF #104**
62" 36" 62" SURFACE COMBUSTION W/ 9,500G. QUENCH 1850°F ..... **REF #104**
62" 36" 62" SURFACE COMBUSTION W/ 9,500G. QUENCH 1850°F ..... **REF #104**
15" 12" 30" Electric c/w load carts 1850°F ..... **REF #104**

CONTINUOUS/BELT FURNACES + OVENS

5"W 36"D 2"H BTU Systems (Inert Gas) Rec. 1922°F . **REF #103**
12"W 48"D 2"H Lindberg (Inert Gas) Elec. 1022°F. .... **REF #103**
12"W 15'D 4"H Sargent&Wilbur'94(Muffle) Gas 2100°F. ..... **REF #103**
16"W 24'D 4"H Abbott-Retort (1996) Elec 2400°F. ..... **REF #103**
24"W 12'D 6"H Heat Industries Elec. 750°F. ..... **REF #103**
24"W 40'D 18"H Despatch Elec. 500°F. ..... **REF #103**
60"W 45'D 12"H Roller Hearth Annealer (Atmos) Gas 1700°F ..... **REF #103**

MARKETPLACE

Manufacturing excellence through quality, integration, materials, maintenance, education, and speed.

AD INDEX

JOE STAMBAUGH
FORGING PRODUCTS GROUP LEADER, AJAX TOCCO MAGNETHERMIC

PLEASE TELL US A LITTLE ABOUT YOUR BACKGROUND AND COMPANY.

My education was in electromechanical technologies. I have spent my 40-year career working in the induction heating industry. I hold two U.S. patents, and I have presented and written numerous technical papers on induction technologies. Presently, I am the International Forging Products group leader for Ajax Tocco Magnethermic.

Ajax Tocco Magnethermic has operations in nine countries. In North America, we have manufacturing facilities in three major locations and eight regional service centers. We design and build all of our power supplies and are able to supply customers with the latest technology. Our domestic and international locations allow us to handle large orders or volume increases while maintaining our commitment to quality, service, and delivery. Ajax Tocco owns and operates Pillar Induction, Saet Induction, and Emmedi. Ajax Tocco is part of ParkOhio Holdings Corp., which provides strategic services and products that allow the world's leading manufacturers to streamline their manufacturing processes and focus their core competencies on the production of high-quality products.

TELL US ABOUT EXHIBITING AT FORGE FAIR.

Attending Forge Fair enables us to better communicate our new technologies to customers and potential customers. Ajax Tocco introduces our state-of-the-art PowerForge and PowerZone induction line of induction billet and bar heating equipment. The new advanced series of PowerForge and PowerZone induction forging equipment is the first induction forging systems designed to incorporate state-of-the-art digital electronics with high-speed fiber optic communication technology between the control and the PowerBlock devices. This technology offers unmatched flexibility with no adjustments required to load match, yet it delivers power to a wide range of billet and bar diameters in a given coil size. The precision of the digital controls affords superior reliability and control of the process. The use of fiber optics offers both superior communication speed and immunity to the electrical noise that can contribute to device failures.

Both the PowerForge and PowerZone designs are completely integrated packages that require minimum floor space, ease of installation, and turnkey operation.

The PowerZone technology provides individual control over each induction forge coil. The PowerZone design allows the use of identical coils at each position along the line. This dramatically reduces the number of spare coils needed. This technology allows the use of various frequencies at each coil and the ability to place more power into the start of the process to provide the best core-to-surface differential. When running lower production levels, the first zones of the line can be turned off. The superb energy efficiency helps the end users reduce their energy bills, which is key in most world markets. Expansion capabilities can also be built into the PowerZone series of equipment via our modular design approach, which can allow for future expansion.

Ajax Tocco also offers the Pro-Solv process setup tool. This tool provides an easy and effective way to set up the equipment to easily achieve the best possible heating of billets and bars. For more difficult jobs and applications, we offer the Pro-Solv Pro service, which can assist you in the analysis of the proper heating of your product and implementation of the process on our equipment.

Ajax Tocco will also provide detailed information on our ForgeView and ForgeView Plus software.

WHAT ARE THE BENEFITS TO BEING A MEMBER OF THE INDUSTRY ASSOCIATION?

Being an active member of the industry association allows us to contribute to the industry by helping us understand the forgers' needs and operations. The annual meetings held by the industry provide information from some of the world's best experts on subjects vital to our industry. Both forging producers and suppliers can find extensive information to help their companies with productivity improvement, new technology, better understanding of worldwide demands, public policies, and safety. Industry associations can also provide design engineering assistance, industry sales information, and benchmarking.

HOW HAS THE FORGING INDUSTRY EVOLVED?

I have seen the forging industry evolve in many areas. The forgings are, in many cases, near net forgings. Many forgers are providing a finished product to the end user as opposed to a rough oversize forging that still needs a considerable amount of machining. Some forgers forge, machine, and heat-treat, providing a finished product to the end user. I have also seen the industry embrace the use of automation to better facilitate the load and unload of the forging in the presses. This automation has dramatically improved throughput by reducing cycle times. Tooling performance has been dramatically enhanced with new technologies and practices.

WHAT INDUSTRY CHALLENGES DO YOU SEE?

There are many challenges for the forging and heat-treating industry. These challenges include product quality, cost of manufacturing, and being competitive in a worldwide market. Changing product designs presents new challenges to both industries. Lightweight forging initiatives are changing the overall designs, because reduction of weight is key to the vehicle-manufacturing market. Ajax Tocco is continually advancing this induction technology and automation to provide the world's most reliable, efficient, and state-of-the-art technology designed to accommodate these demands.

WHAT'S IN AJAX TOCCO'S FUTURE?

Ajax Tocco has developed digital-controlled induction power supplies and continues to develop this technology, which improves the reliability and efficiency of our equipment. Ajax Tocco is one of the few induction equipment manufacturers in the world that maintains a dedicated full-time research and development staff, facility, and programs.

FOR MORE INFORMATION: go to www.ajaxtocco.com

ECM USA Inc
VACUUM FURNACES

ECM TREATED GEARS DRIVE THE WORLD

Low Pressure Vacuum Carburizing Systems

PRODUCTS


ICBP® Nano


ICBP® Jumbo


ICBP® Flex


ICBP® Duo

- Vacuum Carburizing
- Gas Quenching
- Oil Quenching
- Neutral Hardening

INNOVATION

ECM Technologies and ECM USA have installed over 1000 cells of heat treating capacity with almost every Automotive company in the world. These systems provide low pressure vacuum carburizing and gas quenching for millions of parts that bring motion and reliability into our daily lives. From automatic, manual transmissions, dual clutch, CVT, to axles and even airplane engine parts, ECM and our processes are part of your lives. Let us build a system for you.

We are a global manufacturer of ***INDUSTRIAL FURNACES***

WWW.ECM-USA.COM

9505 72nd Ave. Ste 400 • Pleasant Prairie, WI 53158 • 262.605.4810

THE INDUSTRY STANDARD FOR OVER 100 YEARS

RX® ENDOTHERMIC ATMOSPHERE GENERATOR

ALLCASE® BATCH INTEGRAL QUENCH FURNACE

RUGGED RELIABLE QUALITY

For over 100 years, Surface Combustion has focused on applying our technical and practical experience to the pursuit of moving heat treating and furnace technology forward. Innovation is a tradition at Surface, with more than 675 patents and 75 registered trademarks. Having installed more than 250,000 thermal systems worldwide, many in operation for over 50 years, Surface is justifiably proud of its reputation for designing durable and productive furnaces. Surface is committed to providing our customers the best in rugged and reliable thermal processing equipment. Our strength lies in the breadth of our product portfolio, unparalleled process knowledge, and commitment to customer service.

SURFACE COMBUSTION, INC.
1700 INDIAN WOOD CIRCLE, MAUMEE, OH, USA
PHONE: +1-419-891-7150, +1-800-537-8980
INFO@SURFACECOMBUSTION.COM
WWW.SURFACECOMBUSTION.COM

Surface® Combustion